CONTROLLING POLYMER STRUCTURE THROUGH THE COHERENCE OF LIGHT

CONTROLLING POLYMER MICROSTRUCTURE THROUGH THE COHERENCE OF LIGHT

By

WHITNEY E. SHIMMELL, B.SC. (HONS.)

A Thesis

Submitted to the School of Graduate Studies

in Partial Fulfillment of the Requirements

for the Degree

Master of Science in Chemistry

McMaster University

MASTER OF SCIENCE (2009) McMaster University

(Chemistry) Hamilton, Ontario

TITLE: Controlling Polymer Microstructure Through the Coherence of Light

AUTHOR: Whitney E. Shimmell, B.Sc. (Hons.)(McMaster University, Hamilton, Ontario, Canada)

SUPERVISOR: Dr. Kalaichelvi Saravanamuttu

NUMBER OF PAGES: xi, 116

Abstract

This thesis describes modulation instability of a broad beam of partially spatially incoherent laser light propagating in a photopolymerisable organosiloxane. Refractive index changes due to photoinitiated free-radical polymerisation lead to a nonlinear regime in which even weak perturbations in the optical field become amplified. These trigger the spontaneous division of the beam into multiple self-trapped filaments of light. By tuning the spatial coherence of the beam, it was possible to vary the diameter of the self-trapped filaments. Quantitative analyses showed that the relation between filament diameter and spatial incoherence was consistent with a previously developed theoretical model. Because refractive index changes in the photopolymer are irreversible, modulation instability led to a permanent array of self-induced waveguides. In this way, it was possible to control the dimensions of the spontaneously formed polymer microstructure by tuning the incoherence of the optical field.

Acknowledgements

I would like to express my gratitude to my supervisor, Dr. Kalaichelvi Saravanamuttu, for her guidance and assistance, both as an undergraduate as well as a graduate student. Thank you also goes to my defense committee: Dr. Randall Dumont and Dr. Peter Kruse, for their input and suggestions.

I would also like to thank past and present members the Saravanamuttu group: Kailash Kasala, Liqun Qiu, Ana Villafranca, Ian Burgess, Matthew Ponte, Jihua Zhang, Natalie Wood, Idlir Liko, and Robert Welch for their contributions and discussions.

Funding for this research was provided by NSERC, Canadian Foundation for Innovation, Ontario Innovation Trust and McMaster University. Donation of photoinitiator from CIBA Specialty Chemicals is gratefully acknowledged.

Finally, thanks to John and Lorie, my parents, and to Michael, my fiancé, for their love, encouragement, and support.

Table of Contents

List of Figures and Tables

1. Introduction

1.1 Nonlinear propagation of light

1.1.1 Optical self-trapping

In most dielectric media, a beam of continuous wave light will broaden in space as it travels. This is due to the natural diffraction of light, which takes place under linear conditions, that is, when medium is not photoresponsive and where its refractive index remains unchanged in the presence of an optical field.[1]

Under certain conditions, a light beam propagating in a photosensitive medium can cause an increase in refractive index along its path. The increase in refractive index creates a lensing effect, which enables the beam to focus along its propagation path.[1]

1.1.2 Self-trapping and the nonlinear Schrödinger equation

When the natural tendency of the beam to diffract is counterbalanced by its self-focussing, the beam self-traps and propagates over long distances (>> Rayleigh length) without suffering any changes to its spatial intensity profile. When broadening and self-focussing *exactly* balance one another, the resulting beam is known as a soliton.

This balanced relationship is described by the nonlinear Schrödinger equation, as follows:[1]

$$2ikn_o(\frac{\partial \psi}{\partial z}) + \nabla_\perp^2 \psi + k^2(n^2 - n_o^2)\psi = 0 \qquad [1\text{-}1]$$

, where ψ is the electric field amplitude and k, the angular wavenumber. Broadening of the beam in the plane transverse to the propagation axis, z, is given the Laplacian term, $\nabla_{\perp}^{2} = (\partial^2/\partial x^2) + (\partial^2/\partial y^2)$. Broadening of the beam is countered by the self-induced change in refractive index, $\Delta n = n - n_o$.

The balance between the natural diffraction and self-focussing described by Equation [1-1], which leads to self-trapping of the beam is illustrated in **Figure 1.1**.

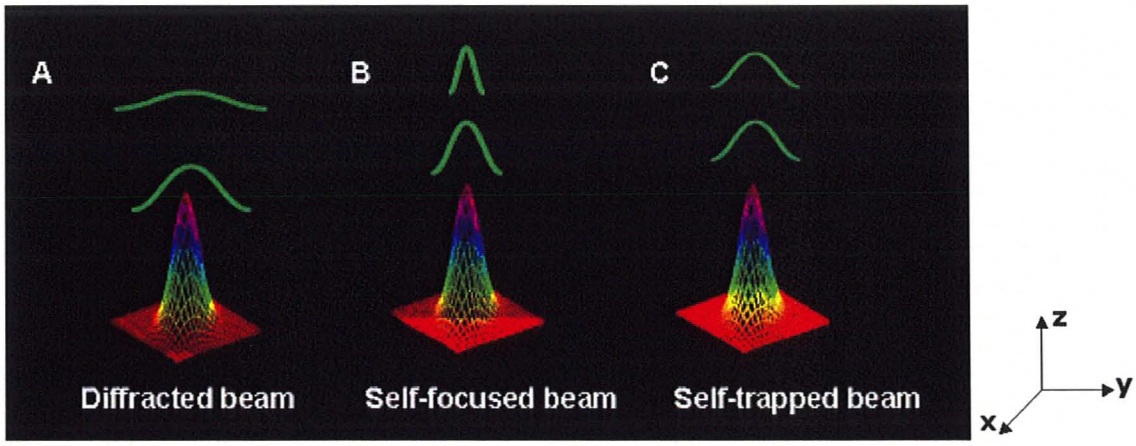

Figure 1.1 Gaussian beam exhibiting (A) diffraction, (B) a self-focussing, and (C) self-trapping due to the competition between (A) and (B).

1.2 Coherent and incoherent light

1.2.1 White light versus continuous wave laser light

Over the last forty years, the majority of studies on self-trapping have been done using coherent laser light.[1, 2, 3, 4, 5, 6, 7, 8, 9] However, in the past decade, increasing attention has been paid to the research of propagation of incoherent light, specifically incoherent white light, in nonlinear optical media.[2, 10, 11, 12, 13] In contrast to coherent

light, which has strong correlation of amplitude and phase, in time and space, light emitted by a white light source is composed of a spectrum of wavelengths with extremely poor spatial and temporal correlation of phase and amplitude (**Figure 1.2**).

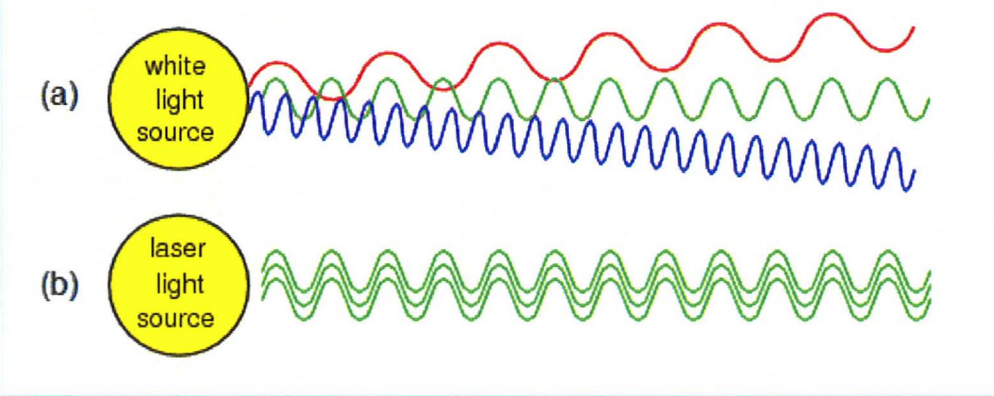

Figure 1.2 Illustrations of (a) an incoherent white light beam depicting weak of correlation of wavelength, amplitude, and phase, in contrast to (b) a coherent light beam, where there is strong correlation of wavelength, amplitude, and phase

As a result, a beam of white light consists of a multitude of intensity speckles, which randomly fluctuate in space on a femtosecond (10^{-15}s) timescale (**Figure 1.3**).[14]

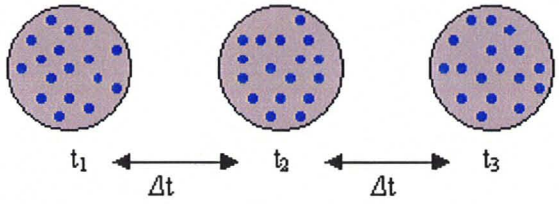

Figure 1.3 Illustration of fluctuating speckles in a beam of white light. $\Delta t \sim 10^{-15}$s.

Since the response time of the human eye is much slower than 10^{-15} seconds, it sees the time-averaged or smoothed profile of a white light beam. Conventional nonlinear optical media, such as Kerr materials, have response times that are equivalent to the femtosecond timescale.[2] Consequently, each of the intensity speckles begins to self-focus, leading to filamentation of the beam. For this reason, self-trapping of white light is

only possible when the response time of the medium is much greater than the timescale of the intensity fluctuations of white light. This was achieved at low laser powers in a photorefractive crystal, which decreased the rate of refractive index change and effectively lengthened the response time of this medium.[15] Alternatively, a material with an inherently longer response time, such as a photopolymer, can be used to elicit self-trapping of white light.[2, 15, 16]

1.2.2 Spatial and temporal coherence

Light emitted by a continuous wave quasi-monochromatic laser has excellent coherence – both spatially and temporally. By contrast, the temporal and spatial coherence of white light emitted by an incandescent source, such as the sun or a tungsten filament, is weak. Temporal coherence refers to the discontinuity in phase that occurs in a beam after propagation through a finite length. Because the phase correlation is examined along the line of propagation, temporal coherence is also referred to as longitudinal coherence. Each segment of the wavetrain has an associated length and lifetime; the average lifetime of the wavetrain is known as the temporal coherence time.

The temporal coherence length (or the length of the coherent pulse), l_t, is the average length of the segmented wavetrains, and can be calculated as follows:

$$l_t = c\tau_0 \cong \frac{\lambda^2}{\Delta\lambda} \qquad [1\text{-}2]$$

, where c is the speed of light, τ_0 is the coherence time, and is the average lifetime of the wavetrain, λ is the wavelength of the light source, and $\Delta\lambda$ is the linewidth.

Temporal coherence is inherent to most light sources due to the difficulty in obtaining a light source that is purely monochromatic.

Spatial coherence on the other hand, can be tuned from excellent to weak to generate the desired spatial coherence length. This tuning process will be covered in detail in section **1.6**. Spatial coherence differs from temporal coherence in that instead of considering the light field along the line of propagation, it refers to the correlation in phase between different points in the plane transverse to the axis of propagation. That is, spatial coherence describes how uniform the phase of the wave front is.[17, 18] A beam with infinite spatial coherence will consist of wavefronts that are identical to one another over the entire width of the beam. When the wavefronts differ from one another, the distance over which there is a correlation between them is the spatial coherence length.

1.3 Use of a photochemical medium for self-trapping

1.3.1 Photopolymerisation as a basis for refractive index change

The majority of research into the nonlinear propagation of spatially and temporally incoherent white light has been carried out by *theoretical* physicists, due to the difficulty in finding a suitable medium.[2, 15, 19] However, it has been recently shown that the nonlinear propagation of white light is experimentally possible in a photopolymerisable system, the response time of which is much longer than 10^{-15} seconds. The photopolymer is an organosiloxane with methacrylate groups, which undergo photoinitiated free-radical polymerisation.[15, 20, 21, 22]

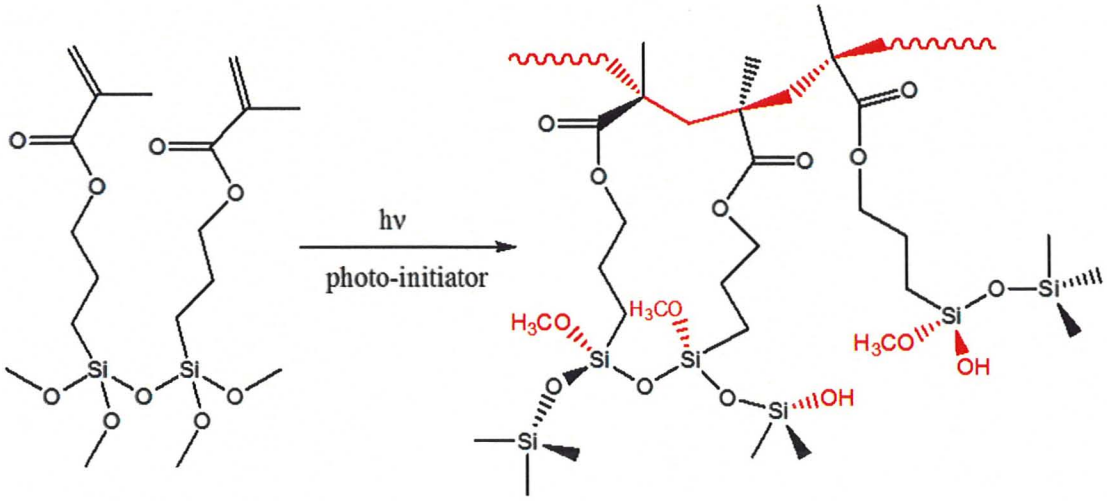

Figure 1.4 Photo-induced polymerisation of organosiloxane

Free radical polymerisation leads to an increase in local density, which in turn gives rise to an increase in refractive index of the medium. Polymerisation and consequent refractive index changes along its propagation path therefore lead to self-trapping of the beam.[23, 24, 25, 26] The refractive index change caused by polymerisation is described by[23, 24, 25, 26]

$$\Delta n(x, y, z, t) = \Delta n_{\max} \left\{ 1 - \exp\left[-\frac{1}{U_0} \int_0^{t-x} \left| E(t) \right|^2 dt \right] \right\}, \qquad [1\text{-}3]$$

in which U_o represents the minimum threshold exposure necessary to induce polymerisation, E(t) is the amplitude of the electric field, Δn is the refractive index change, at a particular point in time (t) and over a specific volume (defined by x, y, z), and Δn_{max} is the index change at saturation.

The plot of Equation [1-3] in **Figure 1.5** shows that the rate of refractive index change is initially large, but gradually decreases as the extent of polymerisation increases, and the medium reaches saturation due to a depletion of available monomer.

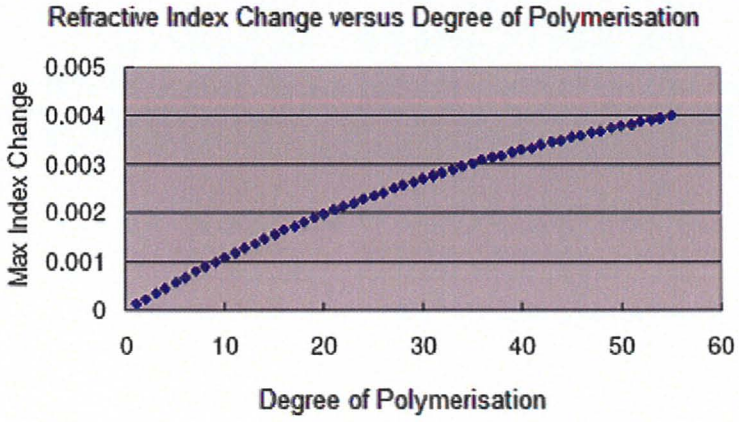

Figure 1.5 A plot describing the change in refractive index by the progression of the polymerisation[27]

1.3.2 Self-trapping of white light in the photopolymerisable organosiloxane

Typical results from self-trapping of a single narrow beam of white light in the photopolymerisable organosiloxane are presented in **Figure 1.6**.[21, 28] These images show the one, two, and three-dimensional spatial intensity profiles of a white light beam propagating in the organosiloxane. At the entrance face of the sample, the input beam is intense and narrow (**Figure 1.6a**), but broadens significantly after traveling through a distance of 6.0 mm (**Figure 1.6b**). Over time, the beam initiates polymerisation and corresponding refractive index changes along its propagation path. A nonlinear condition arises in which there is competition between the self-induced refractive index change and the natural diffraction of the beam. The consequent self-trapping of the beam is evident in the following sequence of images (**Figure 1.6c – m**). After 90 s, the initially broad and

weak beam narrowed and increased in intensity (**Figure 1.6g**), indicating that it retains its profile from the entrance face along its propagation path of 6.0 mm. At long times, the beam broadens slightly and decreases in intensity due to the saturation of refractive index.[28]

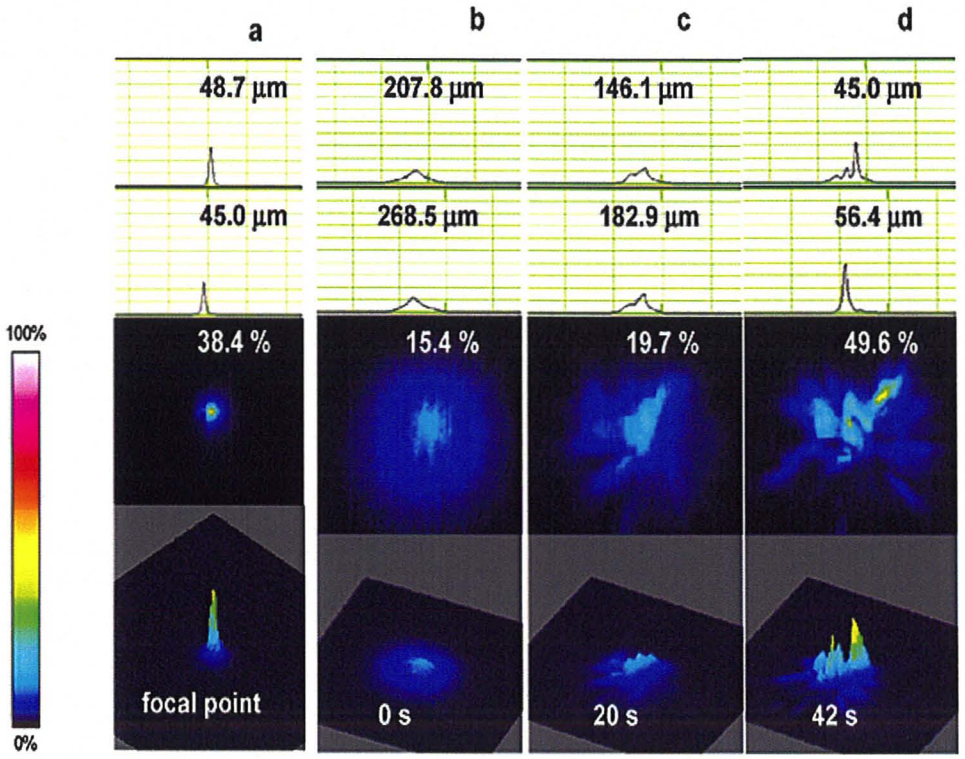

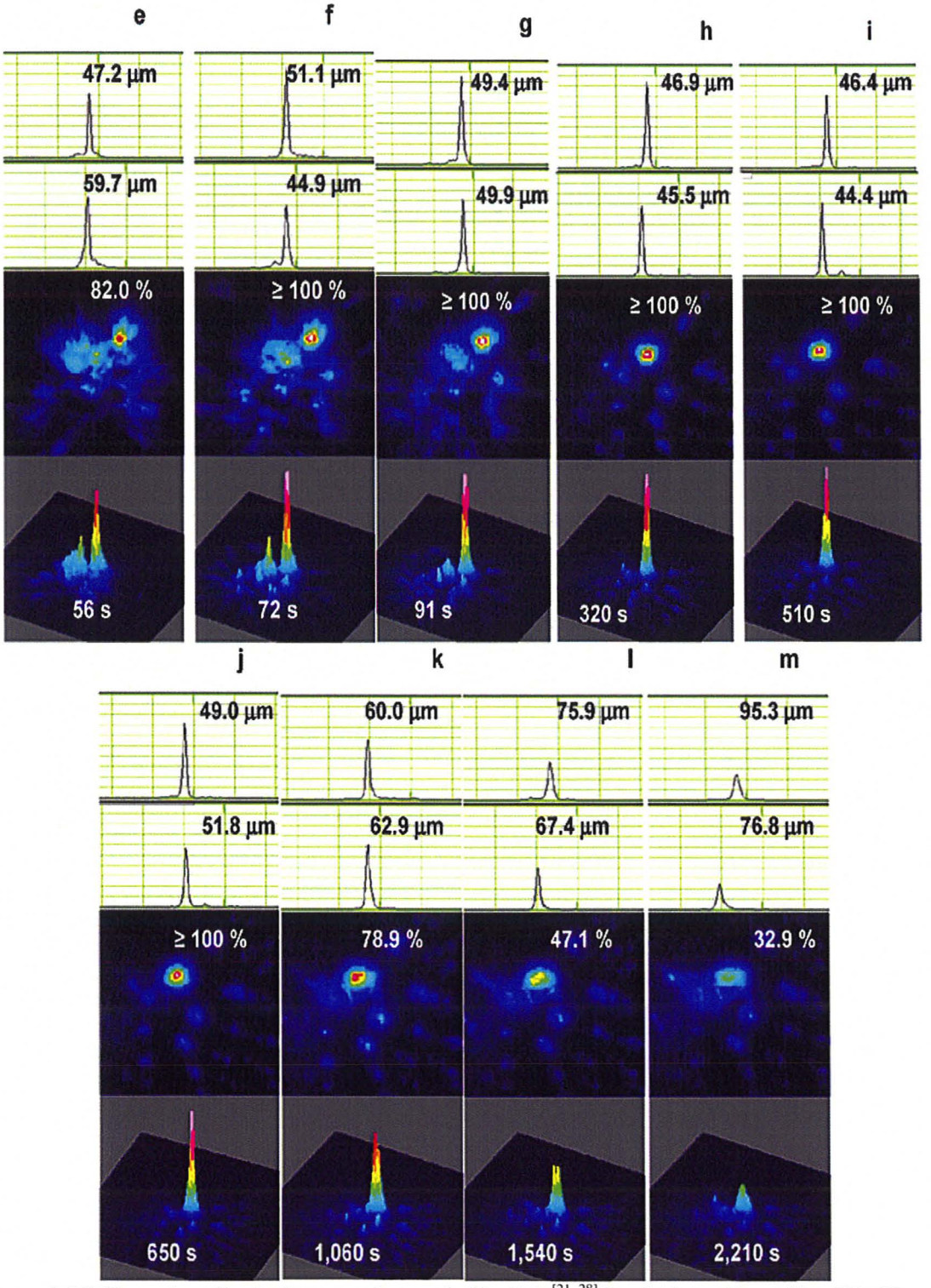

Figure 1.6 Self-trapping of a single narrow beam of white light[21, 28] Spatial intensity profiles (1D, 2D and 3D) of the beam at the entrance face (a), and after 6.0 mm of propagation (b)-(m).
Reprinted with permission from Zhang, J, Kasala, K, Rewari, A and Saravanamuttu, K. *J. Am.Chem.Soc. (Communication)* **2006,** *128*, 406. Copyright 2006 American Chemical Society.

One of the consequences of self-trapping in a photochemical medium is the irreversibility of the refractive index change. This results in a permanent refractive index structure within the medium in the form of a cylindrical fibre. This functions as an optical *waveguide*. A brief treatment of optical dielectric waveguides is provided in **Appendix A**.

1.4 Modulation instability

1.4.1 Modulation instability in photorefractive crystals

The findings of self-trapping of white light described above implied that the *same* competition between diffraction and self-induced refraction would elicit spontaneous pattern formation due to weak amplitude modulations - noise - in a broad, uniform beam of white light. Such a beam propagating under nonlinear conditions can divide *spontaneously* into a multitude of identical filaments of light. This has been predicted by theoretical models and experimentally observed for coherent[1, 29, 30, 31, 32, 33, 34, 35] and partially spatially incoherent[36, 37, 38, 39, 40, 41, 42, 43] light.

A broad beam of light, which may appear uniform under linear conditions, invariably contains weak amplitude fluctuations (noise). These inhomgeneities are amplified under nonlinear conditions due to the same competition between diffraction, and self-induced refraction that gives rise to self-trapping. Because of the nonlinear photoresponse of the medium, regions that experience even slightly elevated intensity, undergo a corresponding elevation in photo-induced refractive index. This causes light from the surrounding area to become confined to these areas of higher refractive index,

strengthening the intensity disparity between these regions, which results in the amplification of these intensity perturbations. These amplified regions then become unstable and divide spontaneously into multiple self-trapped filaments that propagate without broadening over long distances.

The process of modulation instability described above has been both predicted and observed for coherent,[29, 30, 31, 32, 33, 34, 35, 36] as well as for partially spatially incoherent[19, 37, 38, 39, 40, 41, 42, 43] light sources. The temporal evolution of modulation instability of a partially spatially incoherent beam in a strontium-barium-niobate crystal is presented in **Figure 1.7**.[37] These images show the intensity structure of the light field at the exit face of the photorefractive crystal. **Figure 1.7 A** shows the beam before the nonlinearity has been switched on, and thus the light field appears to be uniform. As the refractive index and thus the nonlinearity increases over time, the beam splits apart into a one-dimensional series of stripes (**Figure 1.7 B-D**). Further development of nonlinearity renders the stripes unstable, and they begin to divide further (**Figure 1.7 E**), into the two-dimensional array of spots (**Figure 1.7 F**) characteristic of modulation instability. Each of these spots is a self-trapped beam capable of traveling long distances without broadening.

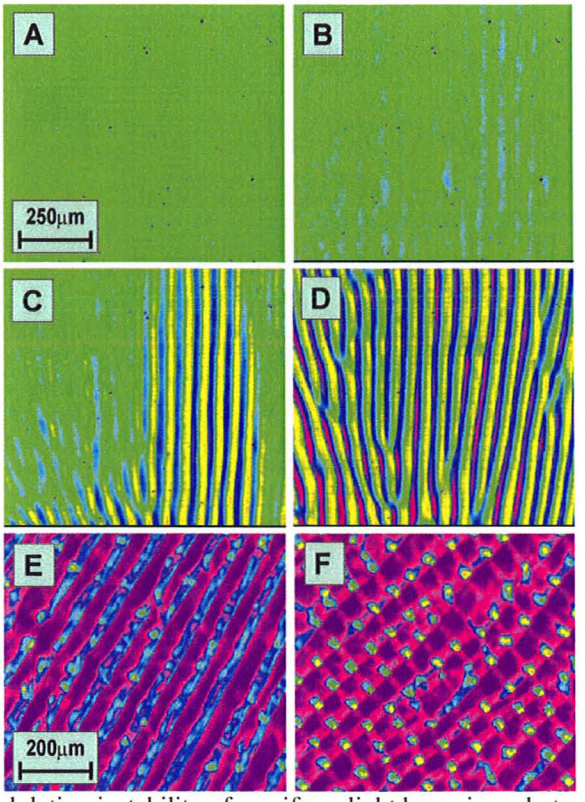

Figure 1.7 Example of modulation instability of a uniform light beam in a photorefractive crystal[37] From Kip, D., Soljacic, M., Segev, M., Eugenieva, E., & Christodoulides, D. N. *Science* **2000** 290 495-498. Reprinted with permission from AAAS.

1.4.2 Modulation instability of spatially and temporally incoherent white light in the photopolymerisable organosiloxane medium

Modulation instability of spatially and temporally incoherent white light is possible when the response time of the photosensitive medium is sufficiently longer than the rate at which the light field undergoes phase and amplitude fluctuations (that is, longer than the femtosecond time-scale).[16] Under identical conditions that elicit self-trapping of a single narrow beam of white light in the photochemical medium, a broad collimated beam of white light was found to transform into multiple self-trapped filaments, due to the competition between diffraction and nonlinearity. This is shown in

Figure 1.8, where a uniform, collimated beam of white light transforms; first into a 1-D periodic pattern of stripes, indicating the amplification of the noise imposed on the sample. This is then followed by each stripe then being affected by instability and spontaneously breaking down into a two-dimensional array consisting of multiple self-trapped beams.[22]

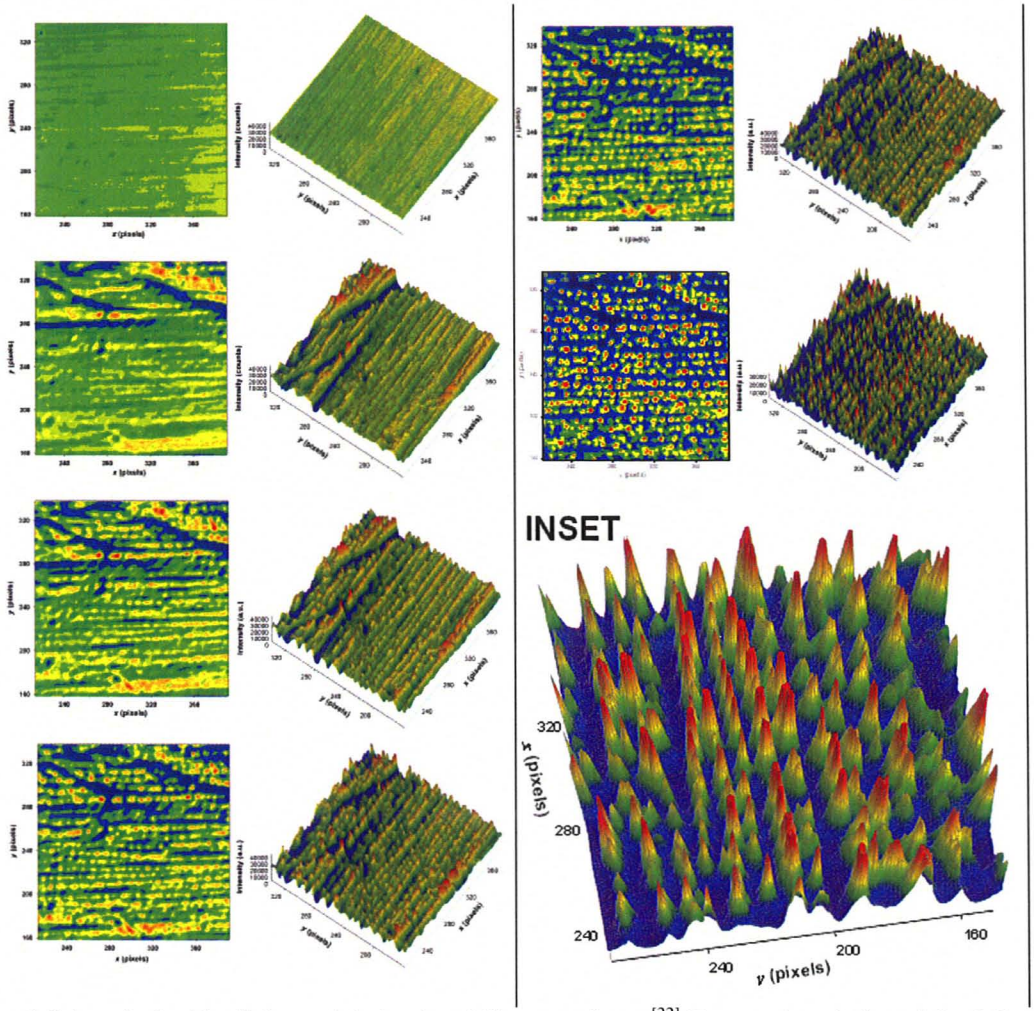

Figure 1.8 A typical white light modulation instability experiment[22] Temporal evolution of the 2-D and 3-D spatial intensity profiles of (a) a uniform beam of white light at a propagation distance of 6.00 mm in photopolymerisable organosiloxane contained in a polymethylmethacrylate cuvette at (b) 385 s, (c) 396 s, (d) 407 s, (e) 418 s, (f) 473 s, and (g) 550 s. The inset is a magnified intensity profile of individual self-trapped filaments of white light at 550 s. Striations of the cuvette were oriented along the *x*-axis. For clarity, intensities were normalized to the maximum peak in images f and g (1 pixel = 9.3 μm x 9.3 μm). Reprinted with permission from Burgess, I. B.; Shimmell, W. E.; Saravanamuttu, K. *J. Am. Chem. Soc.* **2007**, *129*, 4738. Copyright 2007 American Chemical Society.

In the above experiment, the weak amplitude fluctuations are imposed on the medium as a result of longitudinal striations on the poly (methyl methacrylate) cuvette as a result of the extrusion process. This results in the periodic array of stripes that is seen when the polymerisation process begins to amplify the weak noise source. When this weak source of noise is removed, which can be done by instead using an optical glass cuvette, the resulting array is composed of a random distribution of filaments.[22] Conversely, if additional order in the ultimate structure is required, the final pattern can be controlled by imposing the desired amplitude fluctuation onto the sample. This has been accomplished by using an optical mask consisting of light and dark stripes with a periodicity commensurate to the average filament diameter to influence the final distribution of self-trapped beams.

1.4.3 A characteristic self-trapped filament diameter

A series of white light modulation instability experiments in the photopolymerisable medium, were performed at a variety of beam powers in order to determine the effect of optical intensity on the modulation instability process as well as on the resulting filaments. There is a noticeable trend seen in regards to the transformation rate of the beam. As the optical power to which the photochemical medium is exposed is increased, the rate at which the beam divides into stripes and subsequently spots also increases, meaning that these transitions will occur earlier.[22]

The optical power determines the rate of polymerisation and thus the rate of refractive index change (affecting the speed at which these beam transformations occur).

The intensity of the light field to which the photopolymerisable medium is exposed does not affect the size of the filaments that result. Measuring the filament diameter of the spots seen in multiple modulation stability experiments at each optical power examined, always results in self-trapped filament diameters that are statistically equivalent. The characteristic diameter of self-trapped filaments for white light modulation instability (for which the spatial coherence length is approximately 300 nm) in the organosiloxane is 75 ± 5 microns.[22]

1.4.4 Effect of modulation instability on the physical polymer structure

While the refractive index changes in traditional nonlinear media are non permanent and thus, reversible, the refractive index changes that arise due to photopolymerisation in the organosiloxane gel are permanent. This results in the optical fibres leaving a permanent physical imprint in the polymer, giving rise to a bundle of polymer filaments or cylindrical waveguides. These fibre waveguides are shown in the following set of micrographs:

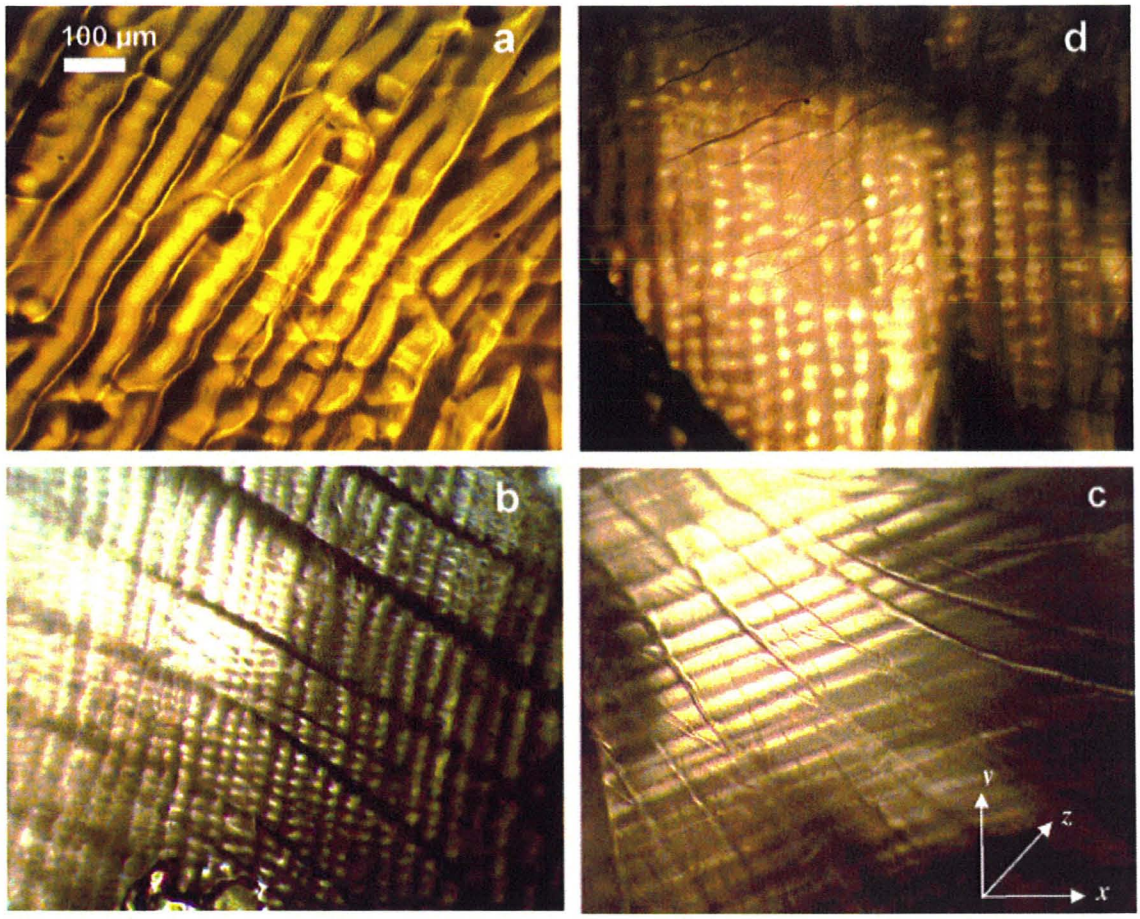

Figure 1.9 Optical micrographs revealing the permanent physical structure imposed in the organosiloxane as a result of the nonlinear process, modulation instability.[22] Reprinted with permission from Burgess, I. B.; Shimmell, W. E.; Saravanamuttu, K. *J. Am. Chem. Soc.* **2007**, *129*, 4738. Copyright 2007 American Chemical Society.

Figure 1.9a exemplifies the permanent polymer microstructure (at a plane orthogonal to the direction of light propagation) that remains in the material after the sample has been exposed to the light field only for enough time to undergo the first transition, where it divides into a series of stripes. The second transition, from stripes to spots, is documented in **Figure 1.9b and c**, which again, show transverse cross-sections of the sample. **Figure 1.9d**, shows the longitudinal cross-section of the same sample, in which the propagation of the cylindrical waveguides traversing the sample are clearly visible.

The consequence of this is that this process is able to permanently affect the structure of the polymer. In this way, modulation instability in a photochemical medium can be employed as a method of using light to trigger the spontaneous organization of polymer structures, as well as to potentially control the physiology of the polymer structure itself.

1.5 Theoretical relationship between spatial coherence length and filament diameter

1.5.1 Modulation instability as a method of controlling polymer microstructure

Modulation instability of broad beams of light represents a method to spontaneously achieve long-range 3-D microstructure in polymers. The experiments with white light yielded a characteristic filament diameter of 75 μm. By exploiting a previously made theoretical relationship between the filament diameter and spatial incoherence of the optical field, this research aims to achieve tenability in the resulting polymer microstructure.

It has been predicted that the spatial coherence length of the light field plays a pivotal role in determining the filament diameter of the self-trapped beams that arise from modulation instability experiments. Mathematically, it has been shown that the perturbation frequency (which is inversely proportional to the filament diameter) has a dependence on the degree of spatial incoherence inherent to the incident electromagnetic field:[40]

$$\frac{g(\alpha)}{k} = -(k_{x0}/k)(|\alpha|/k) + (|\alpha|/k)\sqrt{\frac{\kappa I_0}{n_0} - \left(\frac{\alpha}{2k}\right)^2} \qquad [1\text{-}4]$$

where, g(α) is the growth rate of modulation instability. The term k_{x0}/k is equal to the variable θ_0, which represents the degree of spatial incoherence of the light field, which is related to the coherence length, l_c through:[44]

$$\theta_0 = \frac{\sqrt{2\pi}}{kl_c} \qquad [1\text{-}5]$$

As the beam becomes increasingly coherent, the value of θ_0 approaches zero. That is to say, the greater the value of θ_0, the more incoherent the beam. Purely coherent laser light will have $\theta_0 = 0$. k is the wavevector ($k = k_0 n_e$, and $k_0 = \frac{2\pi}{\lambda_0}$, where n_e is the extraordinary refractive index, and λ_0 is the wavelength of the light). α is the spatial wavevector, or perturbation frequency and is related to the filament diameter (FD) as follows:

$$\alpha = \frac{2\pi}{FD} \qquad [1\text{-}6]$$

I_0 is the uniform background intensity, n_o is the linear refractive index of the material, and $\kappa = \frac{d(\delta n)}{dI}$ is the refractive index change evaluated at I_0.

As seen in the white light modulation instability studies, while there was no effect on filament diameter in changing the intensity of light, the intensity has an effect on the growth rate of modulation instability. This means that holding the intensity constant,

should ensure a constant growth rate. This allows the relationship between the filament diameter and the spatial incoherence of the optical field to be probed.

1.5.2 Research objective

This research will examine modulation instability of a continuous wave laser beam with different degrees of spatial incoherence propagating in the polymerisable organosiloxane. The technique used by Chen and coworkers will be employed to control the degree of spatial incoherence across the beam.[40] Here, the beam will be passed through a diffuser (a thin transparent film with a rough surface consisting of random inhomogeneities), which scatters light, and thus introduces small speckles across the beam. The coherence length, l_c, relates to the distance in which two points on a wave are phase correlated with any other wave in the beam. This corresponds to the average diameter of the speckles, since the light in each individual speckle is purely coherent, but the speckle size imposes a maximum length for which spatial coherence is possible. The diffuser is set into rotation in order for the medium to experience the time-averaged distribution of the beam. The rotation needs to occur more rapidly than the response time of the medium in order for the medium to react to the time-averaged beam, and not the random phase fluctuation of the individual coherent speckles.[37]

The degree of spatial incoherence can be varied by changing the distance between the diffuser and the nonlinear medium. The larger the speckles appear when the diffuser it at rest, the more coherent the beam (resulting in a higher l_c or lower θ_0).

In this way, the spatial coherence length can be tuned, and the effect on filament diameter associated with the self-trapped beams that the light produces within the photoresponsive organosilixane medium, can be elucidated.

References

1 G. Stegeman, M. Segev, *Science*, **1999**, 286, 1518-1523

2 Trillo, S., Torruellas, W. (2001). *Spatial Solitons*. New York: Spinger.

3 Segev, M.; Stegeman, G. I. *Phys. Today* **1998,** *51*, 42-48.

4 Bathelemy, A.; Maneuf, S.; Froehly, C. *Opt. Commun.* **1985**, *55*, 201-206.

5 Maneuf, S.; Desailly, R.; Froehly, C. *Opt. Commun.* **1988**, *65*, 193-198.

6 Aitchison, J.S.; Weiner, A.M.; Silberberg, Y.; Oliver, M.K.; Jackel, J.L.; Leaird, D.E.; Vogel, E.M.; Smith, P.W.E. *Opt. Lett.* **1990**, *15*, 471-473.

7 Aitchison, J.S.; Al-Hemiary, K.; Ironside, C.N.; Grant, R.S.; Sibbet, W. *Electron. Lett.* **1992**, *28*, 1879-1880.

8 Bartuch, U.; Peschel, U.; Gabler, Th.; Waldhaus, R.; Horhold, H.-H. *Opt. Commun.* **1997**, *134*, 49-54.

9 Bjorkholm, J.E.; Ashkin, A. *Phys. Rev. Lett.* **1974**, *32*, 129-132

10 Christodoulides, D. N.; Coskun, T. H.; Joseph, R. I. *Opt. Lett.* **1997**, *22*, 1080-1082.

11 Mitchell, M.; Segev, M.; Coskun, T. H.; Christodoulides, D. N. *Phys. Rev. Lett.* **1997**, *79*, 4990- 4993.

12 Snyder, A.W.; Mitchell, D. J. *Phys. Rev. Lett.* **1998**, *80*, 1422-1424.

13 Christodoulides, D. N.; Coskun, T. H.; Mitchell, M.; Chen, Z.; Segev, M. *Phys. Rev. Lett.* **1998**, *80*, 5113- 5116.

14 Born, M. & Wolf, E. (1999). *Principles of Optics*. London: Cambridge University Press.

15 Mitchell, M. and Segev, M. *Nature* **1997,** *387,* 880-883.

16 Buljan, H.; Šiber, A.; Soljačić, M.; Segev, M.; *Phys. Rev. E* **66**, **2002**, 035601-1 to 035601-4 2002.

17 Pedrotti, S.J, Frank L. & Pedrotti, Leno S. (1993). *Introduction to Optics* (2nd ed.). New Jersey: Prentice Hall.

18 Peřina, Jan. (1971). *Coherence of Light*. New York: Van Nostrand Reinhold Co.

19 Siegman, A. E., *Lasers*, University Science Books, CA, USA (1996) p.50.

20 Kasala, K; Saravanamuttu, K. *Appl. Phys. Lett.* **2008**, *93*, 051111-051113

21 Zhang, J and Saravanamuttu, K. *J. Am.Chem.Soc. (Article)* **2006,** *128*, 14913.

22 Burgess, I. B.; Shimmell, W. E.; Saravanamuttu, K. *J. Am. Chem. Soc.* **2007**, *129*, 4738.

23 Shoji, S., Kawata, S., Sukhorukov, A.A., Kivshar, Y.S., *Opt. Lett.* **2002**, *27*, 185.

24 Shoji, S., Kawata, S. *Appl. Phys. Lett.* **1999**, *75*, 737.

25 Kewitsch, A.; Yariv, A. *Opt. Lett.* **1996**, *21*, 24-26.

26 Kewitsch, A.,Yariv, A. *Appl. Phys. Lett.* **1996**, *68*, 455-457.

27 Lannan, J. & Saravanamuttu, K. Unpublished results. **2006.**

28 Zhang, J, Kasala, K, Rewari, A and Saravanamuttu, K. *J. Am.Chem.Soc. (Communication)* **2006,** *128*, 406.

29 Iturbe-Castillo, M. D.; Torres-Cisneros, M.; Sánchez-Mondragón, J. J.; Chávez-Cerda, S.; Stepanov, S. I.; Vysloukh, V. A.; Torres-Cisneros, G. E.; *Opt. Lett.* **1995**, *20*, 1853-1855.

30 Peccianti, M.; Conti, C.; Assanto, G.; De Luca, A.; Umeton, C.; *Nature* (London) **2004**, *432*, 733-737.

31 Mamaev, A. V.; Saffman, M.; Anderson, D. Z.; Zozulya, A. A.; *Phys. Rev. A* **1996**, *54*, 870-879.

32 Centurion, M.; Pu, Y.; Psaltis, D.; *Opt. Exp.* **2005,** *13*, 6202-6211.

33 Saffman, M.; McCarthy, G.; Królikowski, W.; *J. Opt. B: Quantum Semiclass. Opt.* **2004**, *6*, S397–S403.

34 Shih, M-F.; Jeng, C-C.; Sheu, F-W.; Lin, C-Y.; *Phys. Rev. Lett.* **2002**, *88*, 133902-1 to 133902-4.

35 Meier, J.; Stegeman, G. I.; Christodoulides, D. N.; Silberberg, Y.; Morandotti, R.; Yang, H.; Salamo, G.; Sorel, M.; Aitchison, J. S.; *Phys. Rev. Lett.* **2004**, *92*, 163902-1 to 163902-4.

36 Streppel, U.; Michaelis, D.; Kowarschik, R.; Bräuer, A.; Phys. Rev. Lett. 2005, 95, 073901-1-073901-4.

37 Kip, D., Soljacic, M., Segev, M., Eugenieva, E., & Christodoulides, D. N. *Science* **2000** 290 495-498

38 Klinger, J.; Martin, H.; Zhigang, C.; *Opt. Lett.* **2001**, *26*, 271-273.

39 Kip, D.; Soljačic, M.; Segev, M.; Sears, S. M.; Christodoulides, D. N.; *J. Opt. Soc. Am. B* **2002**, *19*, 502-512.

40 Chen, Z.; Klinger, J.; Christodoulides, D. N. *Physical Review E.* **2002**, *66*, 066601-1.

41 Chen, Z.; McCarthy, K.; *Opt. Lett.* **2002**, *27*, 2019-2021.

42 Soljacic, M.; Segev, M.; Coskun, T.; Christodoulides, D.N.; Vishwanath, A.; *Phys. Rev. Lett.* **2000**, *84*, 467-470.

43 Sears, S. M.; Soljačić, M.; Christodoulides, D. N.; Mordechai, S.; *Phys. Rev. E* **2002**, *65*, 036620-1 to 036620-9.

44 Coskun, T. H., Christodoulides, D. N., Mitchell, M., Chen, Z., and Segev, M. *Optics Letters* **1998**, *23*, 418-420.

45 Degirmenci, M., Onen, A., Yagci, Y., and Pappas, S. P. *Polymer Bulletin* **2001**, *46*, 443-449.

46 Buck, John A. (2004). *Fundamentals of Optical Fibers* (2nd ed.). New Jersey: Wiley-Interscience.

47 Snyder, Allan W. & Love, John D. (1983). *Optical Waveguide Theory*. New York: Chapman and Hall.

48 Okamoto, Katsunari. (2006). *Fundamentals of Optical Waveguides*. New York: Elsevier.

49 **refractive index**. (2009). In *Encyclopædia Britannica*. Retrieved July 15, 2009, from Encyclopædia Britannica Online: http://www.britannica.com/EBchecked/topic/495677/refractive-index

50 Serway, Raymond & Faughn, Jerry S. (2003). *College Physics* (6th ed.). Pacific Grove, CA: Brooks/Cole-Thomson Learning.

51 Stratton, J. A. (1941). *Electromagnetic Theory*. New York: McGraw-Hill.

2. Experimental

2.1 Generating broad laser beams with tunable spatial coherence

2.1.1 Building the rotating diffuser

A diffuser was made by etching a transparent polystyrene petri dish (diameter = 90 mm) with fine-grit aluminium oxide sandpaper, with an average particle size of 92 μm, until the surface of the petri dish was matte (**Figure 2.1 b**). A small hole was made in the centre of the petri dish using a small nail heated with a plasma torch. The diffuser was then mounted on the spindle of the rotating motor (Jameco, motor, DC, 6-18V, 9820RPM, 0.7A), which was attached to a battery pack powered by four double-A batteries (Duracell® ProCell Alkaline battery, PC1500, 1.5V) (**Figure 2.1a**).

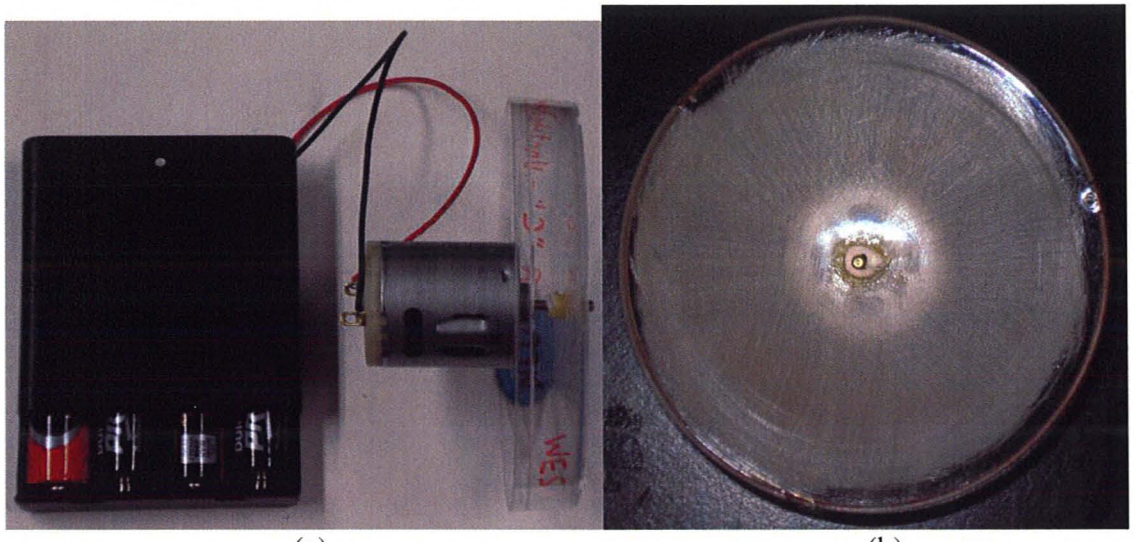

(a) (b)

Figure 2.1 (a) Image of rotating diffuser, (l-r): Battery power source, rotating motor, and diffuser; and (b) a surface view of the diffuser itself, showing etching and the absence of lustre

2.1.2 Determining the spatial coherence of a continuous wave 488 nm laser beam

In order to characterize the spatial coherence lengths accessible with the diffuser, an optical assembly was constructed to acquire the intensity profiles of the resulting speckles as they appeared through the diffuser at varying propagation distances, d. For the first wavelength studied – 488 nm – the optical assembly was as follows:

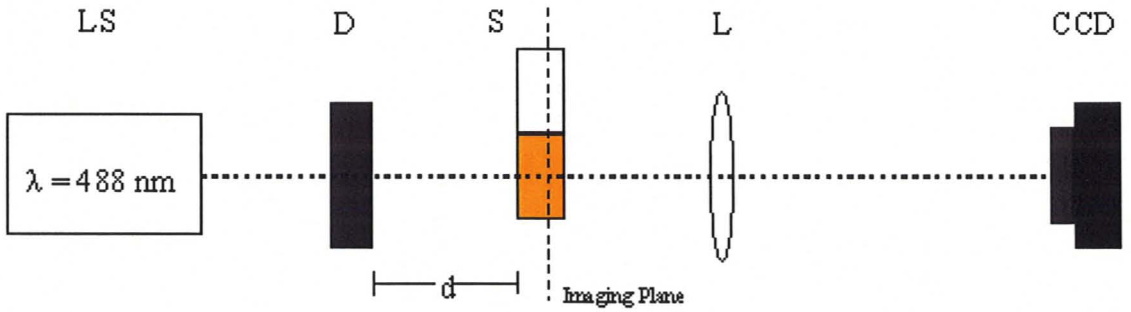

Figure 2.2 General optical assembly used to obtain intensity profiles of modulation instability experiments at a wavelength of 488 nm.

488 nm light from an optically pumped semiconductor laser (Coherent, Sapphire^{TM} 488-20, λ = 488 nm ± 2 nm, output power: 20 mW, beam waist diameter: 0.65 mm – 0.75 mm, Gaussian profile) was passed through the stationary diffuser (D). The beam was then imaged at propagation distances (in air) ranging from 5 mm to 100 mm by a charge-coupled device (CCD) camera. The CCD is driven by the software Dataray® (Version 6.0), which acquires spatial intensity profiles of the beam and calculates parameters such as relative peak intensity and width. Spatial intensity profiles of the speckled beam at different propagation distances are presented in **Figure 2.3**. Each image was processed using SigmaPlot $^{®}$ (Systat Software, Inc.); the average speckle size

of at least a 100 randomly chosen speckles distributed uniformly across each image was then determined using ImageJ® (National Institutes of Health) (**Table 2.1).**

The average speckle diameter at a given propagation distance is the length over which there is strong correlation between the phase of the wavefront and thus represents the spatial coherence length (l_c) of the beam. l_c increases with propagation distance.

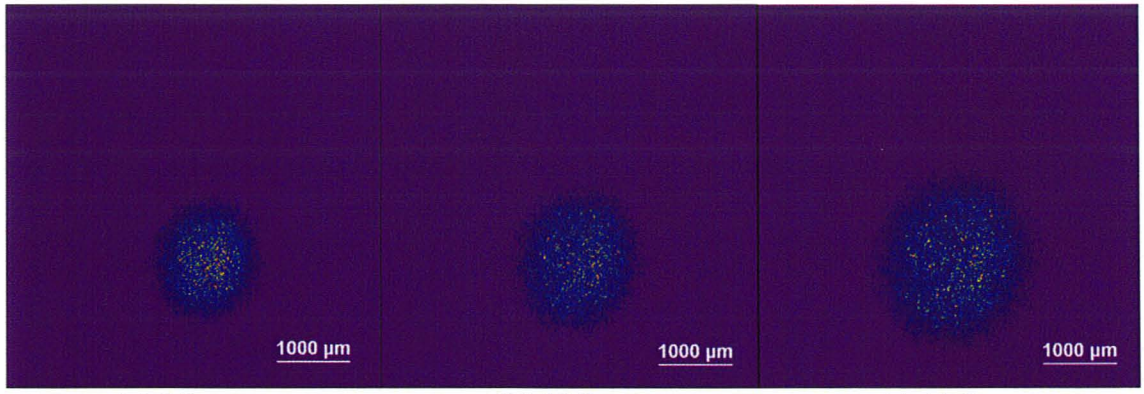

(a) 5.0 mm (b) 10.0 mm (c) 15.0 mm

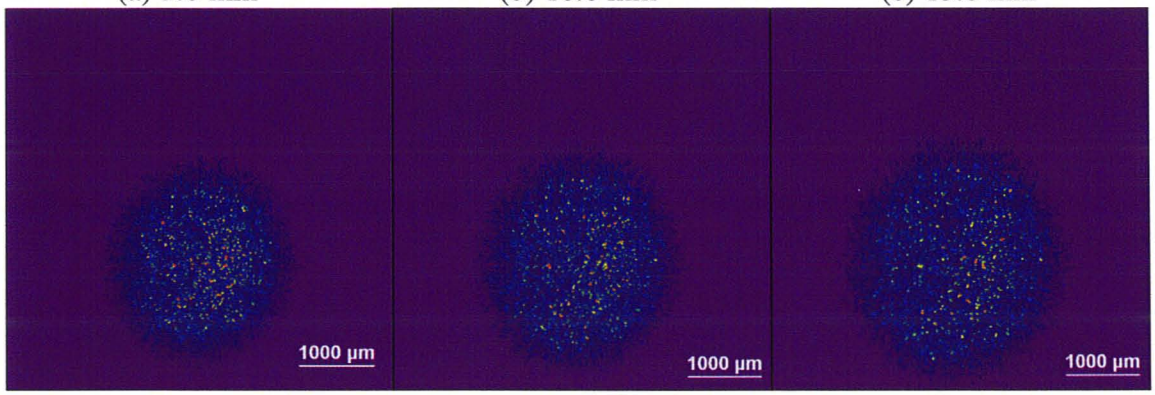

(d) 20.0 mm (e) 25.0 mm (f) 30.0 mm

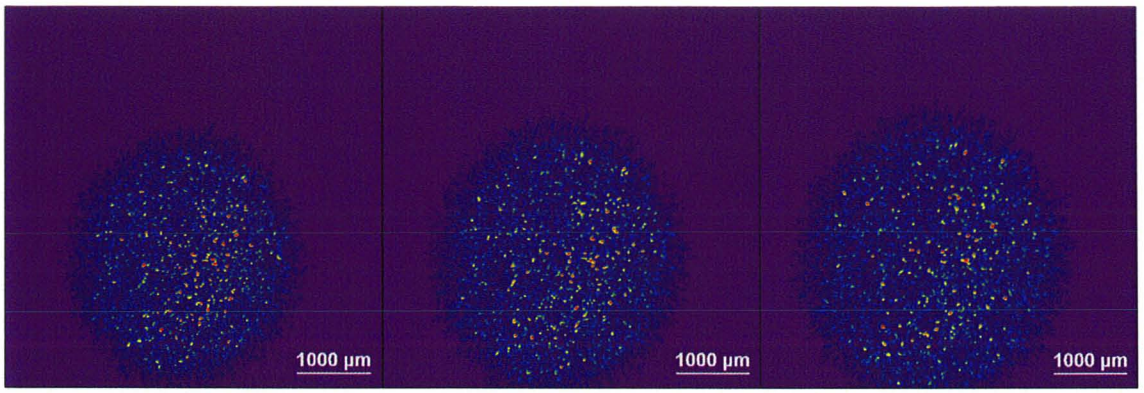

(g) 35.0 mm (h) 40.0 mm (i) 45.0 mm

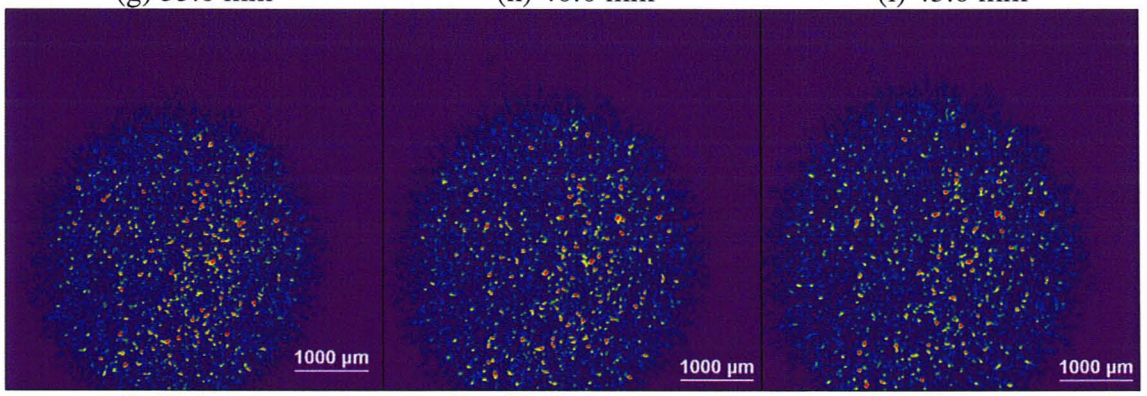

(j) 50.0 mm (k) 55.0 mm (l) 60.0 mm

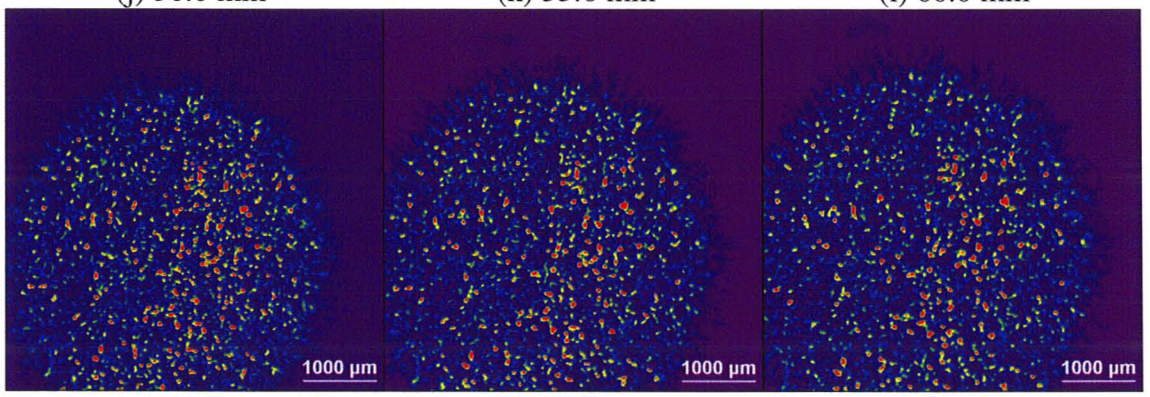

(m) 65.0 mm (n) 70.0 mm (o) 75.0 mm

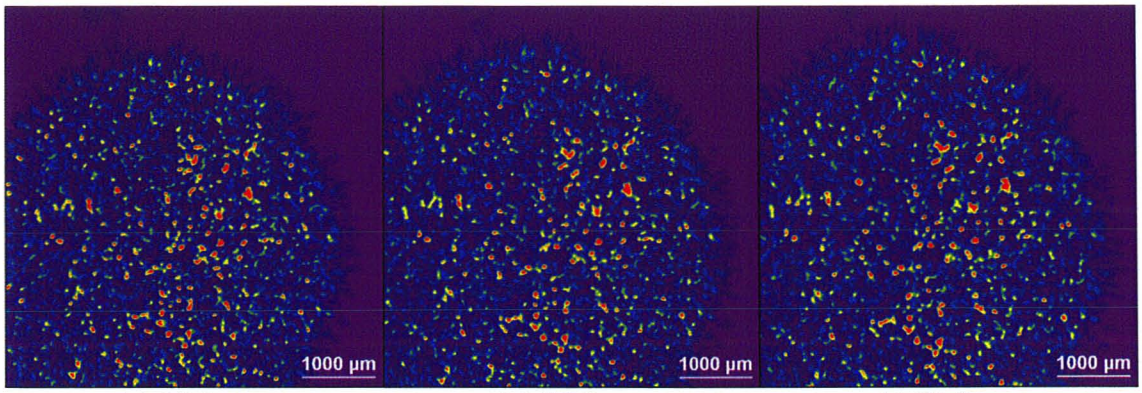

(p) 80.0 mm (q) 85.0 mm (r) 90.0 mm

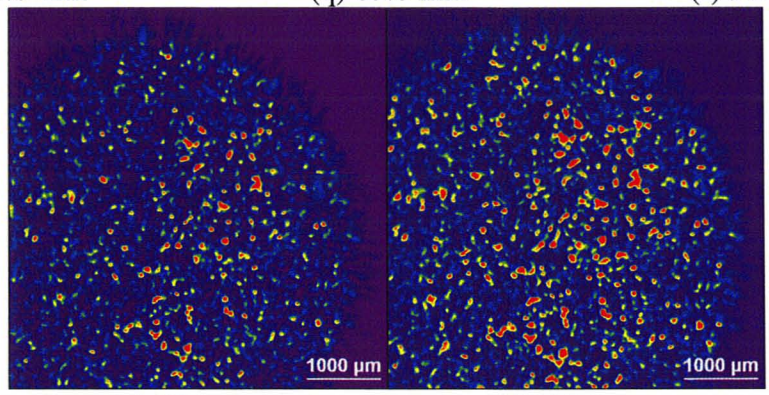

(s) 95.0 mm (t) 100.0 mm

Figure 2.3 2D intensity profiles of the 488 nm laser beam passed through the diffuser at increasing diffuser-cuvette separation distances, d. In each of these images, the blue colour represents regions of low intensity, the yellow and green, intermediate intensity, and the red regions the highest intensity.

Table 2.1 Spatial coherence length measurements for 488 nm wavelength

Diffuser-cuvette separation distance, d (mm)	Number of speckles measured	Average speckle diameter (spatial coherence length, μm)
5.0	100	11 ± 3
10.0	100	15 ± 5
15.0	100	20 ± 6
20.0	100	22 ± 6
25.0	100	27 ± 6
30.0	100	31 ± 6
35.0	100	34 ± 6
40.0	100	37 ± 8
45.0	100	42 ± 10
50.0	100	45 ± 9
55.0	100	49 ± 7
60.0	100	55 ± 8
65.0	100	59 ± 10
70.0	100	59 ± 10
75.0	100	67 ± 13
80.0	100	67 ± 10
85.0	100	71 ± 11
90.0	100	75 ± 9
95.0	100	80 ± 10
100.0	100	86 ± 12

2.1.3 Determining the spatial coherence of a continuous wave 532 nm laser beam

A procedure similar to the one described in the previous section was employed. A separate optical assembly was constructed for the 532 nm beam (**Figure 2.4**).

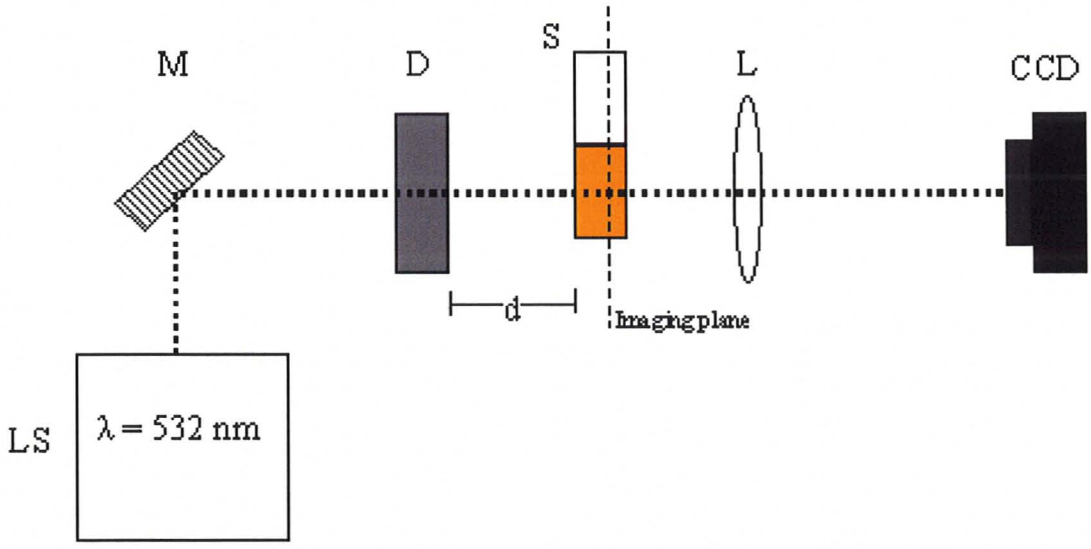

Figure 2.4 General optical assembly used to obtain intensity profiles of modulation instability experiments, when the wavelength is 532 nm.

Here, the light source (LS) was a 532 nm diode-pumped laser (Coherent, Verdi^{TM} V-2, λ = 532 nm, output power: 2 W, beam diameter: 2.25 mm, Gaussian profile). The laser beam was reflected by a mirror (Newport, Broadband SuperMirror, UV-grade fused silica, ion beam sputtered coating, diameter 25.4 mm, thickness 6.35mm, reflectivity 99.9 % at 0-45 deg, 485-700 nm), M, mounted on a precision gimbal optic mount (Newport, 605-2, θ_x and θ_y control) and passed through a diffuser (D). The spatial intensity profile of the beam at varying propagation distances was imaged through a biconvex lens (L), with a focal length of 1.9 cm onto the CCD camera. The lens was positioned to magnify the beam by 4-fold enabling better resolution of the speckles, which were smaller in size

at 532 nm relative to 488 nm. The position of the imaging lens with respect to the diffuser was determined by replacing the diffuser with a slit, which was then imaged onto the CCD. The lens was iteratively moved until the sharpest image with 4-fold magnification was obtained. Once the optical assembly was thus calibrated, the procedure outlined in **Section 2.1.2** for the 488 nm beam was employed to determine l_c of the 532 nm beam at varying propagation distances.

Spatial intensity profiles of the beam were obtained at propagation distances between 5.0 mm to 100.0 mm at 5.0 mm intervals and at 200.0 mm (**Figure 2.5).**

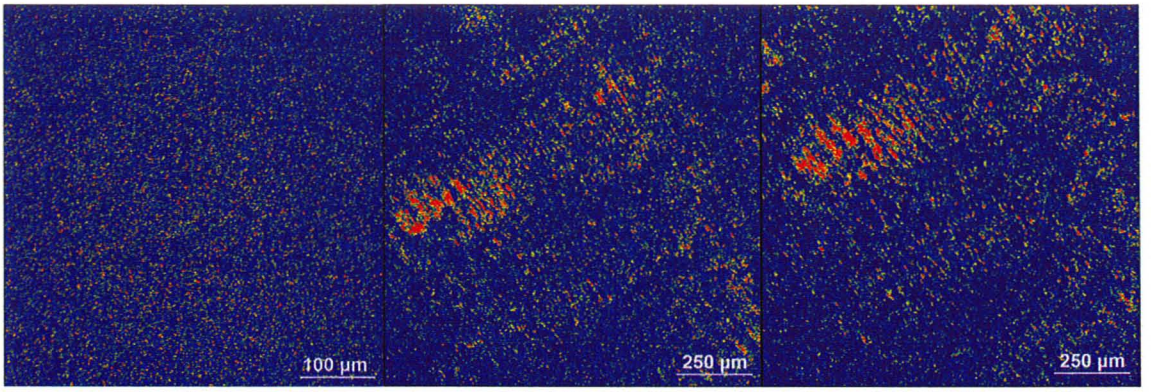

(a) 1.0 mm (b) 5.0 mm (c) 10.0 mm

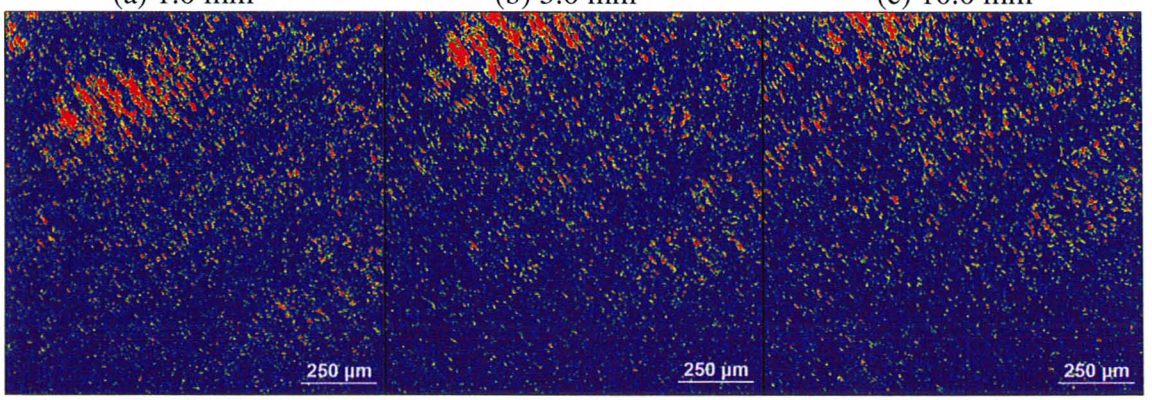

(d) 15.0 mm (e) 20.0 mm (f) 25.0 mm

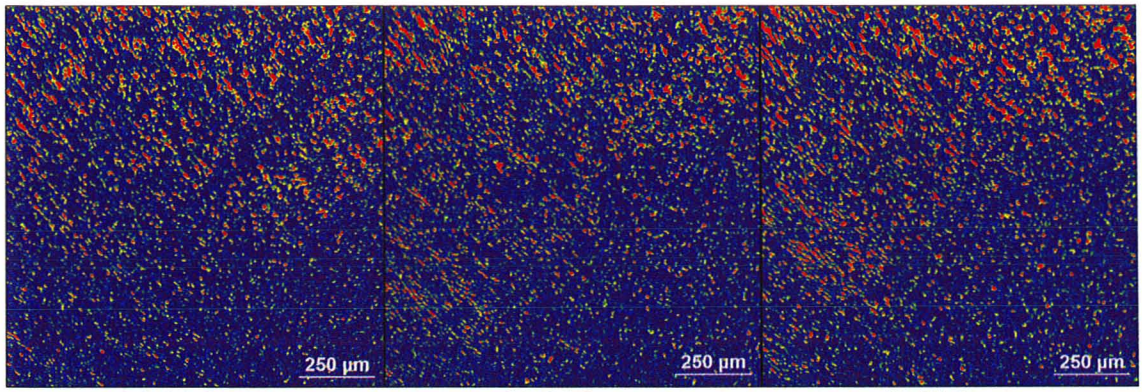

(g) 30.0 mm (h) 35.0 mm (i) 40.0 mm

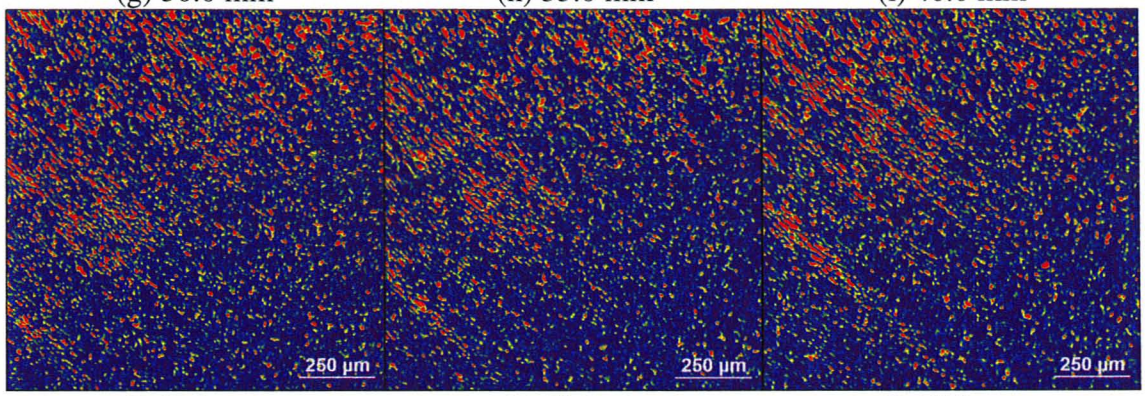

(j) 45.0 mm (k) 50.0 mm (l) 55.0 mm

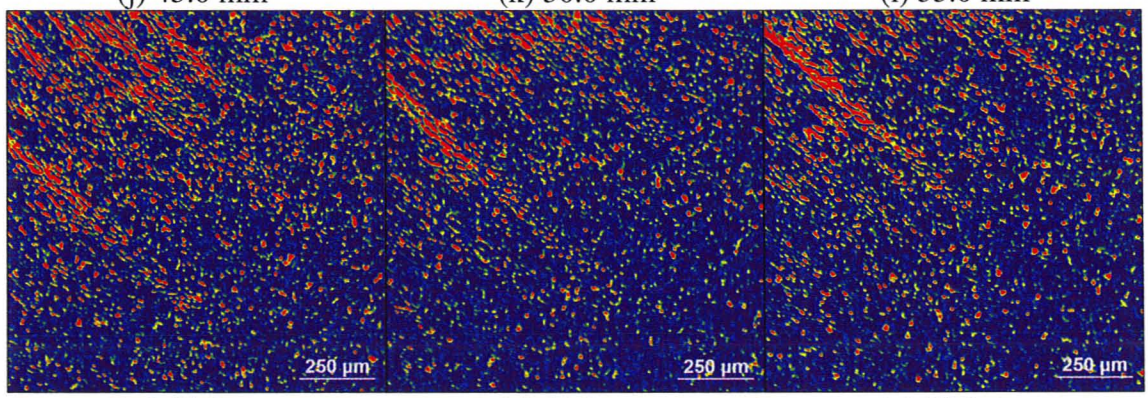

(m) 60.0 mm (n) 65.0 mm (o) 70.0 mm

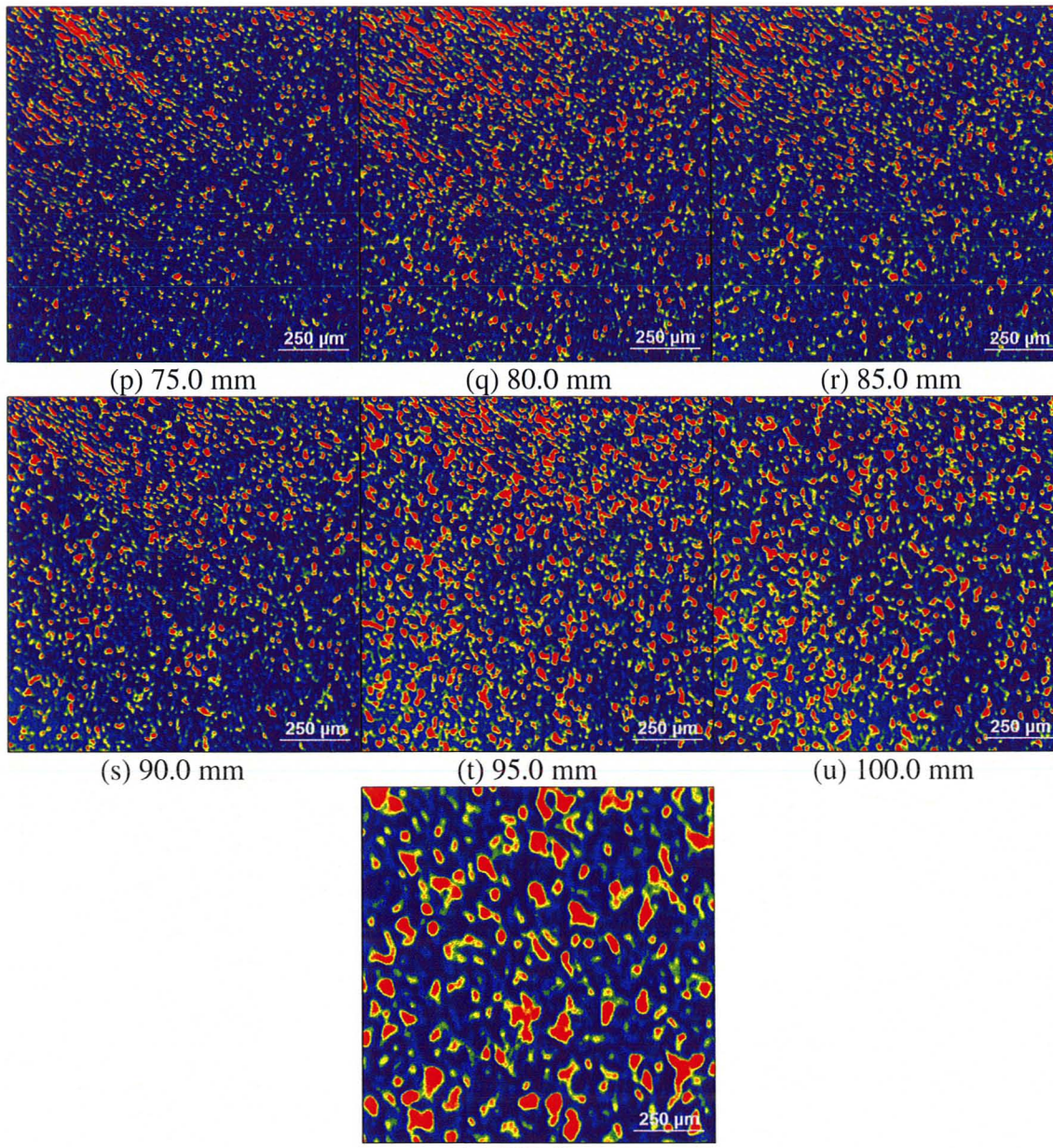

(p) 75.0 mm (q) 80.0 mm (r) 85.0 mm

(s) 90.0 mm (t) 95.0 mm (u) 100.0 mm

(v) 200.0 mm

Figure 2.5 2D intensity profiles of the 532 nm laser beam passed through the diffuser at increasing diffuser-cuvette separation distances, d.

Table 2.2 Spatial coherence length measurements for 532 nm wavelength

Diffuser-cuvette separation distance, d (mm)	Number of speckles measured	Average speckle diameter (spatial coherence length, μm)
1.0	100	1.3 ± 0.2
5.0	100	6 ± 1
10.0	100	7 ± 1
15.0	100	8 ± 1
20.0	100	9 ± 1
25.0	100	10 ± 1
30.0	100	11 ± 1
35.0	100	12 ± 1
40.0	100	13 ± 2
45.0	100	13 ± 2
50.0	100	14 ± 2
55.0	100	16 ± 2
60.0	100	16 ± 2
65.0	100	17 ± 2
70.0	100	18 ± 2
75.0	100	19 ± 2
80.0	100	20 ± 2
85.0	100	21 ± 3
90.0	100	23 ± 3
95.0	100	24 ± 3
100.0	100	25 ± 2
200.0	100	46 ± 5

2.1.4 Overcoming the physical minimum to access shorter coherence lengths

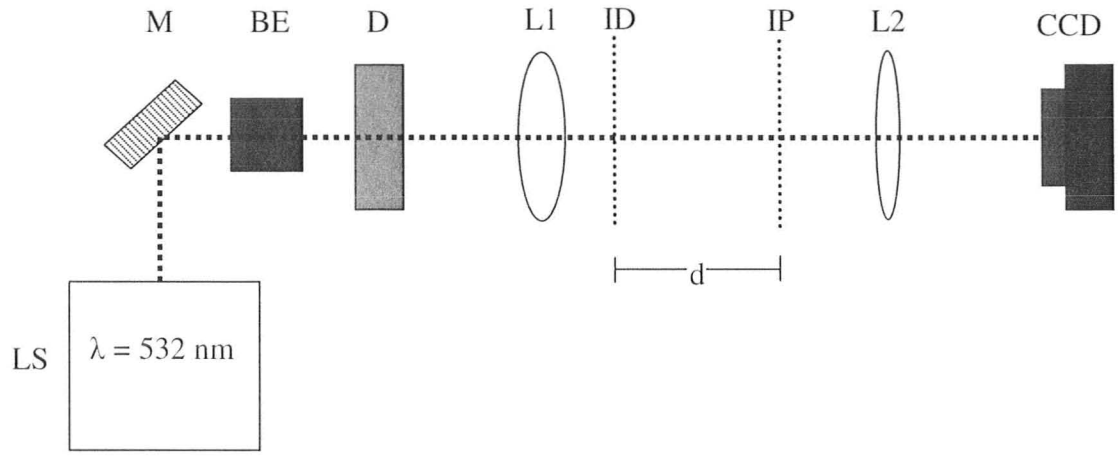

Figure 2.6 Optical assembly used to obtain intensity profiles of speckles that are smaller than the previous minimum.

From the optical assemblies (**Figures 2.2**, **2.4**), a minimum l_c of 11 μm and 6 μm were achieved at 488 nm and 532 nm, respectively. To achieve the shorter l_c value of 1.3 μm, a beam expander was used to expand the beam by 3-fold before it was passed through the diffuser. A biconvex lens with a focal length of 1.9 cm (L1) was then inserted after the diffuser in order to demagnify the speckled beam by 10 fold. Since the resulting speckles are small, the imaging lens was positioned so that it magnified the beam by 10-fold.

2.2 Preparation of photopolymerisable organosiloxane[19, 20, 28]

The photochemical medium used for self-trapping and modulation instability experiments was a methacrylate substituted organosiloxane, prepared by acid-catalysed hydrolysis of 3-(trimethoxysilyl) propyl methacrylate (MAPTMS). This was accomplished by the addition of 1.10 g of 0.05 M hydrochloric acid (5.5×10^{-5} mol) to 17.6 g MAPTMS (0.0708 mol). Initially this mixture exists in two phases, but as the hydrolysis progresses, over five to ten minutes, the mixture becomes homogeneous. (**Figure 2.1**) This produces the compound that is referred to as *blank sol*, which is a viscous, transparent, colourless liquid.

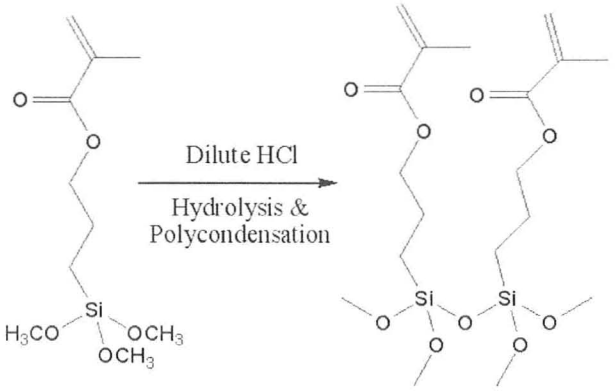

Figure 2.7 Acid-catalysed hydrolysis and condensation of methacryloxypropyltrimethoxy silane

In order to make the mixture sensitive to light in the visible region, and thus make photopolymerisation possible, a titanocene-based free-radical photoinitiator – (bis(η^5cyclopentandienyl) bis(2,6-difluoro-3-(1H-pyrrol-yl)-phenyl) titanium(IV) (Ciba Specialty Chemicals Inc) – was added to the blank sol in proportions of 1.0% by weight.

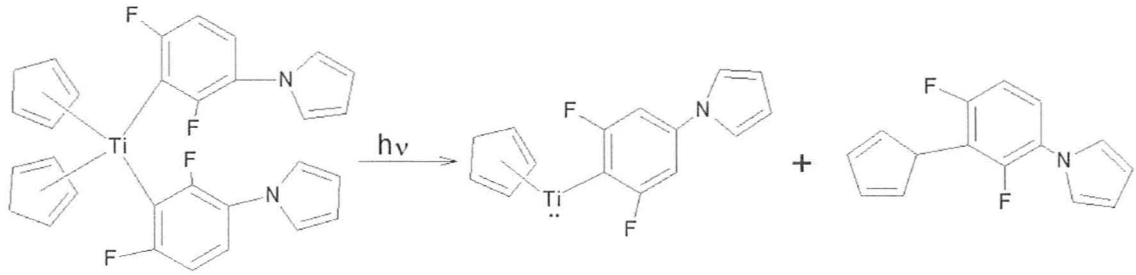

Figure 2.8 Titanocene photoinitiator splitting apart in the presence of light to form titanium-based diradicals.[45]

The sol was shielded from ambient light and stirred for 18-24 hours. Prior to use, the sol, a viscous, transparent, orange-coloured liquid, was filtered through a polytetrafluoroethylene (PTFE) filter with a pore size of 0.2 μm.

2.3 Modulation instability with coherent light

2.3.1 Modulation instability at 488 nm with $l_c = \infty$

Experiments of modulation instability of a broad 488 nm beam were carried out with the optical assembly presented in **Figure 2.2**. The beam was passed through a 3X expander to a width of 2.25 mm and launched directly into a transparent cuvette (S) containing the organosiloxane. At the entrance face of the cuvette, the beam had an intensity between 2.82 mW to 2.86 mW. In this experiment, the diffuser was removed from the assembly so that the spatial coherence of the beam incident on the sample was effectively infinite. The spatial intensity profile of the medium at a propagation distance of 6.0 mm within the medium was focussed onto the CCD and monitored over time.

2.3.2 Modulation Instability at 532 nm with $l_c = \infty$

The method described in **Section 2.3.1** was employed at this wavelength. The beam expander was not needed as the diameter of the beam emitted from the Verdi laser was sufficiently wide (diameter = 2.25 mm). The optical assembly in **Figure 2.4** was employed with the diffuser, D, removed.

2.4 Modulation instability with varying l_c

2.4.1 Modulation instability of partially spatially incoherent 488 nm light with varying l_c

Modulation instability in the organosiloxane was examined at $l_c = 11 \pm 2$ μm, 15 ± 3 μm, 27 ± 6 μm, 34 ± 6 μm, 45 ± 9 μm, and 86 ± 12 μm. For these experiments, the diffuser was reinserted into the optical assembly (**Figure 2.2**), and set to rotate at approximately 3000 RPM. The distance between the diffuser and cuvette containing the organosiloxane was adjusted so that the beam incident on the entrance face of the sample had the appropriate l_c (**Table 2.1**). At the entrance face of the cuvette, the beam had an intensity between 2.82 mW and 2.86 mW. The spatial intensity profile of the medium at a propagation distance of 6.0 mm within the medium was focussed onto the CCD and monitored over time. At least three experiments were carried out at each l_c.

2.4.2 Modulation instability of partially spatially incoherent 532 nm light with varying l_c

Modulation instability in the organosiloxane was examined at $l_c = 1.3 \pm 0.2$ μm, 6 ± 1 μm, 11 ± 1 μm, 15 ± 2 μm, 25 ± 2 μm, and 46 ± 5 μm. The spatial intensity profile of the medium at a propagation distance of 6.0 mm within the medium was focussed onto the CCD and monitored over time. At least three experiments were carried out at each l_c.

2.5 Control experiments

Two experiments were carried out at $l_c = 27 \pm 6$ μm and 45 ± 9 μm, where the diffuser was kept stationary. For these experiments, the optical assembly presented in **Figure 2.2** was modified so that the spatial intensity profile of the beam was imaged with 1:1 magnification through a pair of plano-convex lenses with focal lengths of 25.0 cm.

2.6 Data analysis

The CCD camera is driven by the software DataRay (version 6.0), which acquires 1D, 2D, and 3D spatial intensity profiles of the beam and calculates parameters such as relative peak intensity and width. For the experiments outlined in **Sections 2.3-2.5**, beam profiles were acquired at a rate of one image every 6 s. Typical experiments were run for two hours until the beam had transformed into multiple self-trapped filaments, which were stable over time. For quantitative analysis of the distribution and widths of filaments, the spatial intensity profile of the beam was processed using SigmaPlot®; 100 randomly chosen filaments were then selected and measured using ImageJ®.

3. Results and Discussion

The objective of this study is to show experimentally that modulation instability has a dependence on both spatial coherence length as well as the wavelength of the light used to induce nonlinearity in a photopolymerisable medium. Recall the equation given in the Introduction (**Section 1.5.1**):[40]

$$\frac{g(\alpha)}{k} = -(k_{x0}/k)(|\alpha|/k) + (|\alpha|/k)\sqrt{\frac{\kappa I_0}{n_0} - \left(\frac{\alpha}{2k}\right)^2} \qquad [1\text{-}4]$$

In this equation, k_{x0}/k is equal to the degree of spatial incoherence, [1-5] $\theta_0 = \frac{\sqrt{2\pi}}{kl_c}$, and the filament frequency is calculated by [1-6] $\alpha = \frac{2\pi}{FD}$. [44]

Equation [1-4] can be rearranged to describe the filament frequency, α as a function of the degree of spatial incoherence, θ_0, as follows.

$$\alpha = -\frac{k\sqrt{n_0}\theta_0}{\sqrt{\Delta n}} + \frac{\sqrt{2k\sqrt{n_0}\sqrt{\Delta n} + k^2 n_0 \theta_0^2}}{\sqrt{\Delta n}} \qquad [3\text{-}1]$$

This equation implies a relationship between the spatial coherence length (or degree of spatial incoherence) and the resulting diameter of the self-trapped filaments that exist as a consequence of modulation instability. Specifically, this equation describes a decrease in filament diameter as the incident beam becomes increasingly coherent. There is also a wavelength dependence inherent in this equation. In order to determine this experimentally, a series of modulation instability experiments was designed, varying,

first, the spatial coherence length of the light source, and subsequently, the wavelength. In doing this, it is possible to arrive at an experimental relationship between the three parameters: spatial coherence length, wavelength, and self-trapped filament diameter.

3.1 Modulation instability due to polymerisation at 488 nm

The first type of experiment performed at the 488 nm wavelength, was without the diffuser present, that is, observing the modulation instability of the purely coherent laser beam, $l_c = \infty$, expanded to a width which allows modulation instability rather then single beam self-trapping.

All four of the trials done for this set of experiments showed similar results, and resemble closely the previous findings displayed in incoherent white light experiments. The progression of a representative experiment is shown in **Figure 3.1**.

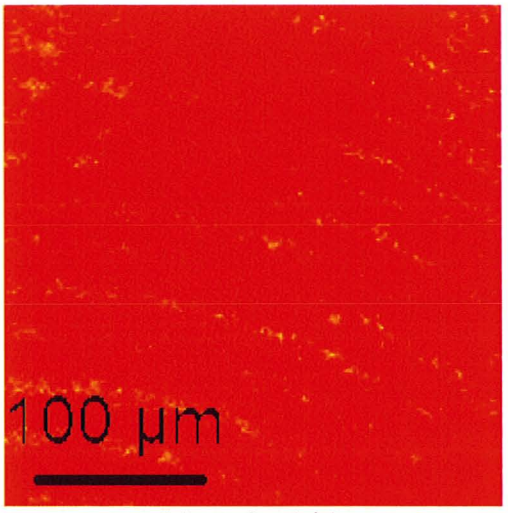

(a) t = 0 s (air)

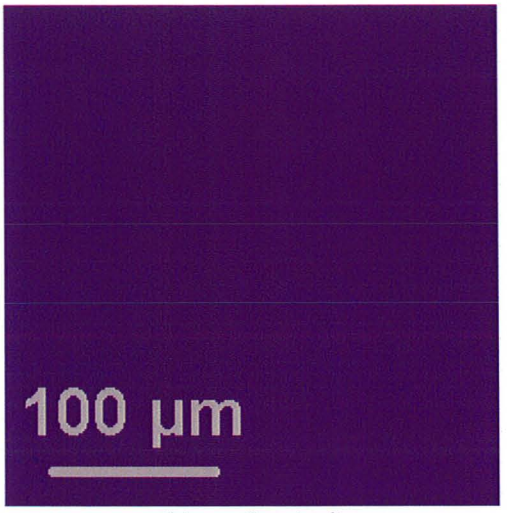

(b) t = 0 s (sol)

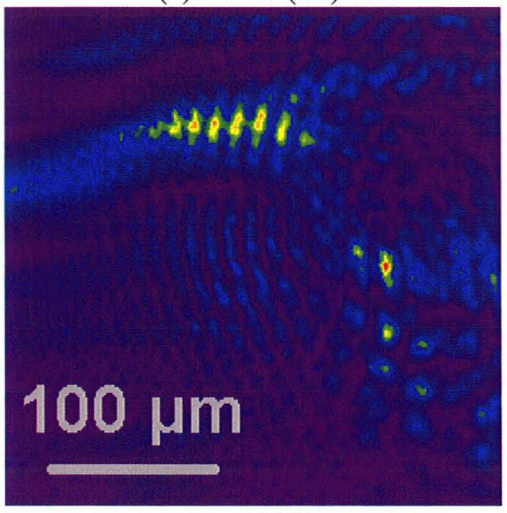

(c) t = 2952 s

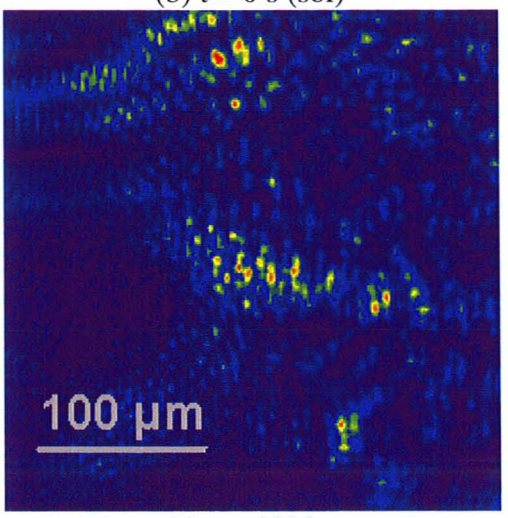

(d) t = 3090 s

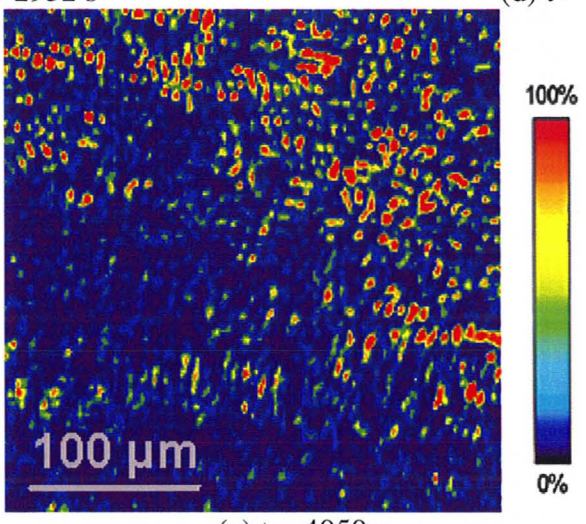

(e) t = 4050 s

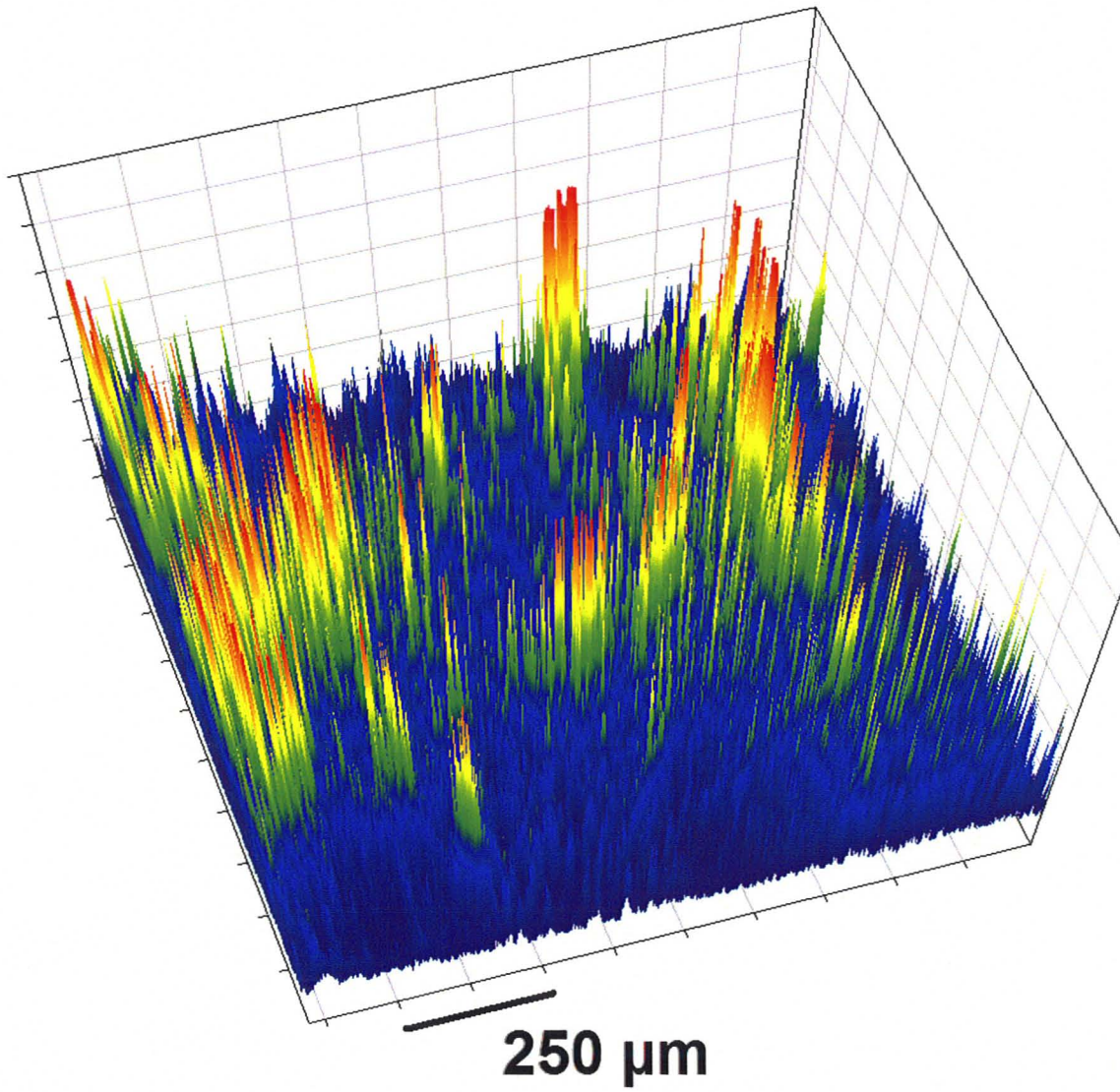

(f) t = 4050 s

Figure 3.1 2D and 3D intensity profiles showing the progression of a coherent light modulation instability experiment. (a) shows the beam under linear conditions (that is, in air), (b) at the start of the experiment, time, t = 0 s, (c) t = 2952 s, (d) t = 3090 s, and (e) t = 4050s, 2D, (f) 3D.

Initially, the beam is not visible at the exit face, which is due to the laser emitting light at a wavelength that is significantly close to the absorption maxima of the photoinitiator used in the nonlinear medium (**Figure 3.1b**). After activating enough photoinitiator, the light beam is able to transmit through the nonlinear medium (**Figure**

3.1c), where it appears in areas that were illuminated with slightly higher intensities than their surroundings, as a result of convection in the sol. These areas of elevated intensity in the sample polymerise and the refractive index increases, leading to increased disparity between high and low intensity regions (**Figure 3.1d**). Further increase in refractive index due to polymerisation counteracts the natural diffraction of the beam, and causes further division of the beam into spots, as seen in **Figure 3.1e**. Each of these spots represents a self-trapped beam which propagates as a waveguide through the sample. During this, the intensity is increasing dramatically. At the commencement of the experiment, the relative peak percentage is 6.5 %. Over time, the peak percent reaches 100 % (at t = 4050 s), which is greater than the relative peak percent of the beam in air (48.2 %). After reaching a maximum, the intensity gradually decreases through until the end of the experiment (total time, 3 hours 20 minutes). This decrease corresponds to the point where the self-trapped filaments pass beyond the imaging plane of the cuvette (6 mm from the front face of the cuvette).

Similar findings were discovered for each of the four trials done using a broad beam of coherent 488 nm wavelength laser light. Significant images, which clearly display the modulation instability phenomenon were selected for each of these experiments. These images can be found in **Appendix B**. Spots were measured for each of the repeat experiments and the results are shown in **Table 3.1**.

Table 3.1 Summary of results for the 488 nm wavelength experiments with an infinite spatial coherence length

Trial	1	2	3	4
Time elapsed (s)	4050	4800	7200	6000
Age of sol (days)	7	2	1	43
Cuvette material*	Plastic	Glass	Glass	Plastic
# of spots measured	100	100	100	100
Average spot diameter (μm)	7 ± 1	6.7 ± 0.9	6.7 ± 0.9	7 ± 1

*Note: Experiments performed in plastic tend to exhibit greater ordering of the self-trapped filaments, due to noise imposed by striations present on the faces of the plastic cuvettes.

When the diffuser is present, the incident light can now be said to be partially spatially incoherent, with a spatial coherence length that is equivalent to the average speckle size seen when the diffuser is at rest. The modulation instability experiments done with this partially spatially incoherent light were done using spatial coherence lengths of 11 ± 2 μm, 15 ± 3 μm, 27 ± 6 μm, 34 ± 6 μm, 45 ± 9 μm, and 86 ± 12 μm. The diffuser was rotated at approximately 3000 RPM; because the response time of the medium is on order of ms to s, it sees only the *time-averaged* version of the optical field. Three or four experiments were done at each coherence length, and a sample experiment demonstrating the temporal evolution of the beam under nonlinear conditions is shown for each coherence length, in the following set of figures. These figures are interspersed with data tables which summarise the results from all of the experiments done at a given coherence length. Intensity profiles corresponding to the repeat experiments can be found in **Appendix B**.

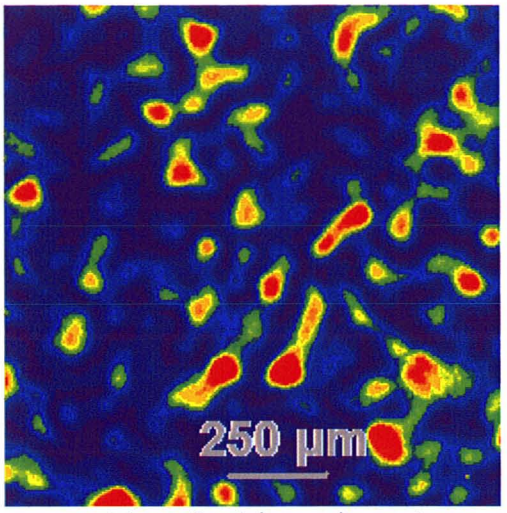

(a) t = 0 s (air, stationary)

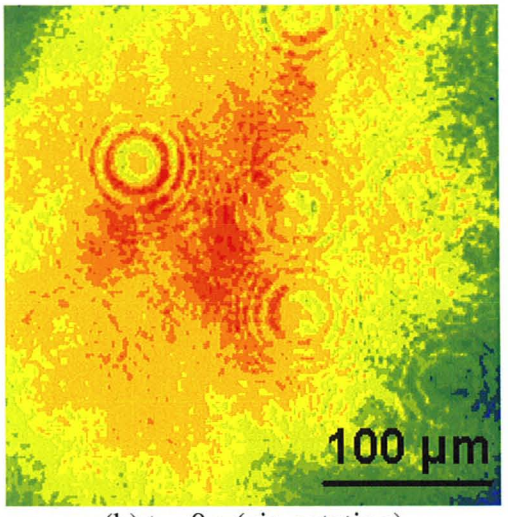

(b) t = 0 s (air, rotating)

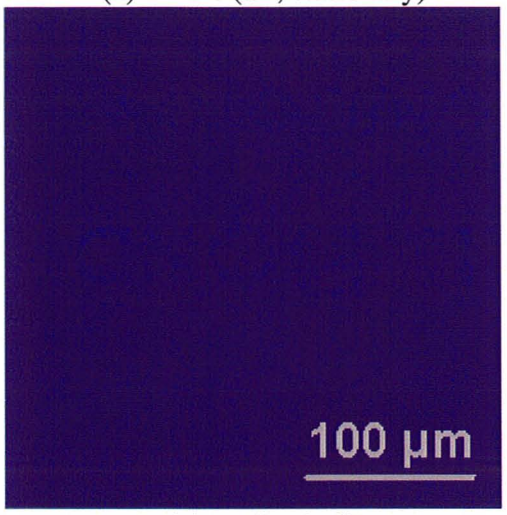

(c) t = 0 s (sol)

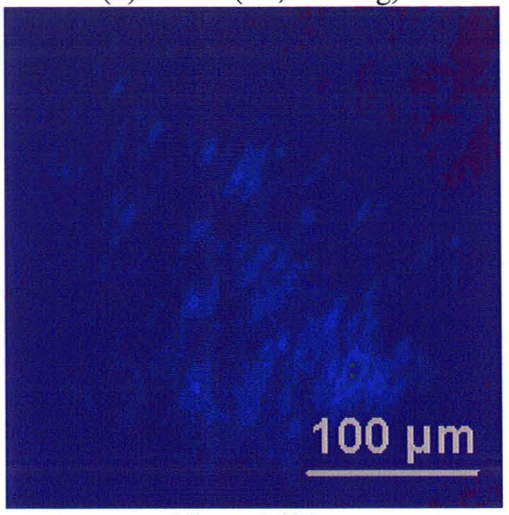

(d) t = 1692 s

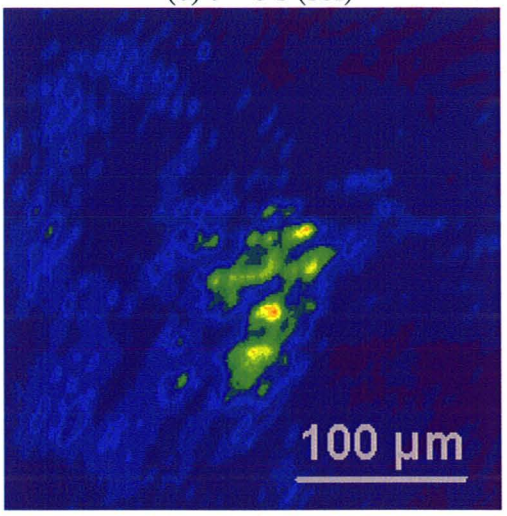

(e) t = 1788 s

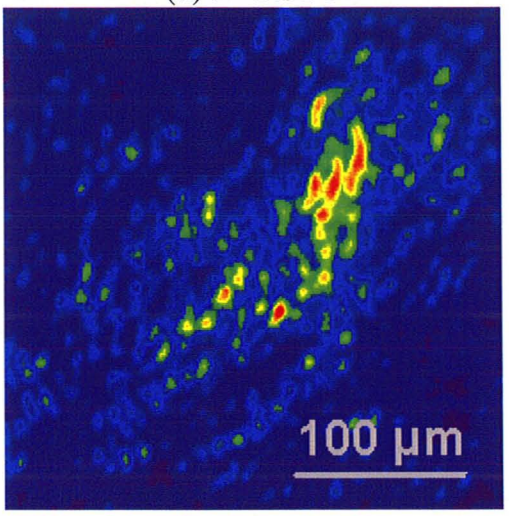

(f) t = 1842 s

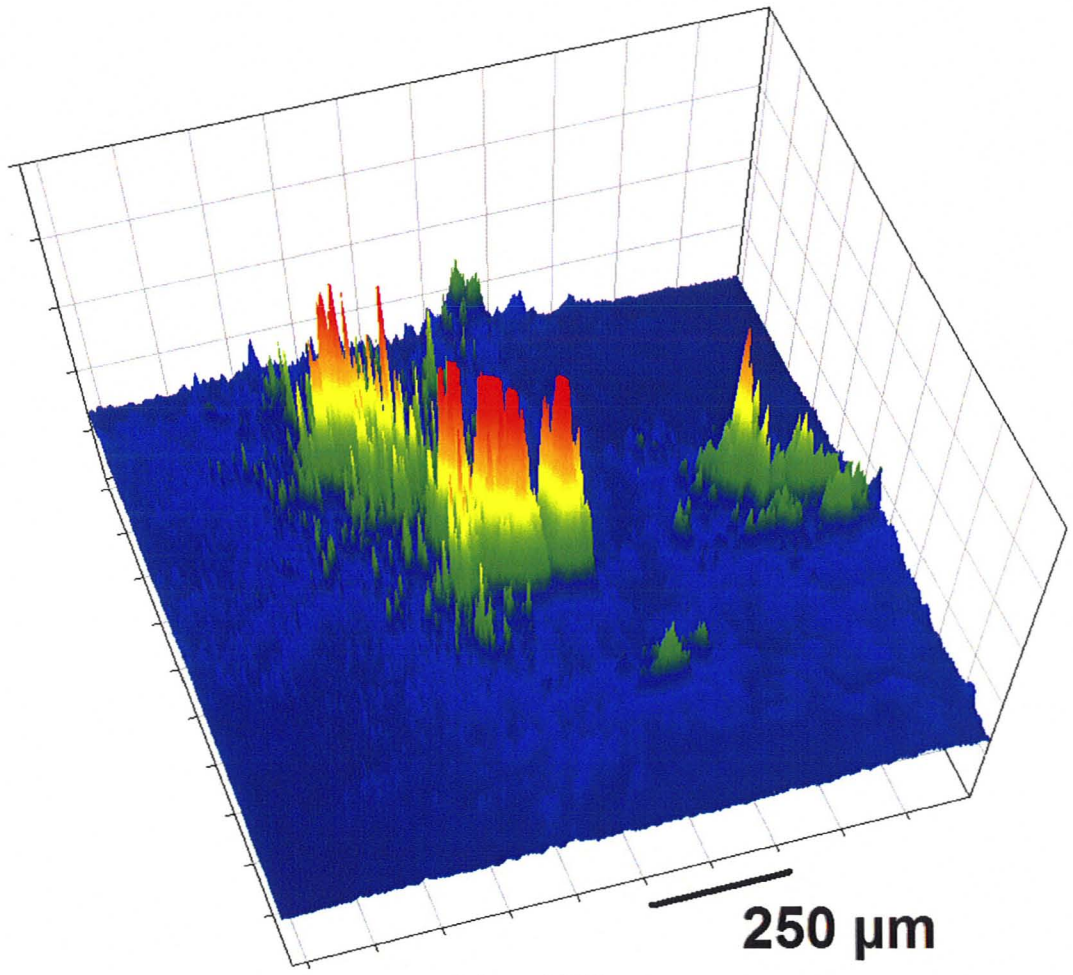

(g) t = 1842 s

Figure 3.2 2D and 3D intensity profiles showing the progression of a partially spatially incoherent light modulation instability experiment, with a spatial coherence length of 86 ± 12 µm. (a) shows the beam under linear conditions (that is, in air), when the diffuser in stationary, (b) the beam in air with the diffuser rotating, (c) at the start of the experiment, time, t = 0 s, (d) t = 1692 s, (e) t = 1788 s, and (f) t = 1842 s, 2D, (g) 3D.

Table 3.2 Summary of results for the 488 nm wavelength experiments with a spatial coherence length of 86 ± 12 µm

Trial	1	2	3
Time elapsed (s)	1842	2982	4488
Age of sol (days)	1	3	3
Cuvette material*	Glass	Glass	Plastic
# of spots measured	100	100	100
Average spot diameter (µm)	9 ± 1	9 ± 1	9 ± 1

*Note: Experiments performed in plastic tend to exhibit greater ordering of the self-trapped filaments, due to noise imposed by striations present on the faces of the plastic cuvettes.

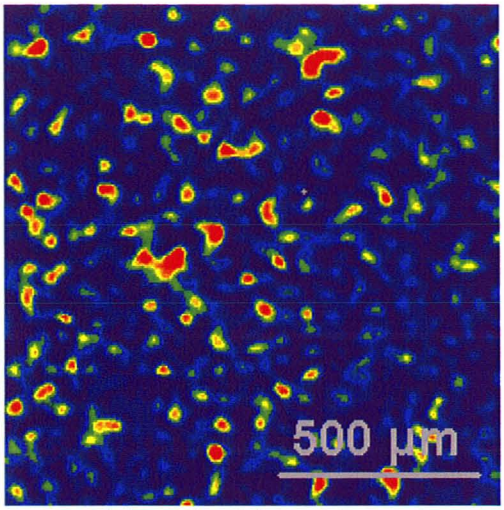

(a) t = 0 s (air, stationary)

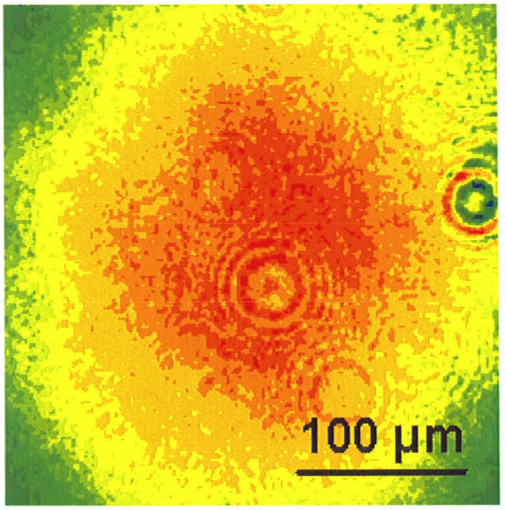

(b) t = 0 s (air, rotating)

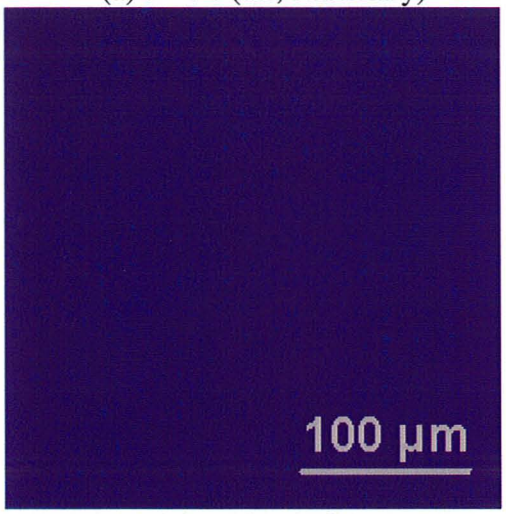

(c) t = 0 s (sol)

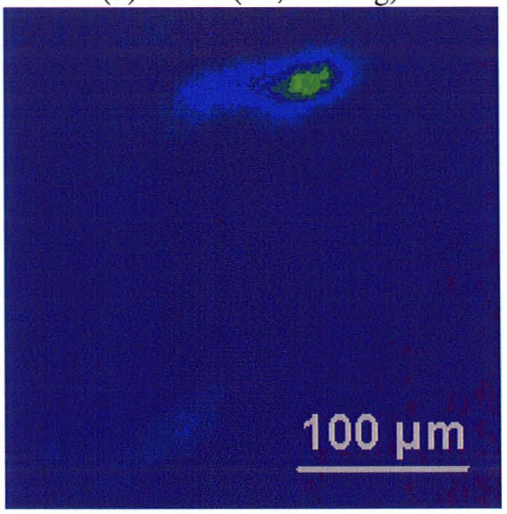

(d) t = 960 s

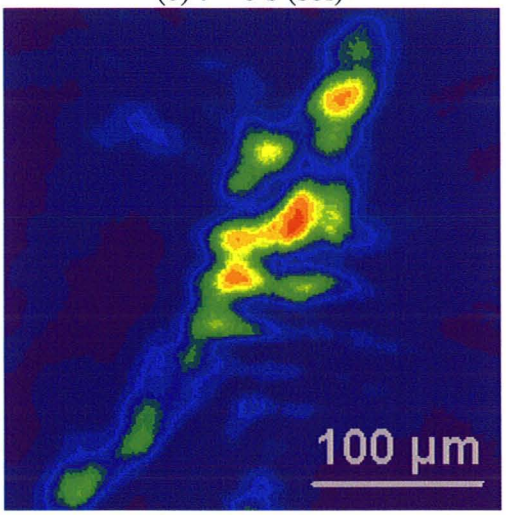

(e) t = 1224 s

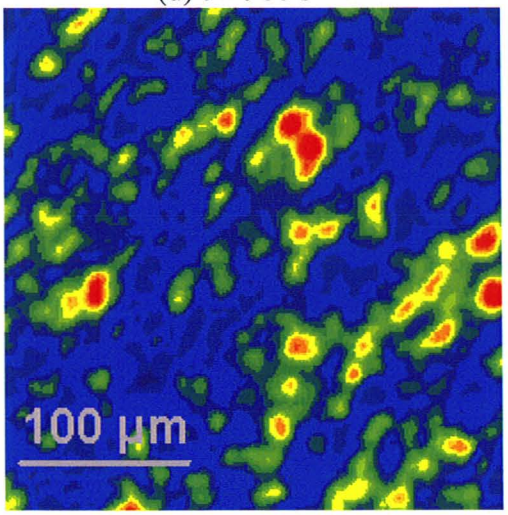

(f) t = 2508 s

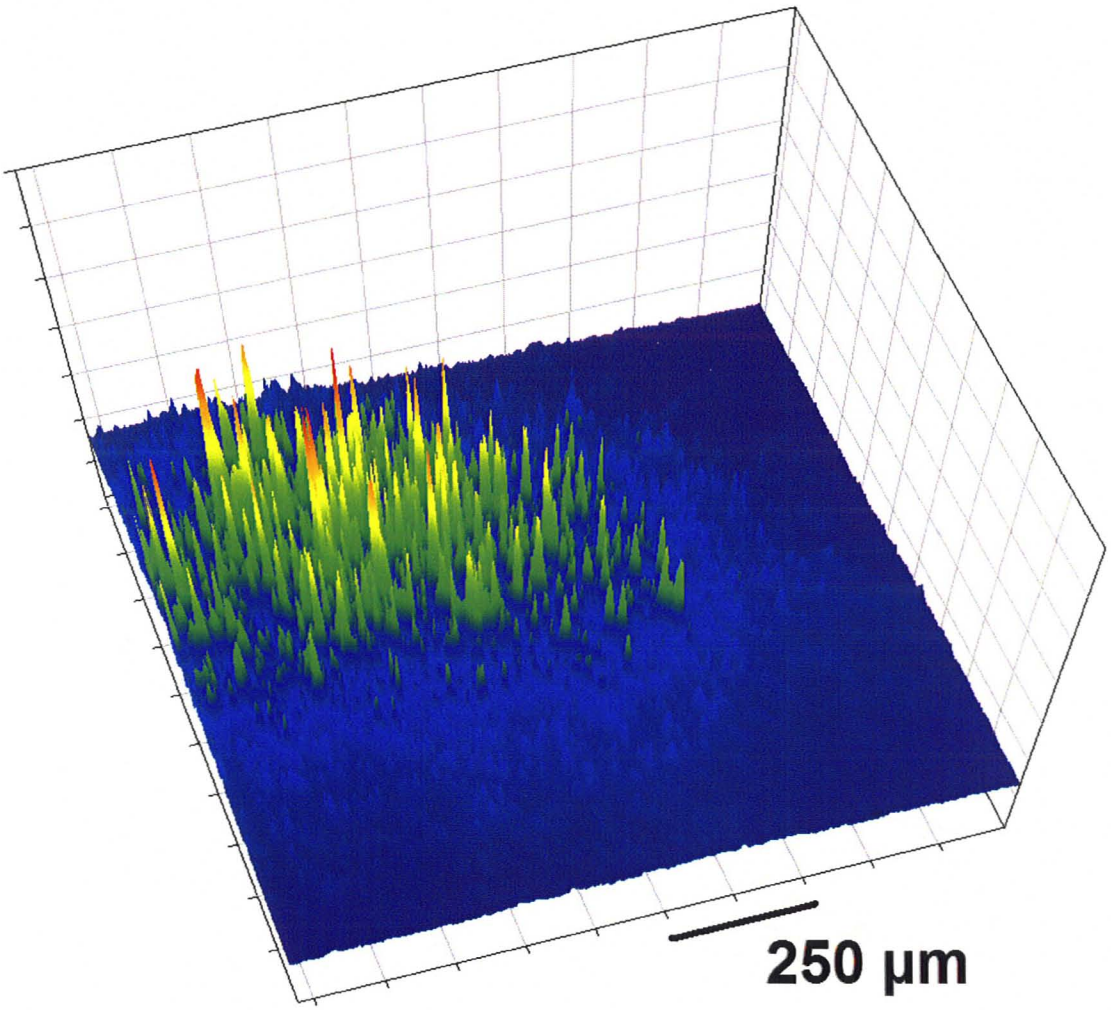

(g) t = 2508 s

Figure 3.3 2D and 3D intensity profiles showing the progression of a partially spatially incoherent light modulation instability experiment, with a spatial coherence length of 45 ± 9 µm. (a) shows the beam under linear conditions (that is, in air), when the diffuser in stationary, (b) the beam in air with the diffuser rotating, (c) at the start of the experiment, time, t = 0 s, (d) t = 960 s, (e) t = 1224 s, and (f) t = 2508 s, 2D, (g) 3D.

Table 3.3 Summary of results for the 488 nm wavelength experiments with a spatial coherence length of 45 ± 9 µm

Trial	1	2	3
Time elapsed (s)	2508	3006	4224
Age of sol (days)	3	1	2
Cuvette material*	Plastic	Glass	Glass
# of spots measured	100	100	100
Average spot diameter (µm)	12 ± 2	12 ± 2	12 ± 2

*Note: Experiments performed in plastic tend to exhibit greater ordering of the self-trapped filaments, due to noise imposed by striations present on the faces of the plastic cuvettes.

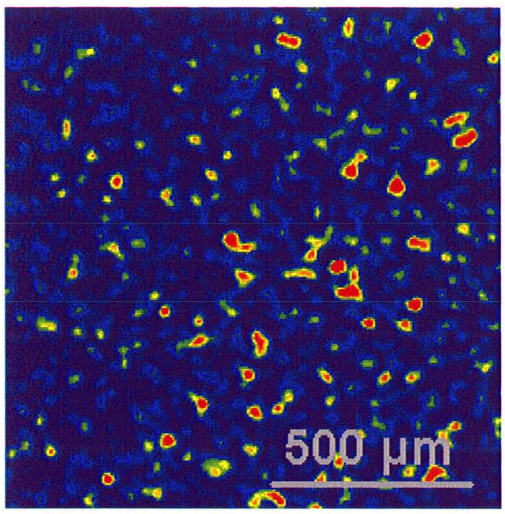

(a) t = 0 s (air, stationary)

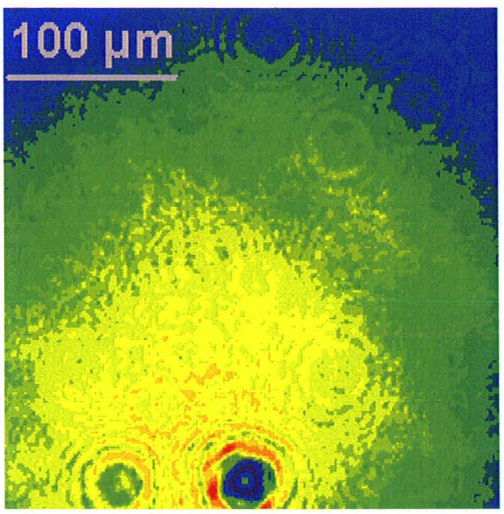

(b) t = 0 s (air, rotating)

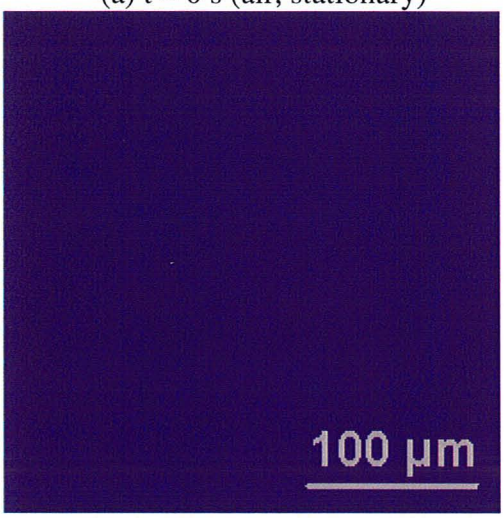

(c) t = 0 s (sol)

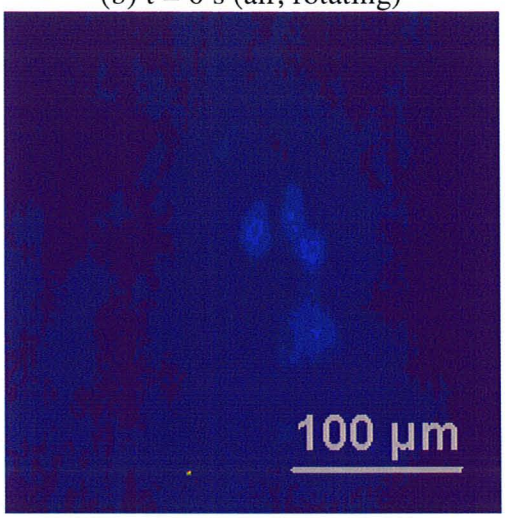

(d) t = 912 s

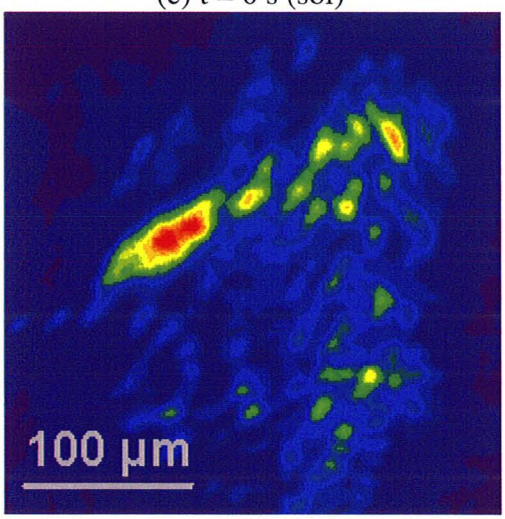

(e) t = 1170 s

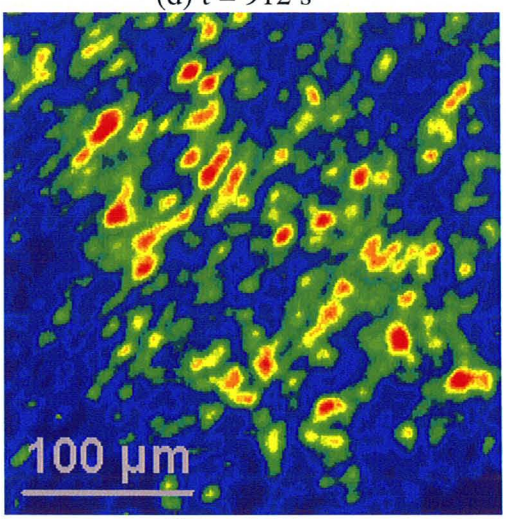

(f) t = 1278 s

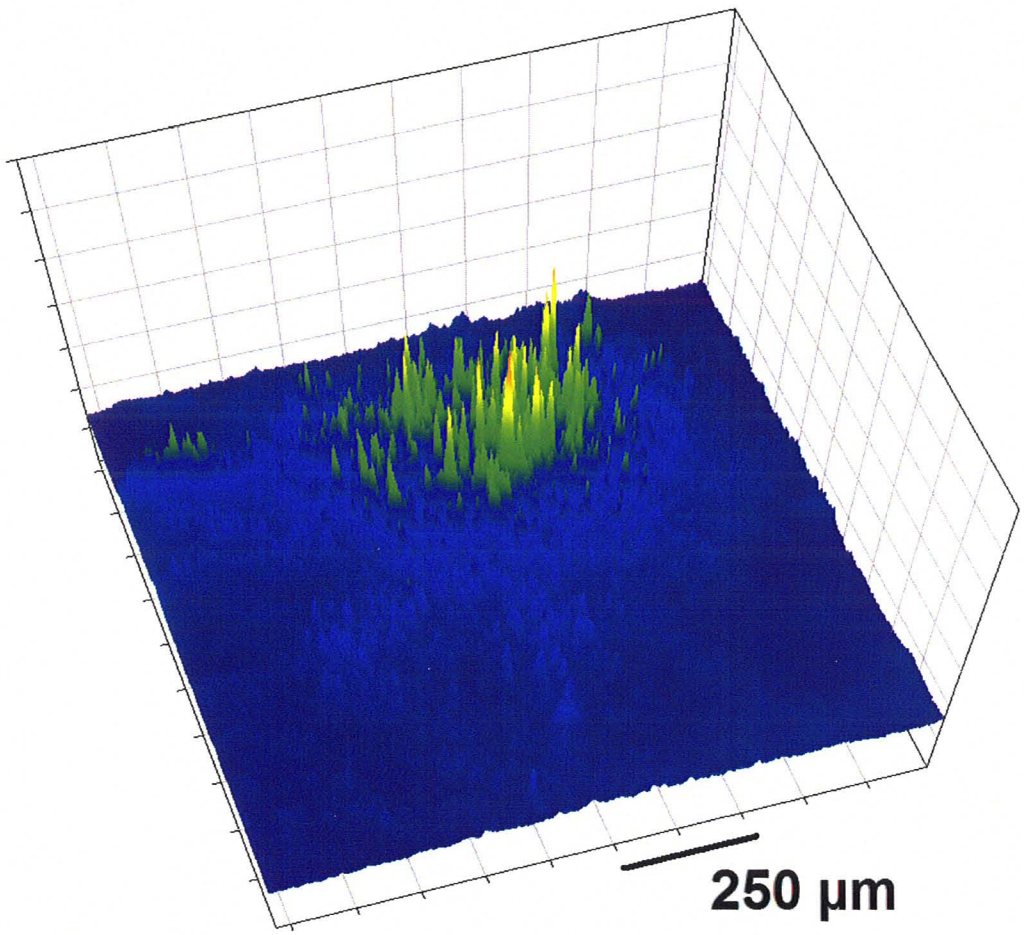

(g) t = 1278 s

Figure 3.4 2D and 3D intensity profiles showing the progression of a partially spatially incoherent light modulation instability experiment, with a spatial coherence length of 34 ± 6 µm. (a) shows the beam under linear conditions (that is, in air), when the diffuser in stationary, (b) the beam in air with the diffuser rotating, (c) at the start of the experiment, time, t = 0 s, (d) t = 912 s, (e) t = 1170 s, and (f) t = 1278 s, 2D, (g) 3D.

Table 3.4 Summary of results for the 488 nm wavelength experiments with a spatial coherence length of 34 ± 6 µm

Trial	1	2	3	4
Time elapsed (s)	1278	5280	3174	4206
Age of sol (days)	3	3	7	1
Cuvette material*	Glass	Glass	Plastic	Plastic
# of spots measured	100	100	100	100
Average spot diameter (µm)	14 ± 1	14 ± 2	14 ± 1	14 ± 1

*Note: Experiments performed in plastic tend to exhibit greater ordering of the self-trapped filaments, due to noise imposed by striations present on the faces of the plastic cuvettes.

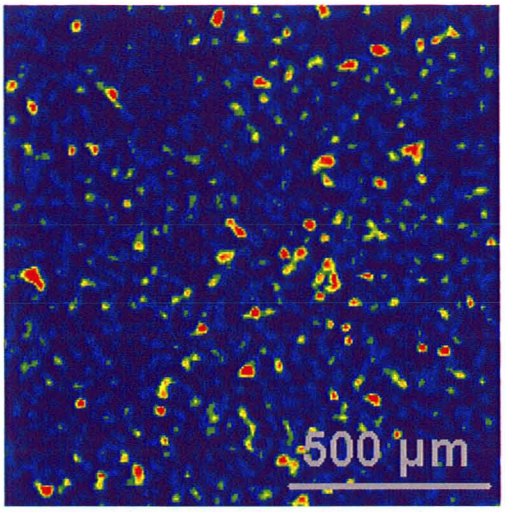

(a) t = 0 s (air, stationary)

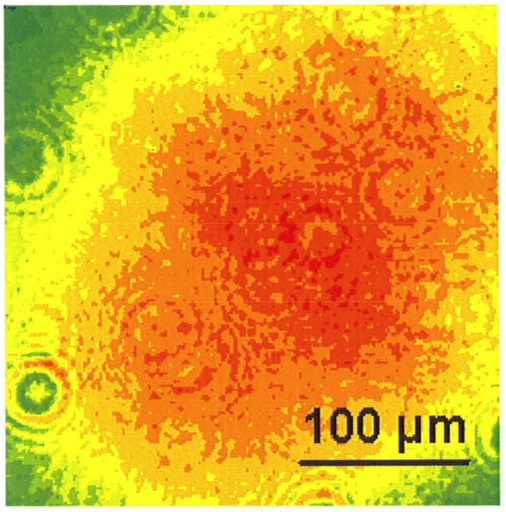

(b) t = 0 s (air, rotating)

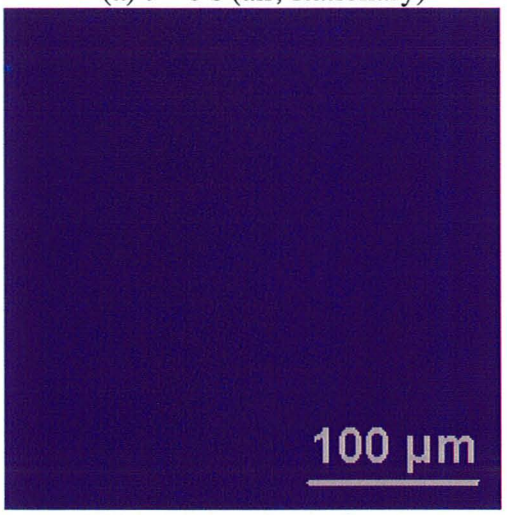

(c) t = 0 s (sol)

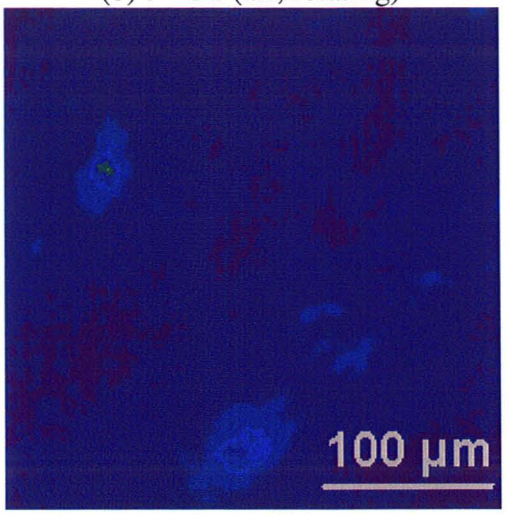

(d) t = 606 s

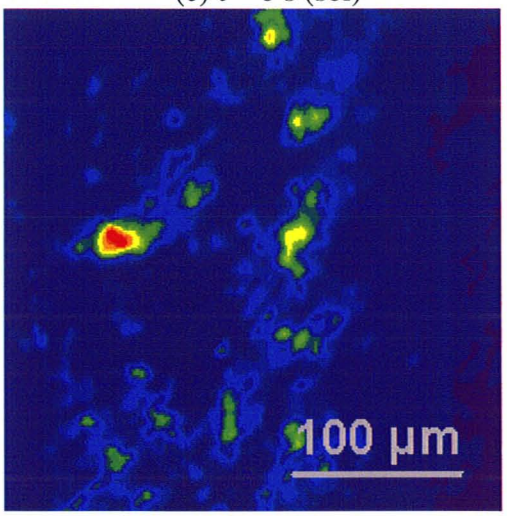

(e) t = 1230 s

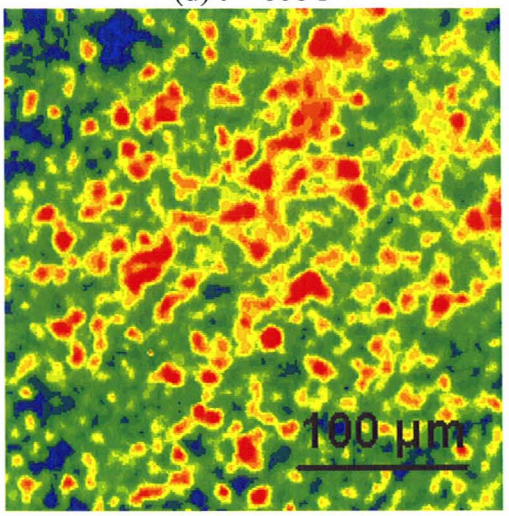

(f) t = 2544 s

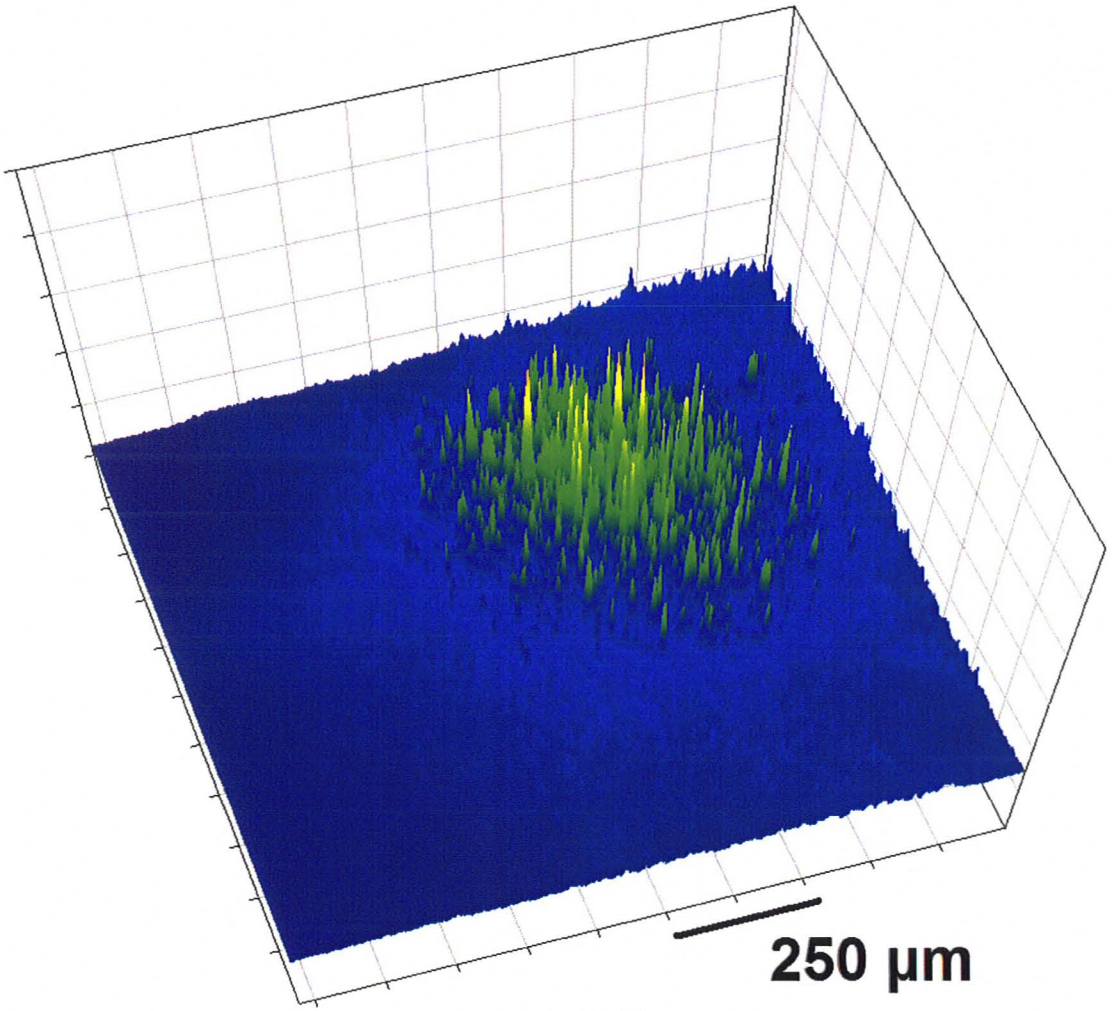

(g) t = 2544 s

Figure 3.5 2D and 3D intensity profiles showing the progression of a partially spatially incoherent light modulation instability experiment, with a spatial coherence length of 27 ± 6 µm. (a) shows the beam under linear conditions (that is, in air), when the diffuser in stationary, (b) the beam in air with the diffuser rotating, (c) at the start of the experiment, time, t = 0 s, (d) t = 606 s, (e) t = 1230 s, and (f) t = 2544 s, 2D, and (g) 3D.

Table 3.5 Summary of results for the 488 nm wavelength experiments with a spatial coherence length of 27 ± 6 µm

Trial	1	2	3
Time elapsed (s)	2544	1494	1968
Age of sol (days)	3	3	1
Cuvette material*	Glass	Glass	Plastic
# of spots measured	100	100	100
Average spot diameter (µm)	16 ± 2	16 ± 2	15 ± 2

*Note: Experiments performed in plastic tend to exhibit greater ordering of the self-trapped filaments, due to noise imposed by striations present on the faces of the plastic cuvettes.

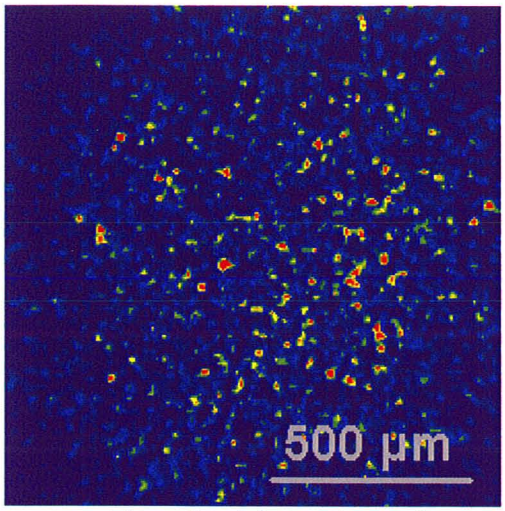

(a) t = 0 s (air, stationary)

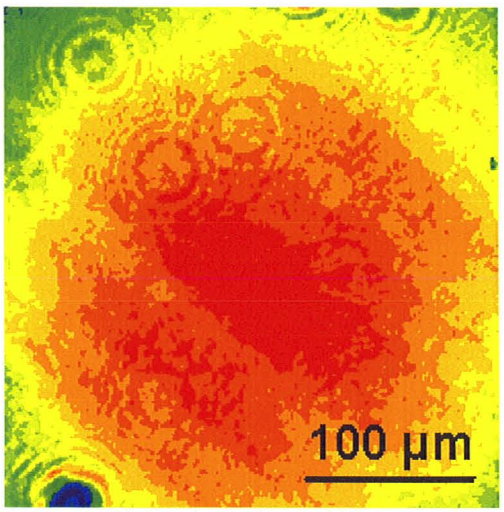

(b) t = 0 s (air, rotating)

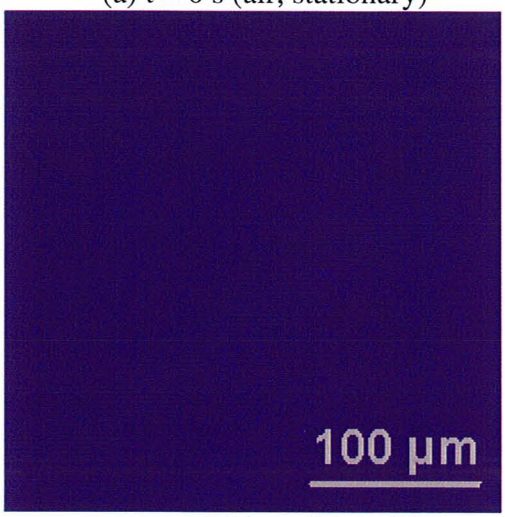

(c) t = 0 s (sol)

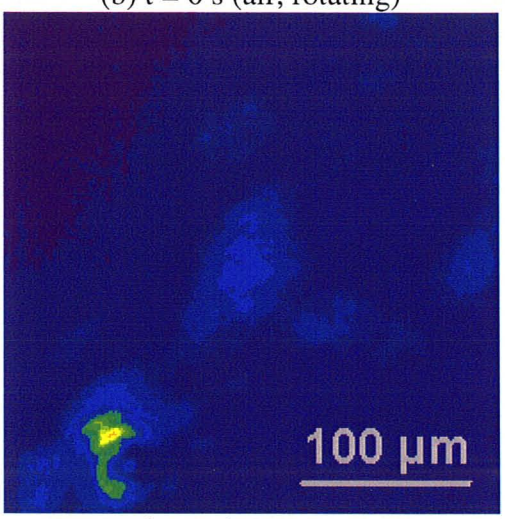

(d) t = 594 s

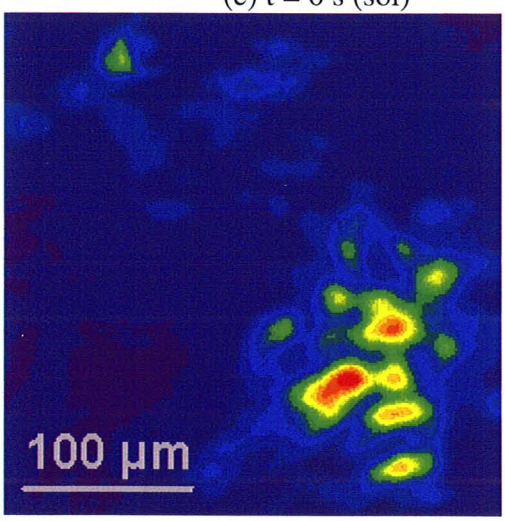

(e) t = 624 s

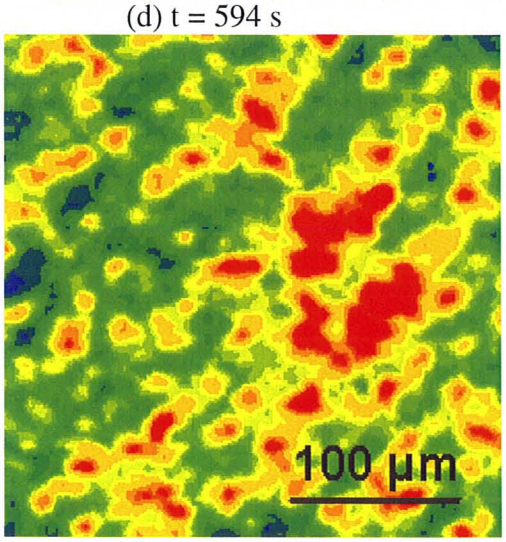

(f) t = 906 s

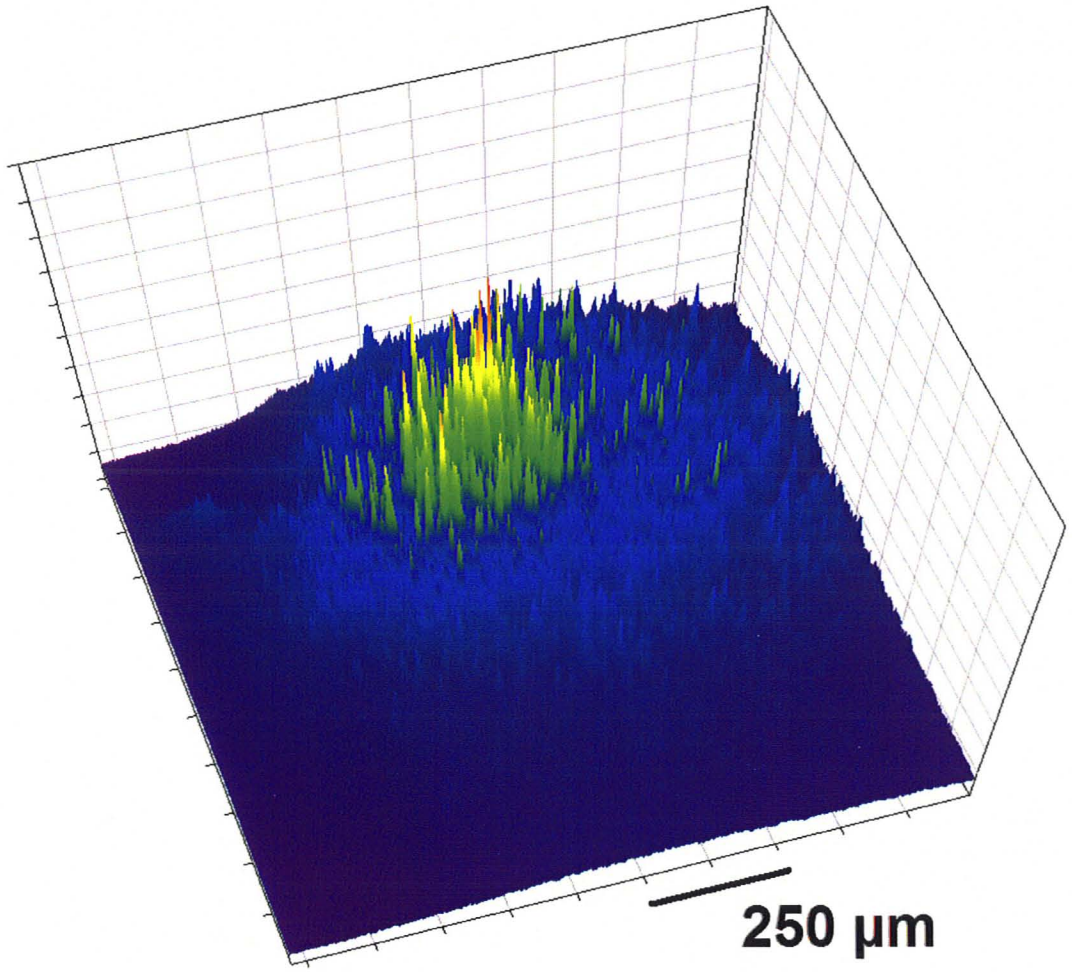

(g) t = 906 s

Figure 3.6 2D and 3D intensity profiles showing the progression of a partially spatially incoherent light modulation instability experiment, with a spatial coherence length of 15 ± 3 µm. (a) shows the beam under linear conditions (that is, in air), when the diffuser in stationary, (b) the beam in air with the diffuser rotating, (c) at the start of the experiment, time, t = 0 s, (d) t = 594 s, (e) t = 624 s, and (f) t = 906 s, 2D, (g) 3D.

Table 3.6 Summary of results for the 488 nm wavelength experiments with a spatial coherence length of 15 ± 3 µm

Trial	1	2	3
Time elapsed (s)	906	1038	1086
Age of sol (days)	43	2	2
Cuvette material*	Plastic	Glass	Glass
# of spots measured	100	100	100
Average spot diameter (µm)	18 ± 2	20 ± 3	19 ± 2

*Note: Experiments performed in plastic tend to exhibit greater ordering of the self-trapped filaments, due to noise imposed by striations present on the faces of the plastic cuvettes.

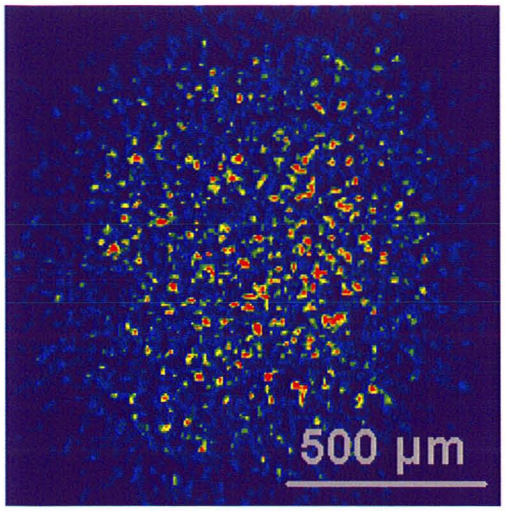

(a) t = 0 s (air, stationary)

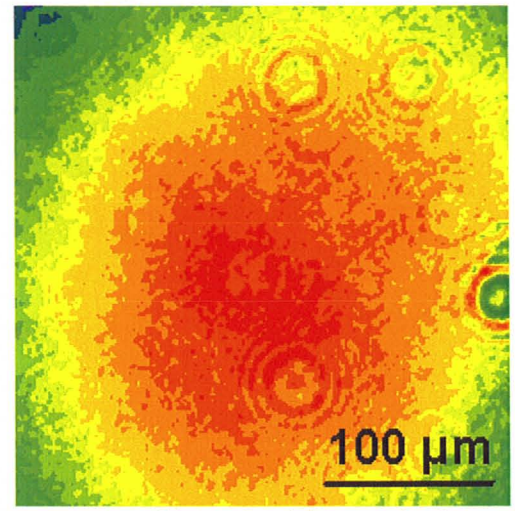

(b) t = 0 s (air, rotating)

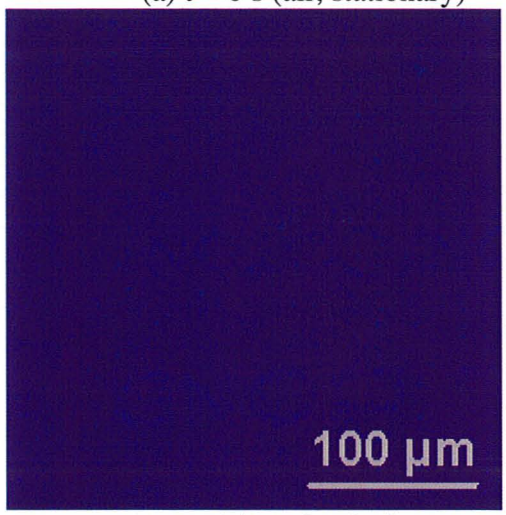

(c) t = 0 s (sol)

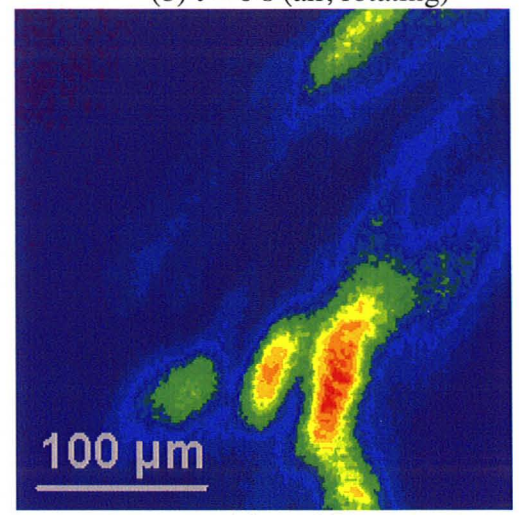

(d) t = 870 s

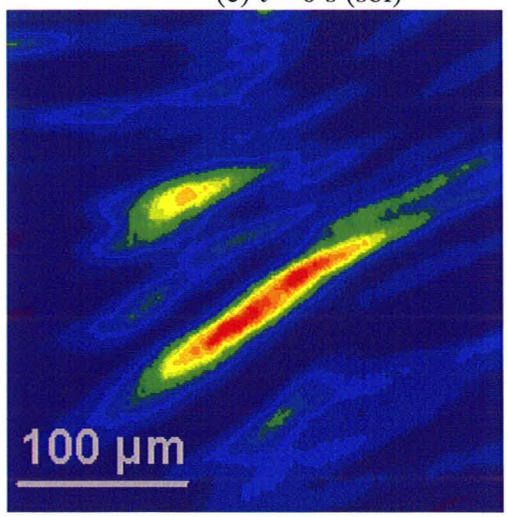

(e) t = 1158 s

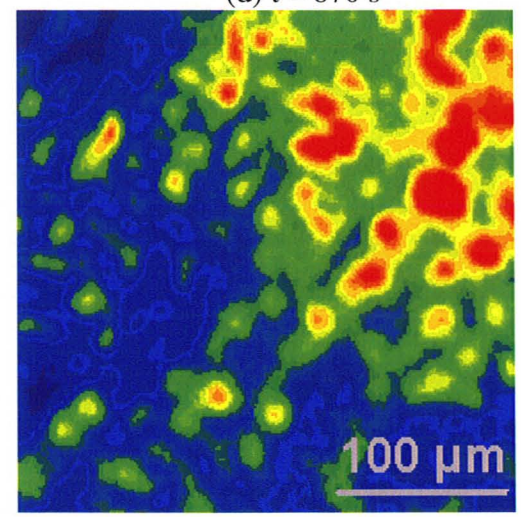

(f) t = 2142 s

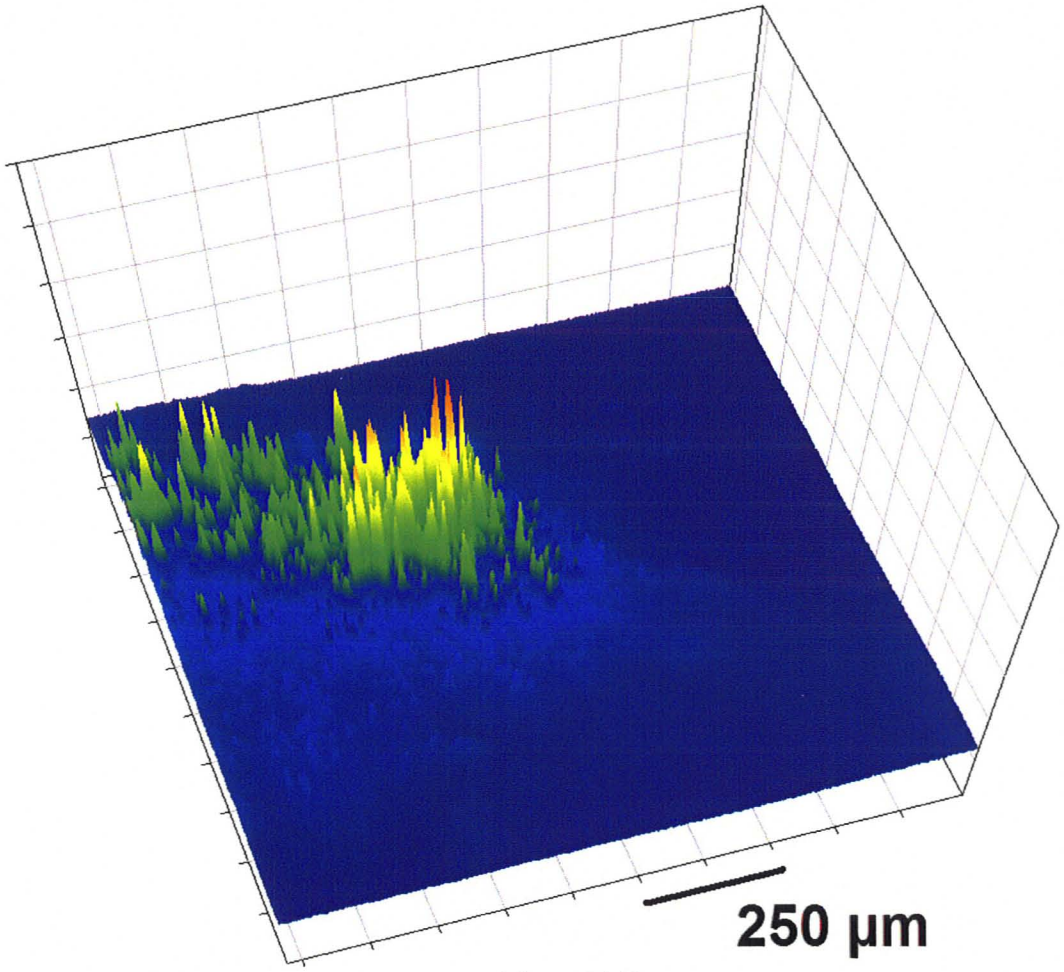

(g) t = 2142 s

Figure 3.7 2D and 3D intensity profiles showing the progression of a partially spatially incoherent light modulation instability experiment, with a spatial coherence length of 11 ± 2 µm. (a) shows the beam under linear conditions (that is, in air), when the diffuser in stationary, (b) the beam in air with the diffuser rotating, (c) at the start of the experiment, time, t = 0 s, (d) t = 870 s, (e) t = 1158 s, and (f) t = 2142 s, 2D, (g) 3D.

Table 3.7 Summary of results for the 488 nm wavelength experiments with a spatial coherence length of 11 ± 2 µm

Trial	1	2	3
Time elapsed (s)	2142	2856	2640
Age of sol (days)	4	4	4
Cuvette material*	Glass	Glass	Glass
# of spots measured	100	100	100
Average spot diameter (µm)	22 ± 2	22 ± 2	20 ± 3

*Note: Experiments performed in plastic tend to exhibit greater ordering of the self-trapped filaments, due to noise imposed by striations present on the faces of the plastic cuvettes.

All of the experiments carried out with partially spatially incoherent light progress in the same way as the purely coherent experiments, demonstrating modulation instability. The beam, while not initially visible, begins to emerge and the intensity increases in random areas based on convection, due to heat, within the medium. This corresponds to the first stage of modulation instability, where random noise and inhomogeneneities imperceptible under linear conditions, are reinforced due to the nonlinearity of the system created by polymerisation.[22] These areas of increased intensity eventually become unstable and spontaneously split up into a random array of virtually identical self-trapped filaments, the size of which depends on the spatial coherence length of the incident light field.

The data from the preceding experiments is summarised in the following table. The degree of spatial incoherence, calculated from the spatial coherence length using equation [1-5], $\theta_0 = \frac{\sqrt{2\pi}}{kl_c}$, and the filament frequency, calculated from equation [1-6], $\alpha = \frac{2\pi}{FD}$, are included, as well.

Table 3.8 Summary of 488 nm wavelength data

Spatial coherence length (μm)	Self-trapped filament diameter (μm)	Degree of spatial incoherence, θ_0	Filament Frequency, α (μm^{-1})	Time elapsed (s)
∞	7 ± 1	0	0.9 ± 0.1	5512 ± 1382
86 ± 12	9 ± 1	0.0015 ± 0.0002	0.7 ± 0.1	3104 ± 1327
45 ± 9	12 ± 2	0.0030 ± 0.0006	0.53 ± 0.08	3246 ± 883
34 ± 6	14 ± 1	0.0039 ± 0.0007	0.44 ± 0.05	3484 ± 1704
27 ± 6	16 ± 2	0.005 ± 0.001	0.40 ± 0.05	2002 ± 526
15 ± 3	19 ± 3	0.009 ± 0.002	0.33 ± 0.05	1010 ± 93
11 ± 2	21 ± 3	0.012 ± 0.002	0.30 ± 0.04	2546 ± 366
*0.3	75 ± 5	0.444	0.084 ± 0.006	N/A

*White light experiments[22]

From this data, the visible trend is that a decrease in spatial coherence length results in an increase in the self-trapped filament diameter. The relationship between the degree of spatial incoherence and the filament frequency can be further characterised by plotting the data and comparing it to the theoretical curve. The theoretical curve is made up of the calculated values of the filament frequency, α, corresponding to the degree of spatial coherence (θ_0) values used for the study. The calculated values of alpha were done so using a rearrangement of equation [1-4], as follows:

$$\alpha = -\frac{k\sqrt{n_0}\theta_0}{\sqrt{\Delta n}} + \frac{\sqrt{2k\sqrt{n_0}\sqrt{\Delta n} + k^2 n_0 \theta_0^2}}{\sqrt{\Delta n}} \qquad [3\text{-}1]$$

These calculated values were treated with a scaling as well as a displacement factor, using the least squares method to fit the data.

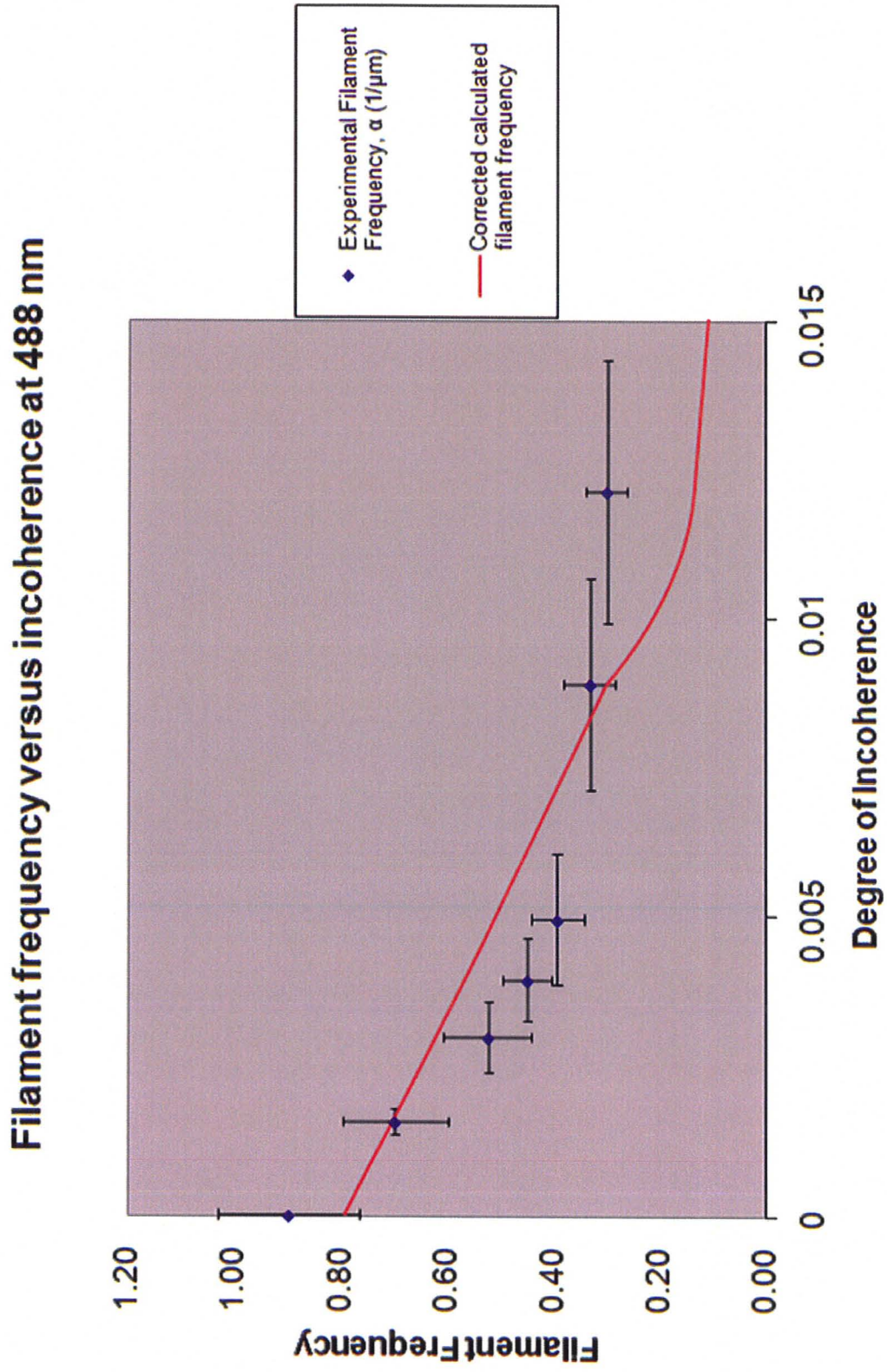

Figure 3.8 Plot of filament frequency versus degree of spatial incoherence for wavelength 488 nm

This data, which displays the relationship between self-trapped filament frequency and degree of spatial incoherence, shows an increase in the filament frequency, as the degree of incoherence is decreased (i.e. when the light field is more coherent). The experimental data (shown in blue) corresponds closely to the theoretically calculated data (the red curve), both showing the inverse relationship between degree of spatial coherence and filament frequency. The experimental data fits the theoretical more closely when the degree of incoherence is small, but begins to deviate as the degree of incoherence becomes larger, as the experimental curve begins to level off more quickly than that of the theoretical.

In addition to a link between spatial coherence and filament diameter, there is also a trend in the time that it takes for the medium to reach the point in the modulation instability process at which the beam has divided into individual identical self-trapped filaments. This transition time seems to have a dependence on the spatial coherence length as well. In general, it appears that this transition happens later, the more coherent the beam.

3.2 Modulation instability due to polymerisation at 532 nm

This study was repeated with a second wavelength – 532 nm, in order to establish a wavelength dependence for the self-trapped filament diameter, as well as reinforce the dependence of filament diameter on spatial coherence seen at a wavelength of 488 nm. Several spatial coherence lengths were selected for experiments. The first was an infinite spatial coherence accessed by using light from the laser that is not diffused, $l_c = \infty$. Three experiments were done at this coherence length, and a sample experiment demonstrating the temporal evolution of the beam under nonlinear conditions is shown in the following figure.

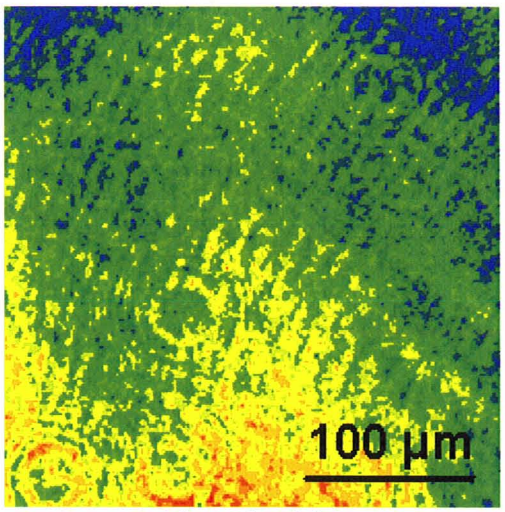

(a) t = 0 s (air)

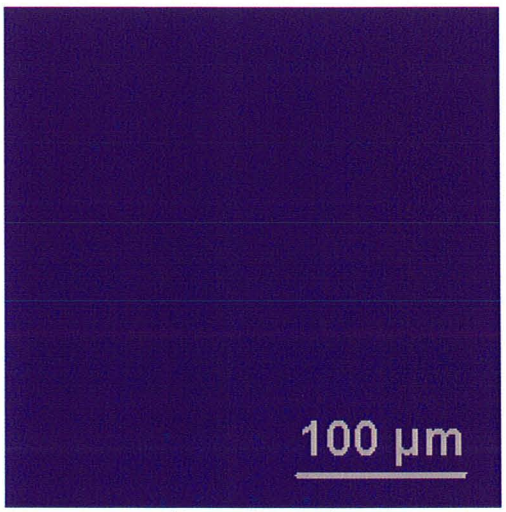

(b) t = 0 s (sol)

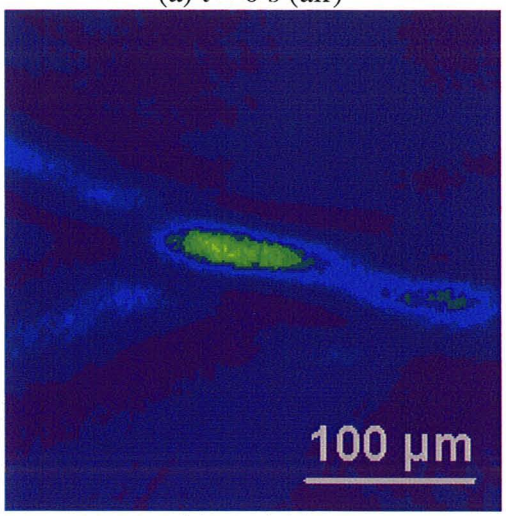

(c) t = 144 s

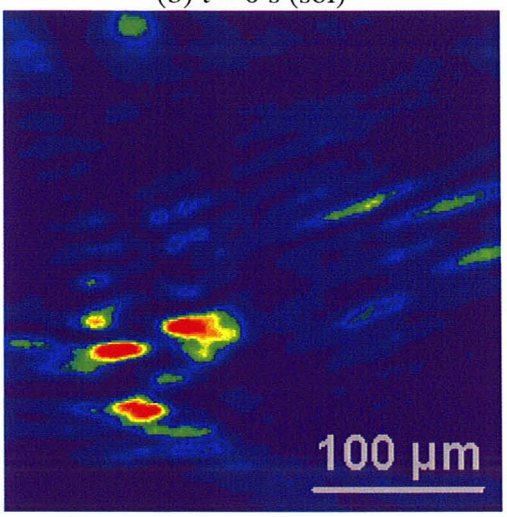

(d) t = 600 s

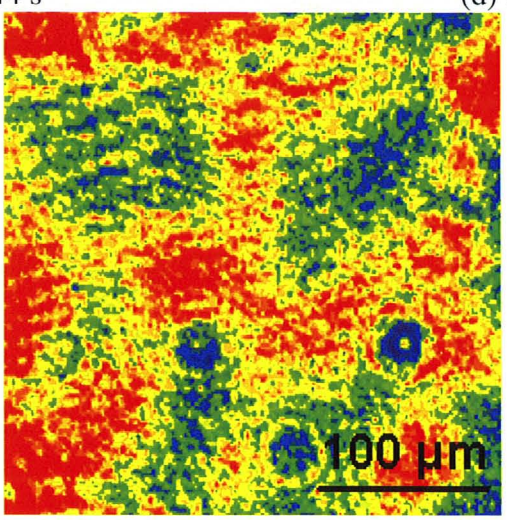

(e) t = 3486 s

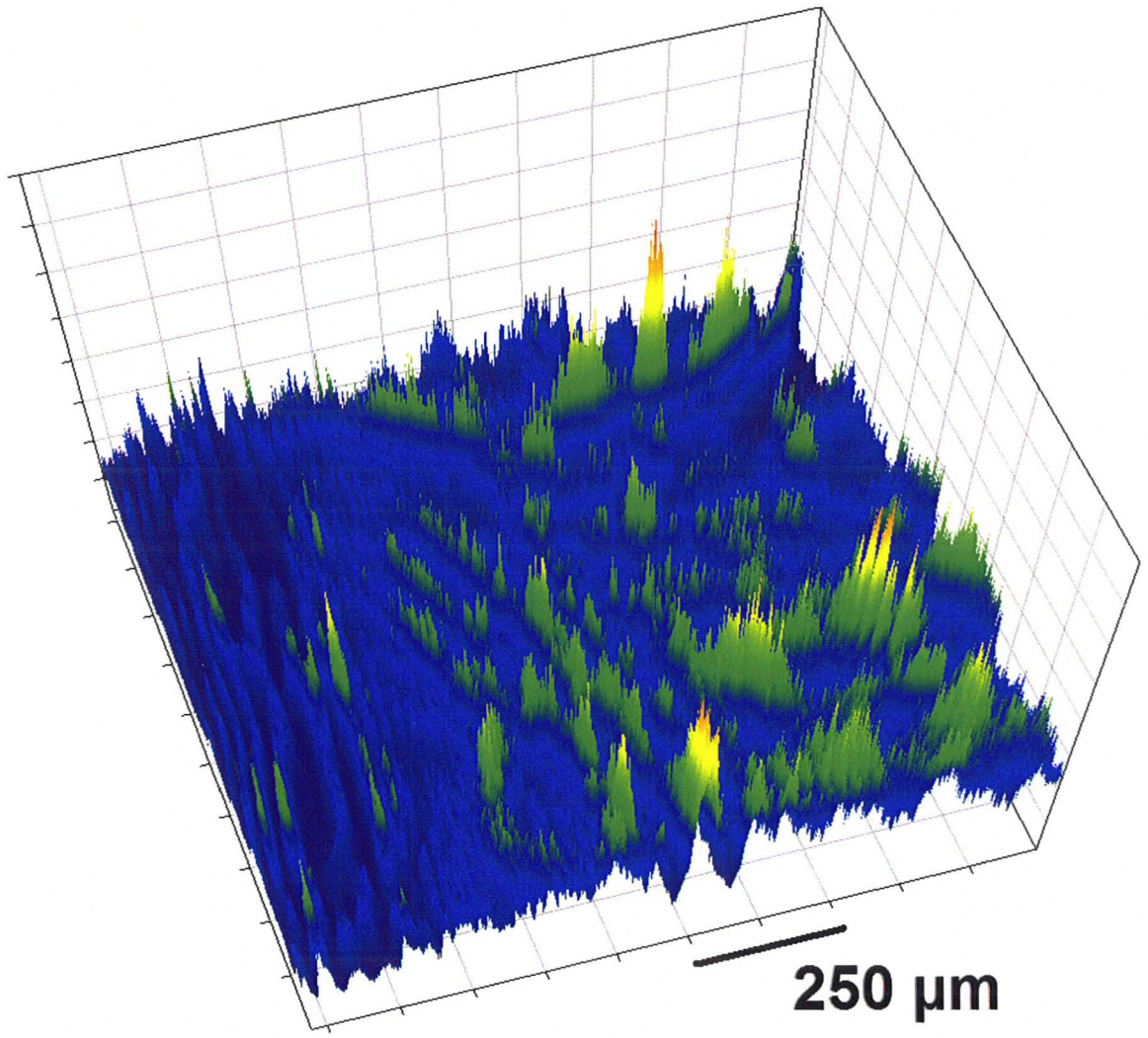

(f) t = 3486 s

Figure 3.9 2D and 3D intensity profiles showing the progression of a purely coherent light modulation instability experiment, with an infinite spatial coherence length. (a) shows the beam under linear conditions (that is, in air) (b) at the start of the experiment, time, t = 0 s, (c) t = 144 s, (d) t = 600 s, and (e) t = 3486 s, 2D, (f) 3D.

These experiments progress in the same way as the purely coherent experiments seen with the 488 nm laser, where, the beam, while not initially visible, begins to emerge and the intensity increases in random areas based on convection within the medium.

These areas of increased intensity eventually become unstable and spontaneously split up into a random array of virtually identical self-trapped filaments.

Similar findings were discovered for each of the three trials done using a broad beam of purely coherent laser light with a wavelength of 532 nm and an infinite spatial coherence length. Significant images, which clearly display the modulation instability phenomenon were selected for each of these experiments. These are shown in **Table 3.9**.

Table 3.9 Summary of results for the 532 nm wavelength experiments with an infinite spatial coherence length

Trial	1	2	3
Time elapsed (s)	3486	3456	2544
Age of sol (days)	2	2	2
Cuvette material*	Glass	Glass	Plastic
# of spots measured	100	100	100
Average spot diameter (μm)	5.9 ± 0.6	6.2 ± 0.8	6.2 ± 0.5

*Note: Experiments performed in plastic tend to exhibit greater ordering of the self-trapped filaments, due to noise imposed by striations present on the faces of the plastic cuvettes.

As with the 488 nm experiments, the diffuser was set into rotation, producing a light field that is partially spatially incoherent. The spatial coherence lengths studied at the 532 nm wavelength are 1.3 ± 0.2 μm, 6 ± 1 μm, 11 ± 1 μm, 15 ± 2 μm, 25 ± 2 μm, and 46 ± 5 μm. Temporal progressions for each coherence length are shown in the following series of figures, along with a table summarising the results for repeat experiments at each spatial coherence length. Intensity profiles for the repeat experiments are available in **Appendix B**.

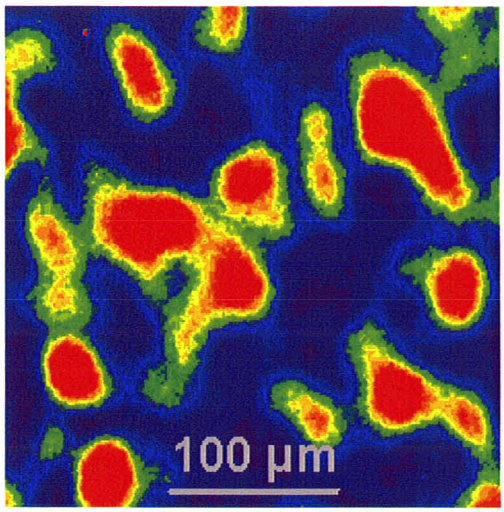

(a) t = 0 s (air, stationary)

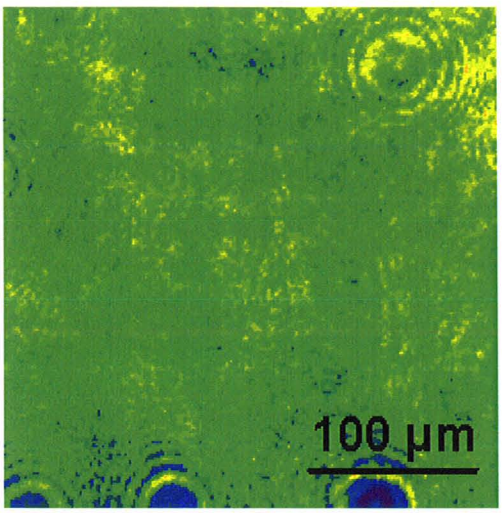

(b) t = 0 s (air, rotating)

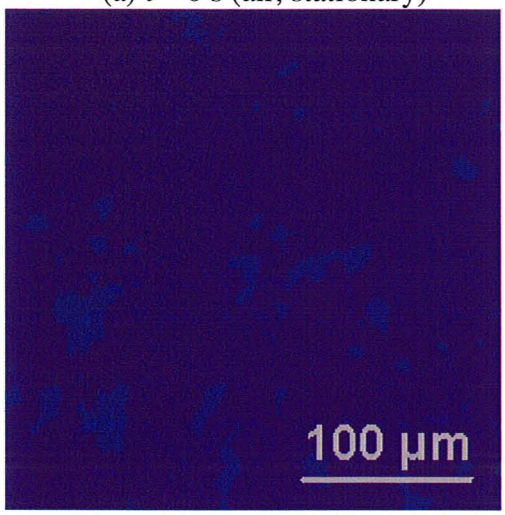

(c) t = 0 s (sol)

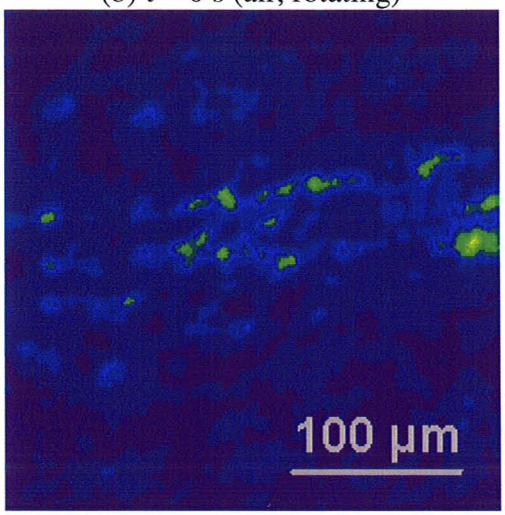

(d) t = 96 s

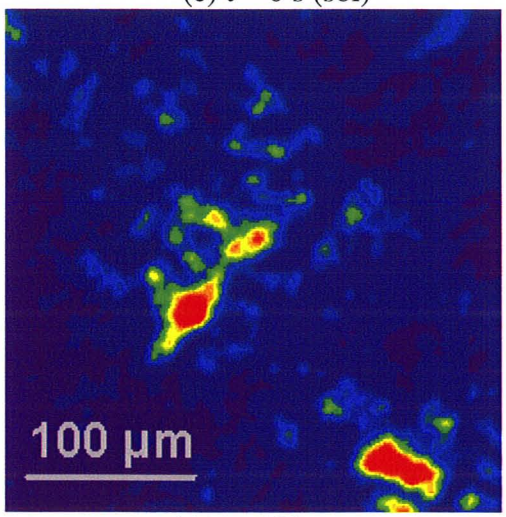

(e) t = 450 s

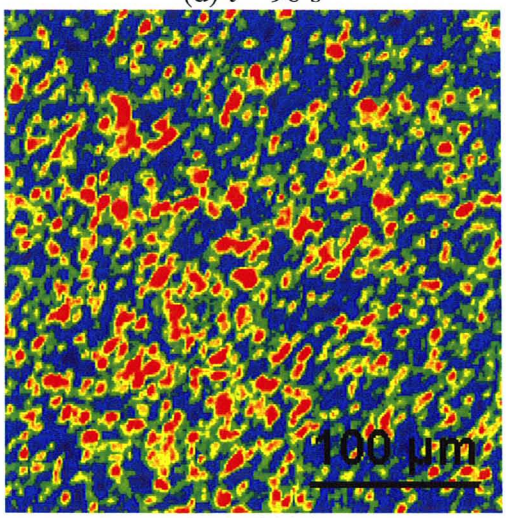

(f) t = 2184 s

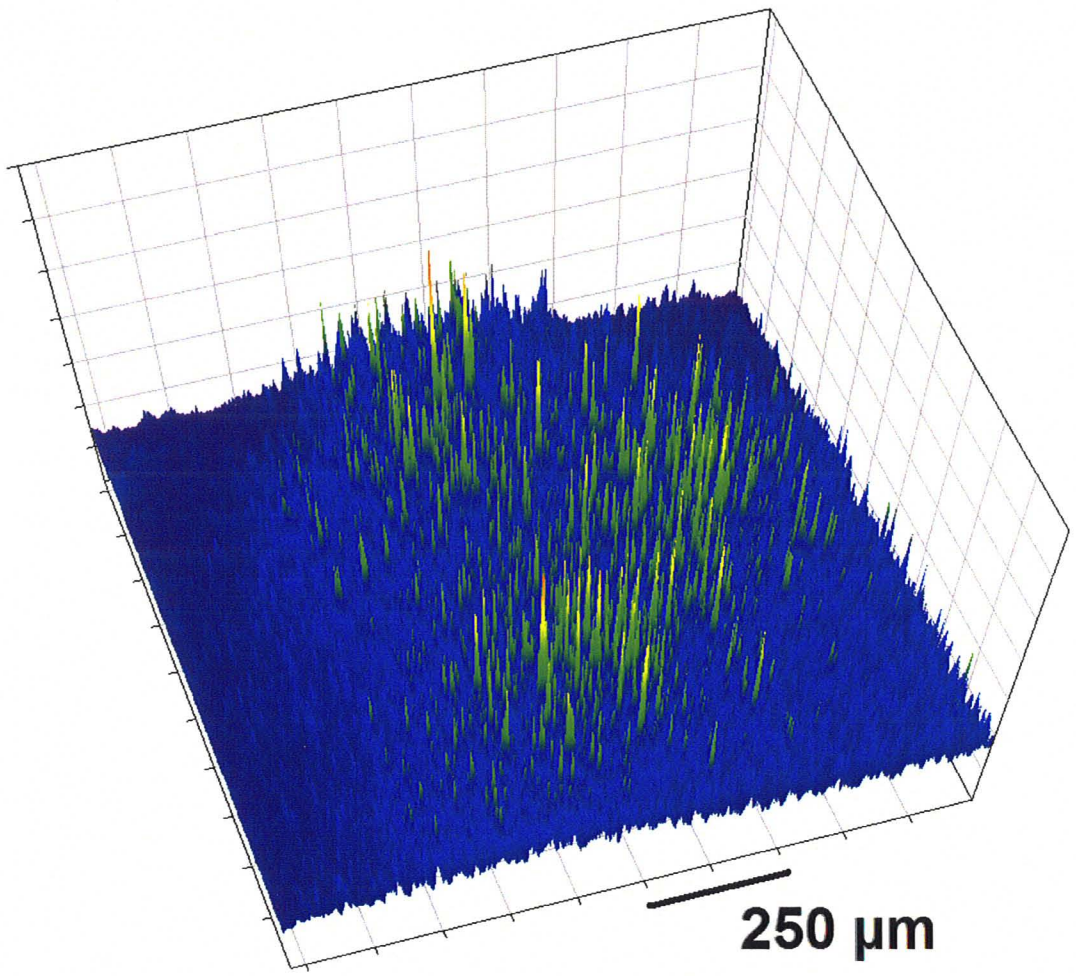

(g) t = 2184 s

Figure 3.10 2D and 3D intensity profiles showing the progression of a partially spatially incoherent light modulation instability experiment, with a spatial coherence length of 46 ± 5 µm. (a) shows the beam under linear conditions (that is, in air), when the diffuser in stationary, (b) the beam in air with the diffuser rotating, (c) at the start of the experiment, time, t = 0 s, (d) t = 96 s, (e) t = 450 s, and (f) t = 2184 s, 2D, (g) 3D

Table 3.10 Summary of results for the 532 nm wavelength experiments with a spatial coherence length of 46 ± 5 µm

Trial	1	2	3
Time elapsed (s)	2184	2100	2772
Age of sol (days)	2	2	2
Cuvette material*	Glass	Plastic	glass
# of spots measured	100	100	100
Average spot diameter (µm)	7.2 ± 0.7	8 ± 1	7.8 ± 0.8

*Note: Experiments performed in plastic tend to exhibit greater ordering of the self-trapped filaments, due to noise imposed by striations present on the faces of the plastic cuvettes.

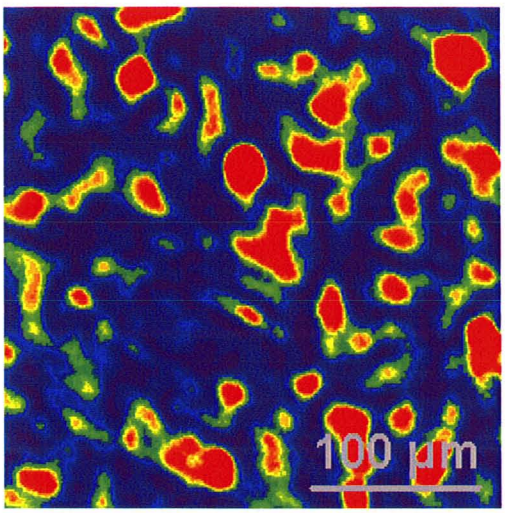

(a) t = 0 s (air, stationary)

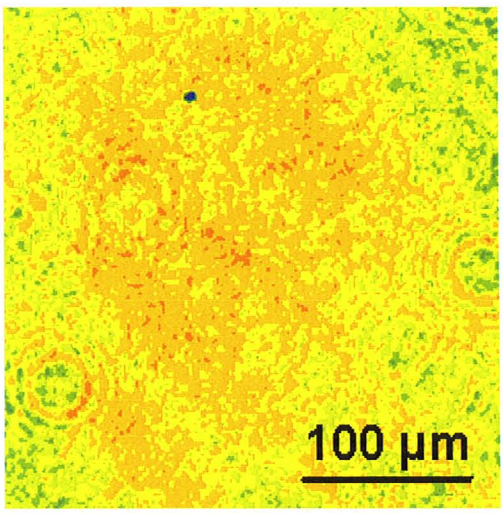

(b) t = 0 s (air, rotating)

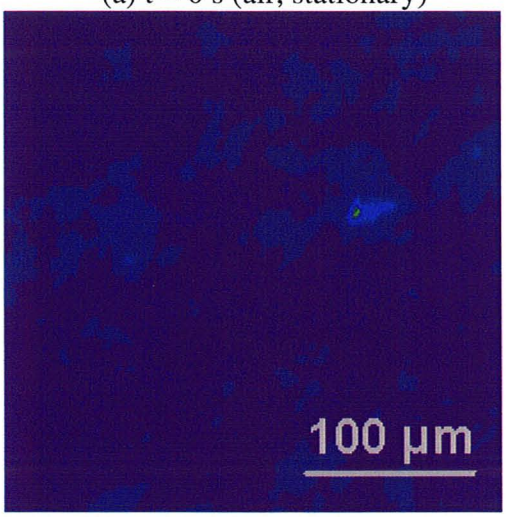

(c) t = 0 s (sol)

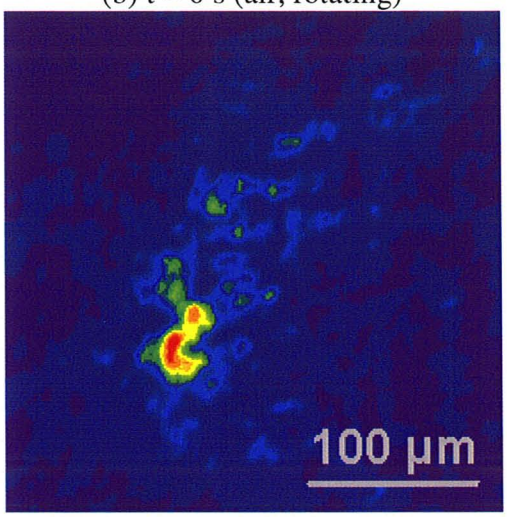

(d) t = 144 s

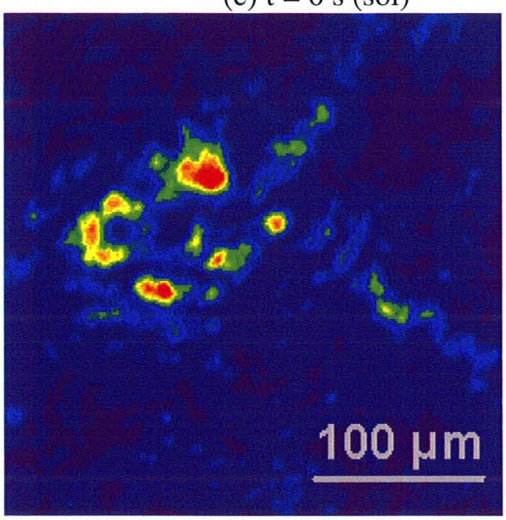

(e) t = 600 s

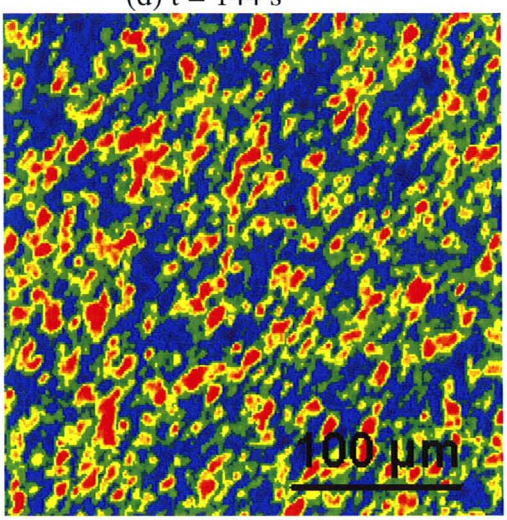

f) t = 1104 s

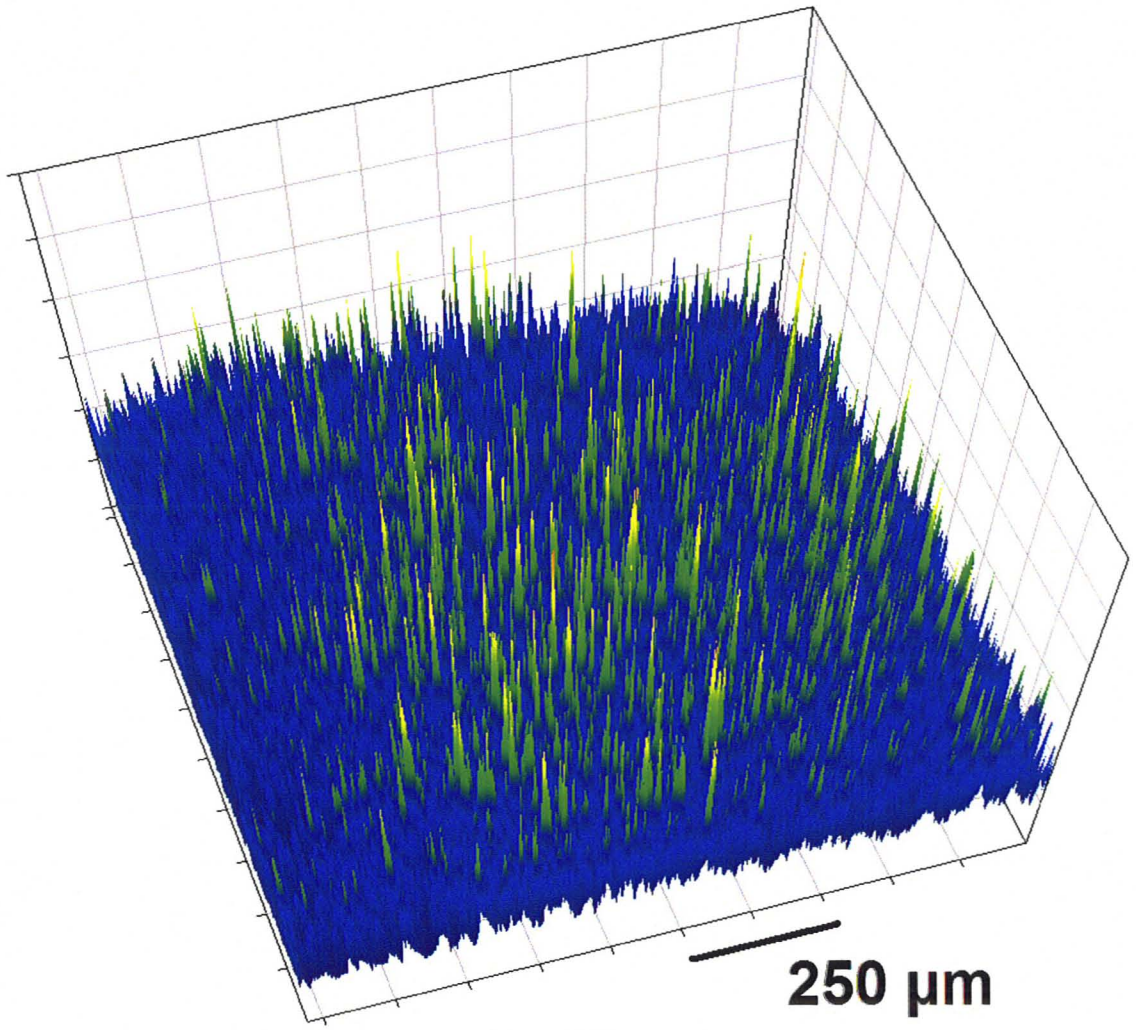

(g) t = 1104 s

Figure 3.11 2D and 3D intensity profiles showing the progression of a partially spatially incoherent light modulation instability experiment, with a spatial coherence length of 25 ± 2 µm. (a) shows the beam under linear conditions (that is, in air), when the diffuser in stationary, (b) the beam in air with the diffuser rotating, (c) at the start of the experiment, time, t = 0 s, (d) t = 144 s, (e) t = 600 s, and (f) t = 1104 s, 2D, (g) 3D.

Table 3.11 Summary of results for the 532 nm wavelength experiments with a spatial coherence length of 25 ± 2 µm

Trial	1	2	3
Time elapsed (s)	1104	1176	906
Age of sol (days)	1	2	1
Cuvette material*	Glass	Plastic	Glass
# of spots measured	100	100	100
Average spot diameter (µm)	9 ± 1	9 ± 1	8.2 ± 0.9

*Note: Experiments performed in plastic tend to exhibit greater ordering of the self-trapped filaments, due to noise imposed by striations present on the faces of the plastic cuvettes.

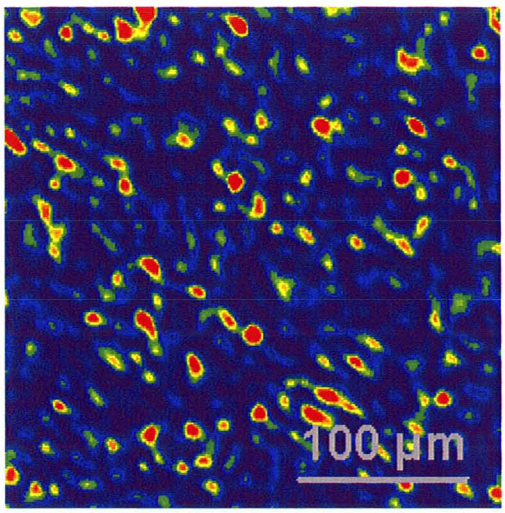

(a) t = 0 s (air, stationary)

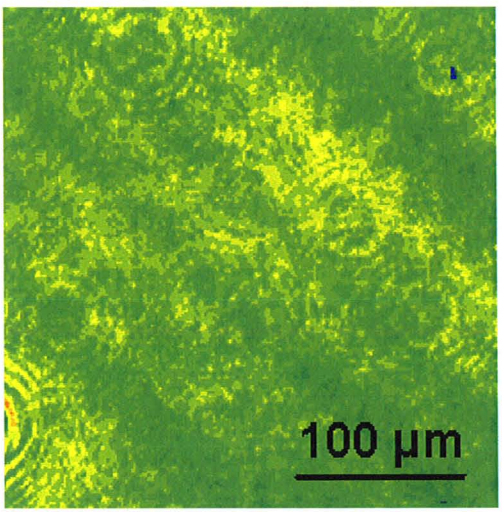

(b) t = 0 s (air, rotating)

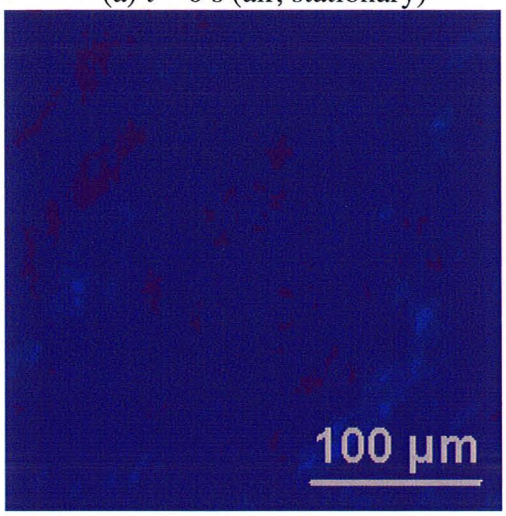

(c) t = 0 s (sol)

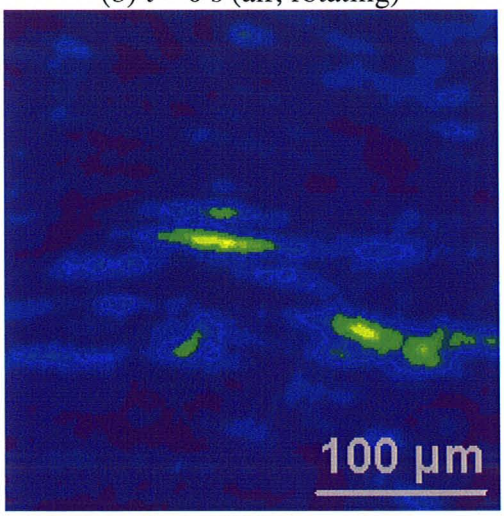

(d) t = 306 s

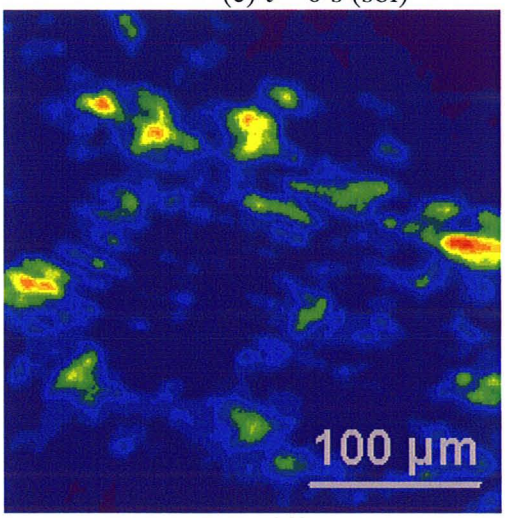

(e) t = 558 s

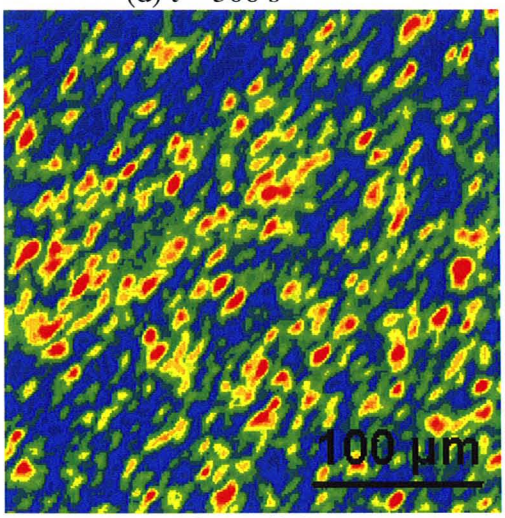

(f) t = 696 s

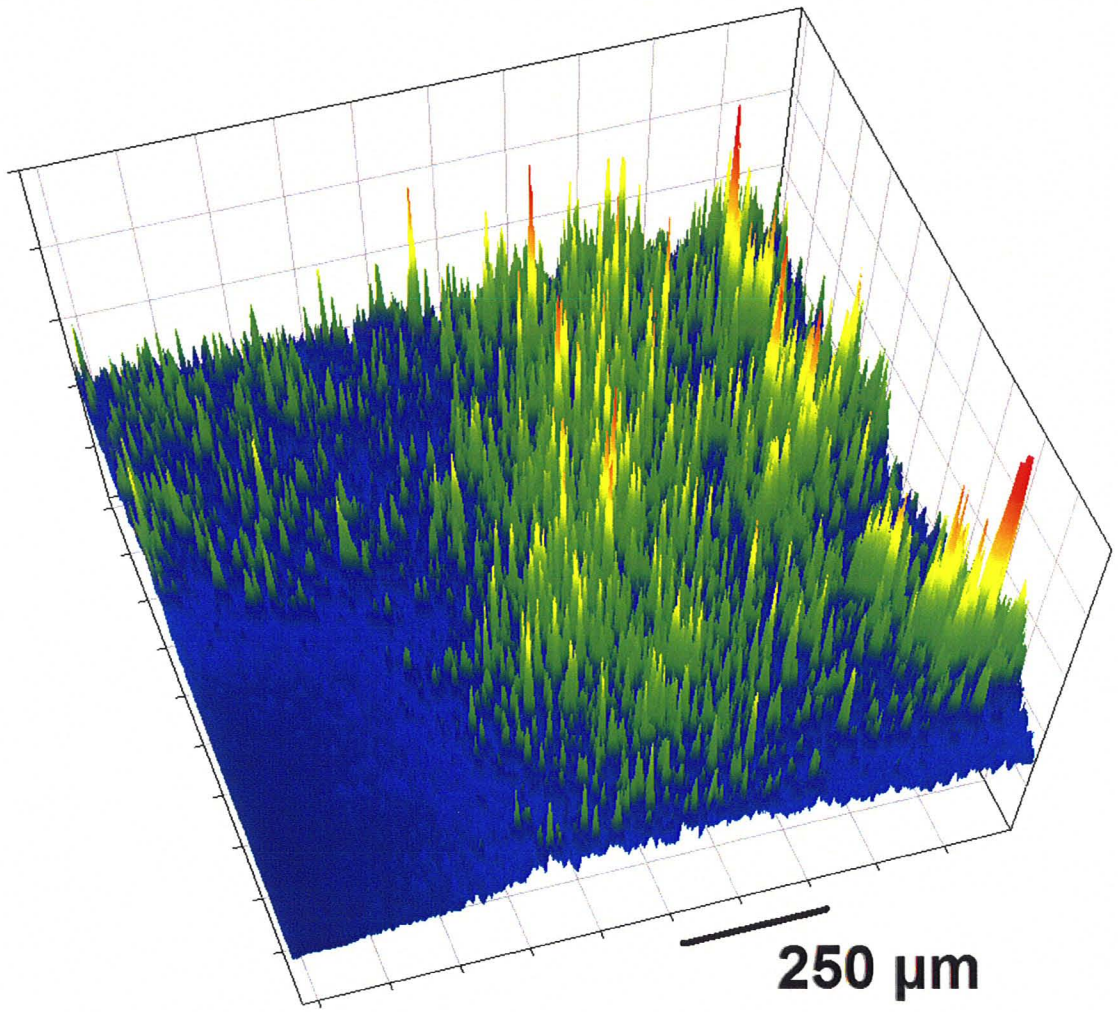

(g) t = 696 s

Figure 3.12 2D and 3D intensity profiles showing the progression of a partially spatially incoherent light modulation instability experiment, with a spatial coherence length of 15 ± 2 µm. (a) shows the beam under linear conditions (that is, in air), when the diffuser in stationary, (b) the beam in air with the diffuser rotating, (c) at the start of the experiment, time, t = 0 s, (d) t = 306 s, (e) t = 558 s, and (f) t = 696 s, 2D, (g) 3D.

Table 3.12 Summary of results for the 532 nm wavelength experiments with a spatial coherence length of 15 ± 2 µm

Trial	1	2	3
Time elapsed (s)	696	1296	858
Age of sol (days)	2	2	2
Cuvette material*	Glass	Glass	Plastic
# of spots measured	100	100	100
Average spot diameter (µm)	9.6 ± 0.9	10 ± 1	9.8 ± 0.9

*Note: Experiments performed in plastic tend to exhibit greater ordering of the self-trapped filaments, due to noise imposed by striations present on the faces of the plastic cuvettes.

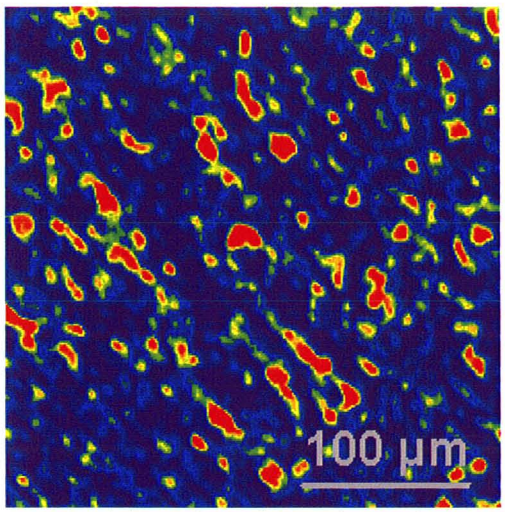

(a) t = 0 s (air, stationary)

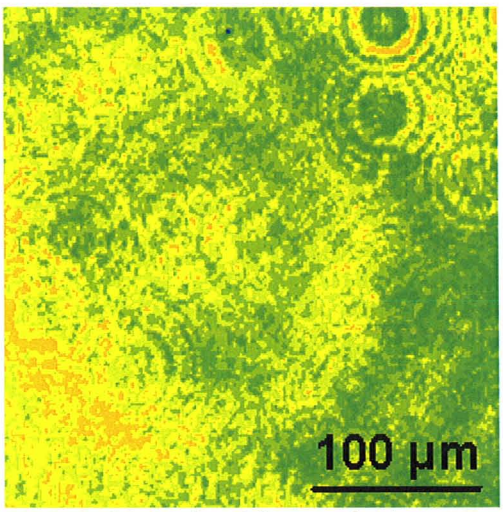

(b) t = 0 s (air, rotating)

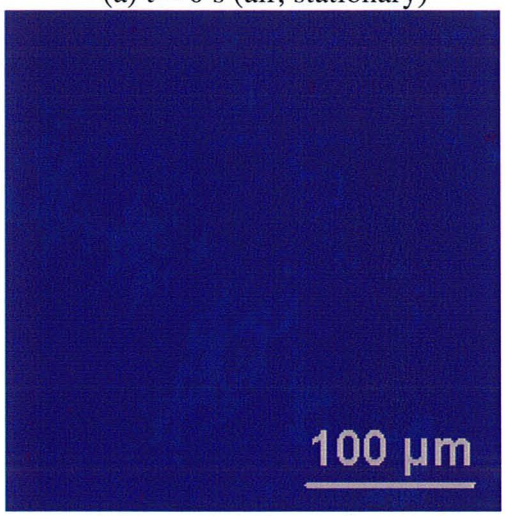

(c) t = 0 s (sol)

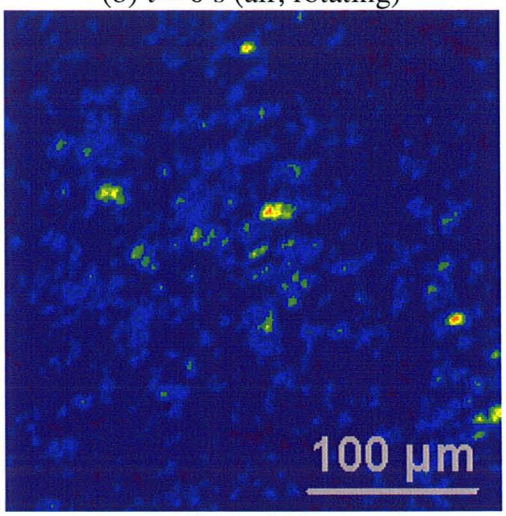

(d) t = 210 s

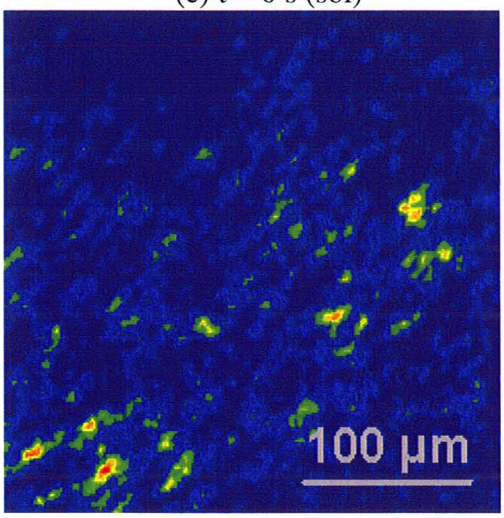

(e) t = 312 s

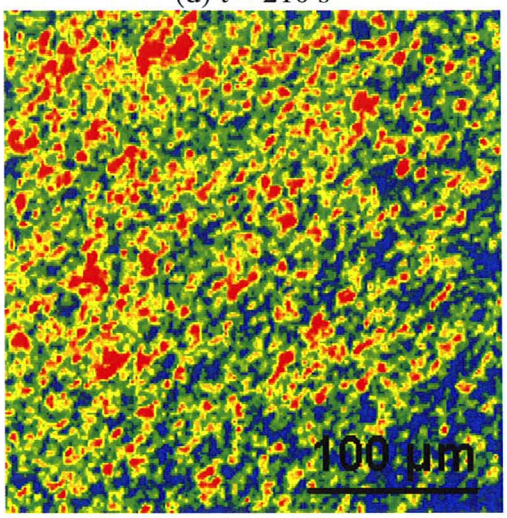

(f) t = 702 s

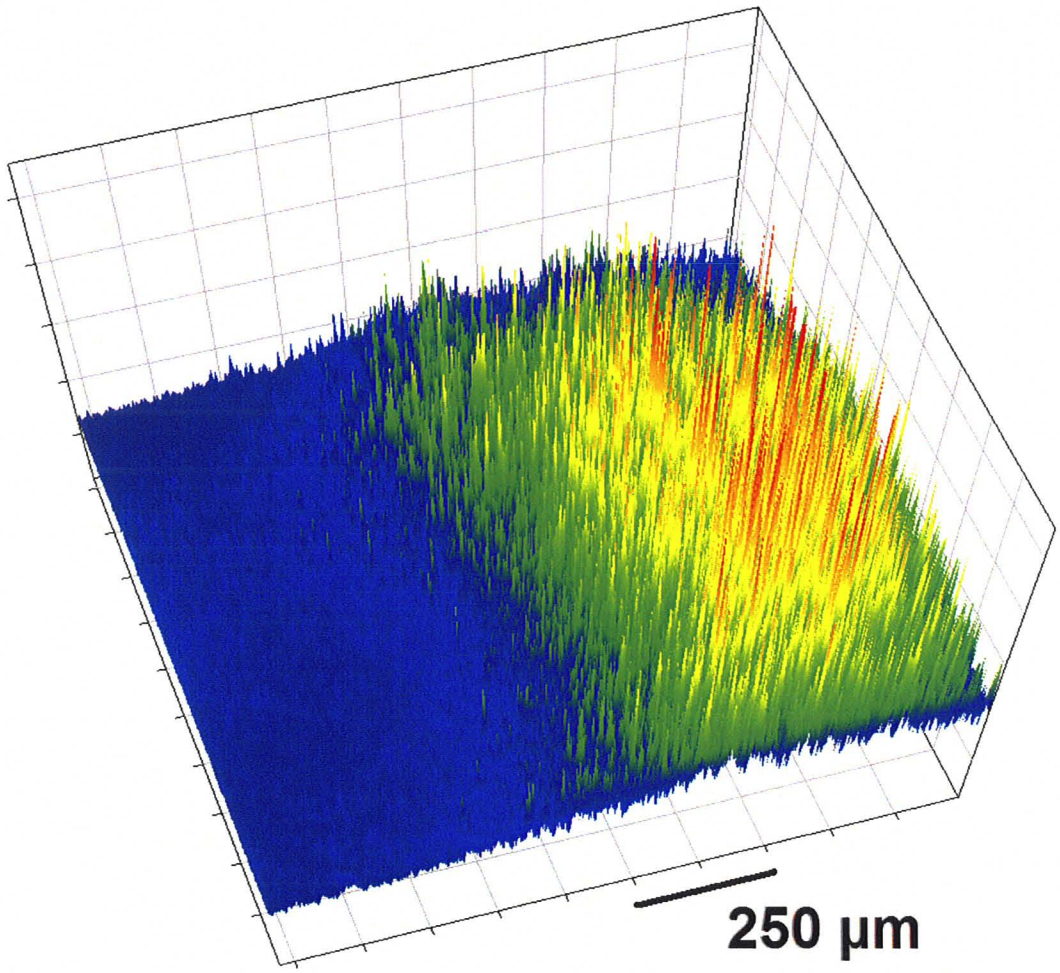

(g) t = 702

Figure 3.13 2D and 3D intensity profiles showing the progression of a partially spatially incoherent light modulation instability experiment, with a spatial coherence length of 11 ± 1 µm. (a) shows the beam under linear conditions (that is, in air), when the diffuser in stationary, (b) the beam in air with the diffuser rotating, (c) at the start of the experiment, time, t = 0 s, (d) t = 210 s, (e) t = 312 s, and (f) t = 702 s, 2D, (g) 3D

Table 3.13 Summary of results for the 532 nm wavelength experiments with a spatial coherence length of 11 ± 1 µm

Trial	1	2	3	4
Time elapsed (s)	702	2664	702	768
Age of sol (days)	1	3	1	1
Cuvette material*	Glass	Plastic	Plastic	Glass
# of spots measured	100	100	100	100
Average spot diameter (µm)	13.2 ± 0.9	14 ± 1	13.6 ± 0.9	13.3 ± 0.8

*Note: Experiments performed in plastic tend to exhibit greater ordering of the self-trapped filaments, due to noise imposed by striations present on the faces of the plastic cuvettes.

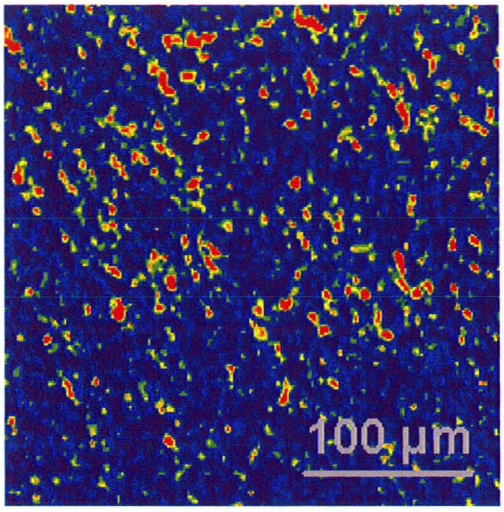

(a) t = 0 s (air, stationary)

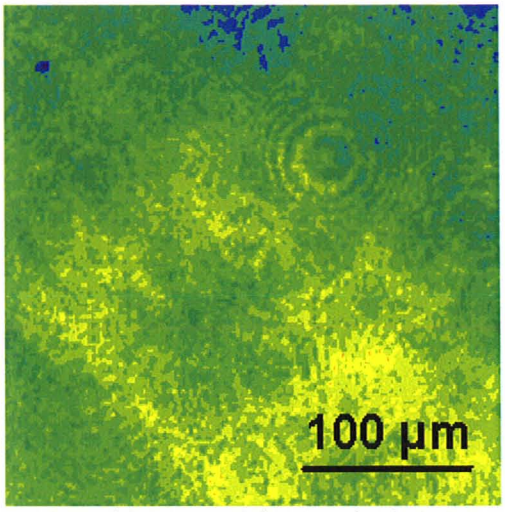

(b) t = 0 s (air, rotating)

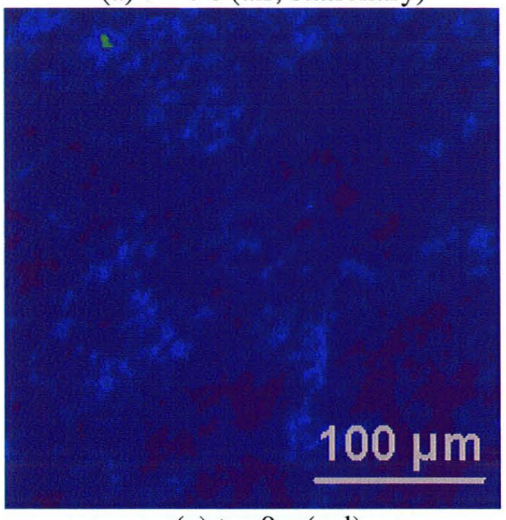

(c) t = 0 s (sol)

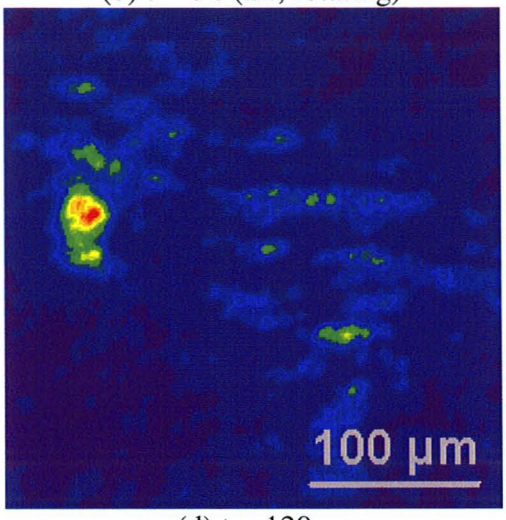

(d) t = 120 s

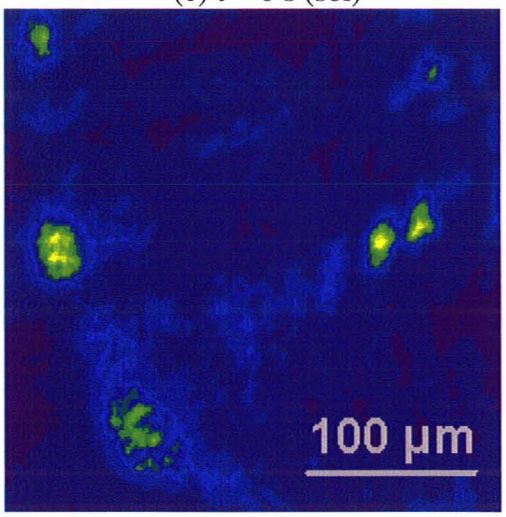

(e) t = 438 s

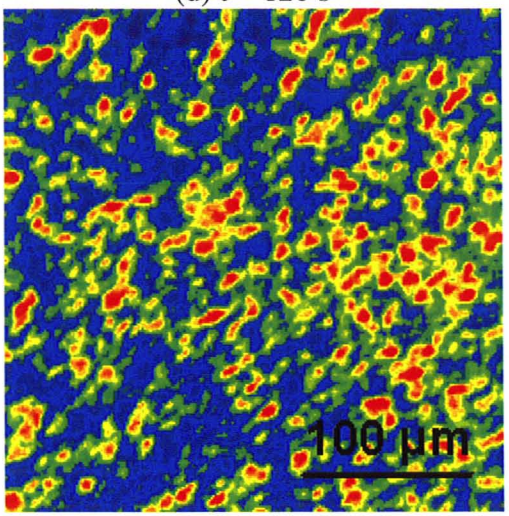

(f) t = 2106 s

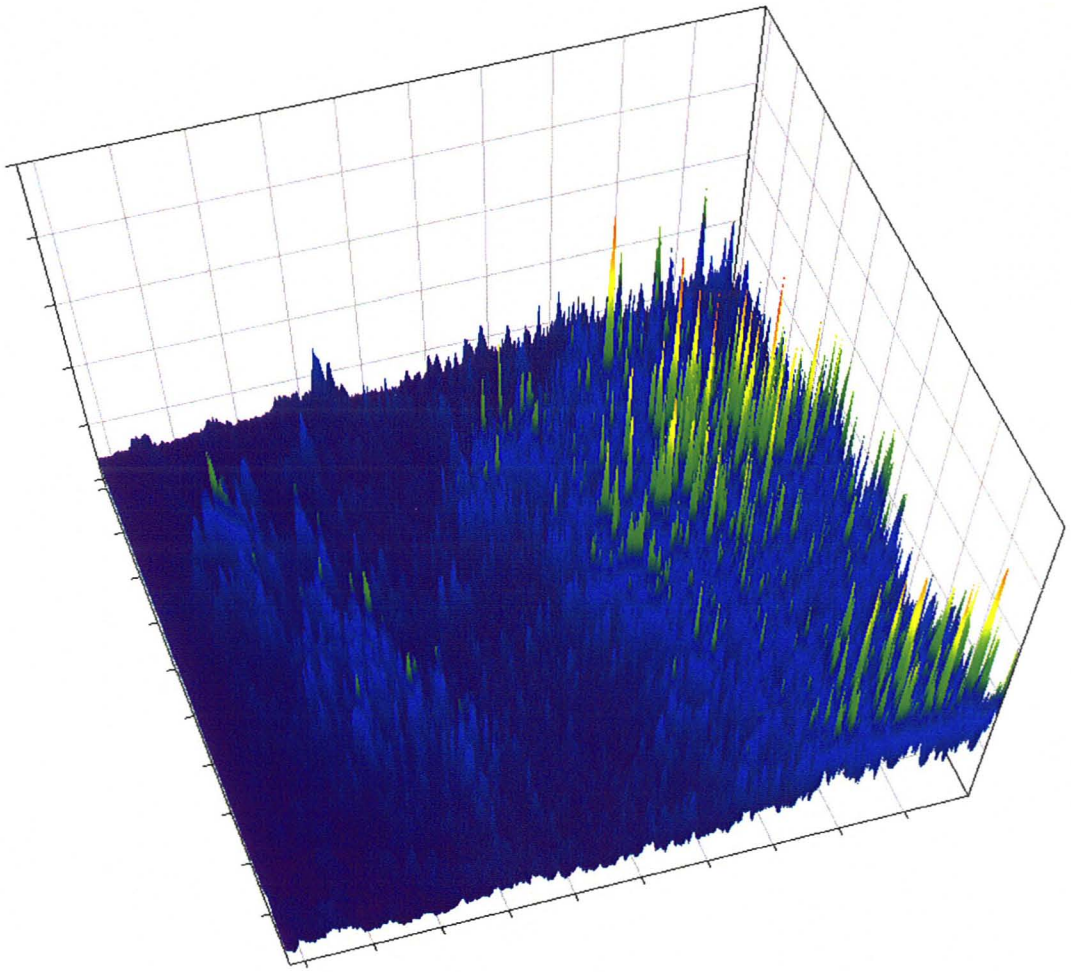

(g) t = 2106 s

Figure 3.14 2D and 3D intensity profiles showing the progression of a partially spatially incoherent light modulation instability experiment, with a spatial coherence length of 6 ± 1 μm. (a) shows the beam under linear conditions (that is, in air), when the diffuser in stationary, (b) the beam in air with the diffuser rotating, (c) at the start of the experiment, time, t = 0 s, (d) t = 120 s, (e) t = 438 s, and (f) t = 2106 s, 2D, (g) 3D.

Table 3.14 Summary of results for the 532 nm wavelength experiments with a spatial coherence length of 6 ± 1 μm

Trial	1	2	3	4
Time elapsed (s)	2106	684	666	300
Age of sol (days)	3	3	3	3
Cuvette material*	Glass	Plastic	Glass	Plastic
# of spots measured	100	100	100	100
Average spot diameter (μm)	16 ± 2	16.6 ± 0.9	16 ± 1	16 ± 2

*Note: Experiments performed in plastic tend to exhibit greater ordering of the self-trapped filaments, due to noise imposed by striations present on the faces of the plastic cuvettes.

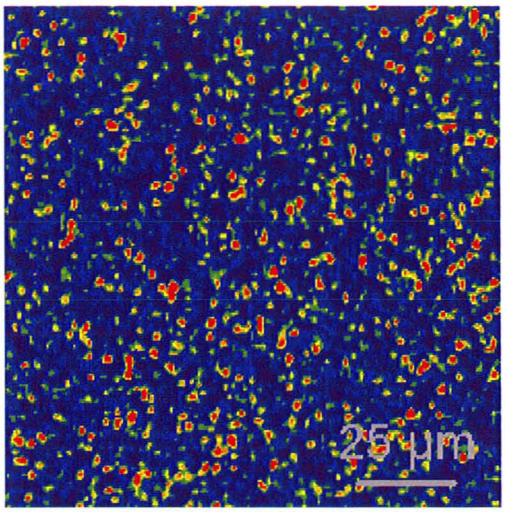

(a) t = 0 s (air, stationary)

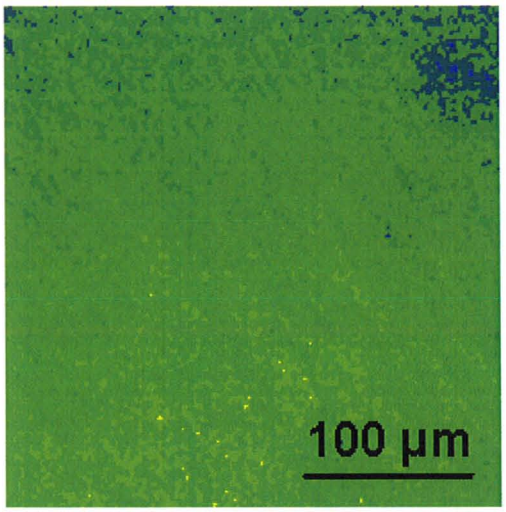

(b) t = 0 s (air, rotating)

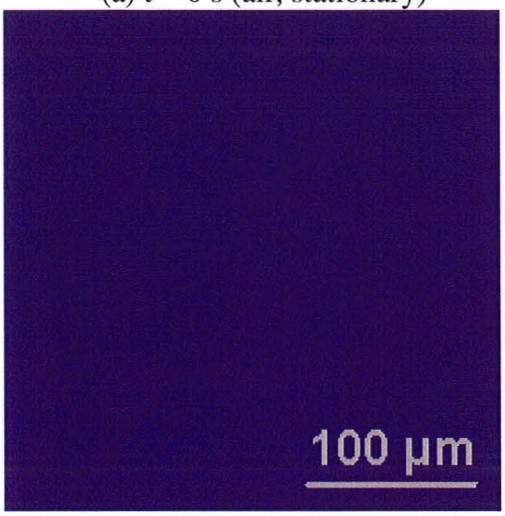

(c) t = 0 s (sol)

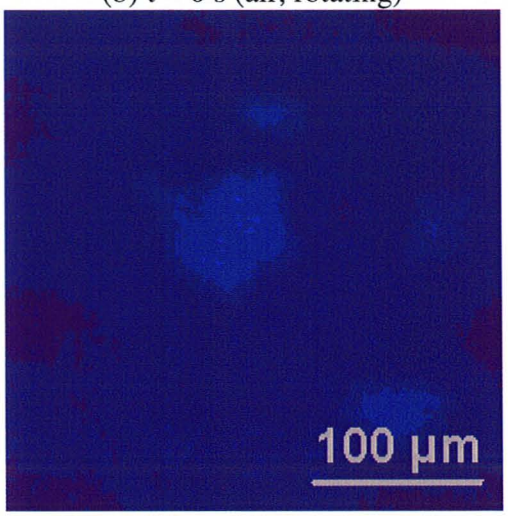

(d) t = 30 s

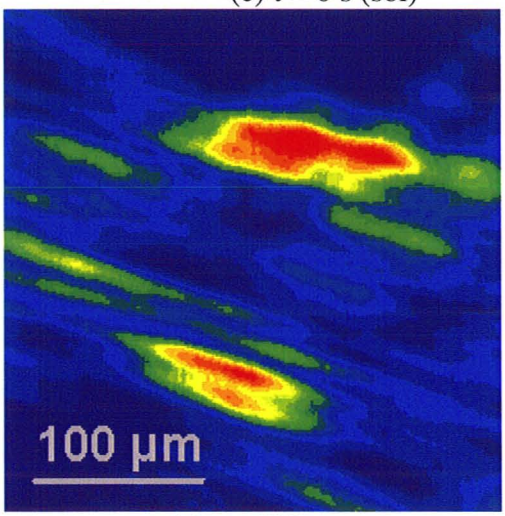

(e) t = 528 s

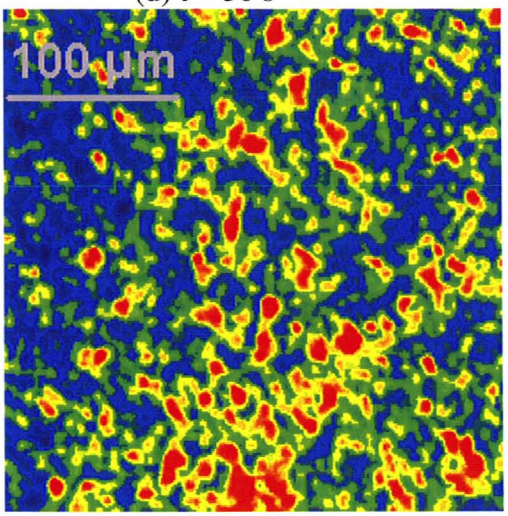

(f) t = 1506 s

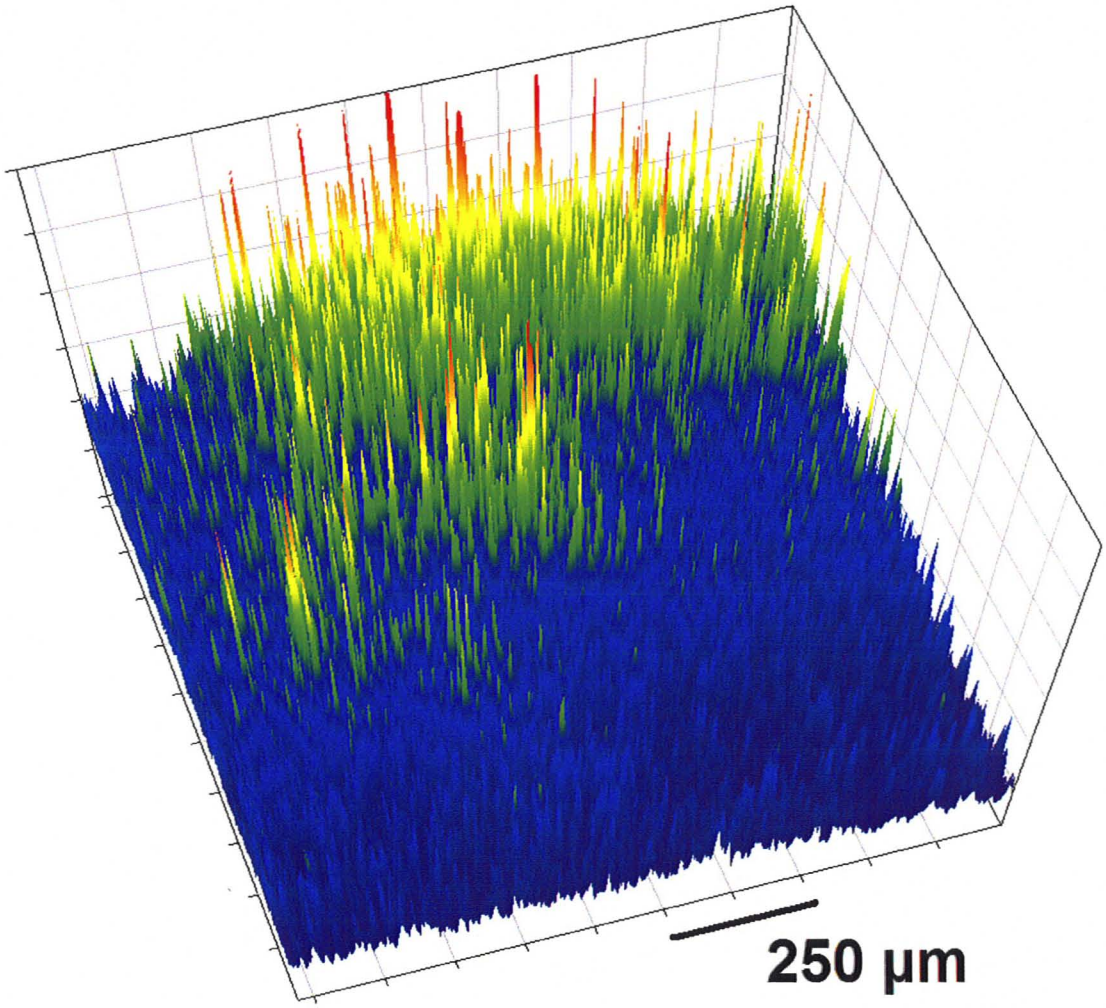

(g) t = 1506 s

Figure 3.15 2D and 3D intensity profiles showing the progression of a partially spatially incoherent light modulation instability experiment, with a spatial coherence length of 1.3 ± 0.2 µm. (a) shows the beam under linear conditions (that is, in air), when the diffuser in stationary, (b) the beam in air with the diffuser rotating, (c) at the start of the experiment, time, t = 0 s, (d) t = 30 s, (e) t = 528 s, and (f) t = 1506 s, 2D, (g) 3D.

Table 3.15 Summary of results for the 532 nm wavelength experiments with a spatial coherence length of 1.3 ± 0.2 µm

Trial	1	2	3
Time elapsed (s)	1506	1716	1206
Age of sol (days)	3	3	3
Cuvette material*	Plastic	Glass	Glass
# of spots measured	100	100	100
Average spot diameter (µm)	18 ± 2	18 ± 1	18 ± 1

*Note: Experiments performed in plastic tend to exhibit greater ordering of the self-trapped filaments, due to noise imposed by striations present on the faces of the plastic cuvettes.

As with the 488 nm experiments, these 532 nm wavelength experiments demonstrate modulation instability. At every coherence length, the light field exhibits an increase in intensity due to the nonlinearity generated by the photopolymerisation reaction. Following this, is the division of the beam into an array of approximately identical spots, each of which represents a self-trapped beam. The resulting data shows a trend in the diameter of these self-trapped filaments that is dependent on the spatial coherence length of the incident beam.

The data from these experiments is summarised in the following table. The degree of spatial incoherence, calculated from the spatial coherence length using equation [1-5], $\theta_0 = \frac{\sqrt{2\pi}}{kl_c}$, and the filament frequency, calculated from equation [1-6], $\alpha = \frac{2\pi}{FD}$, are included, as well.

Table 3.16 Summary of 532 nm wavelength data

Spatial coherence length (μm)	Self-trapped filament diameter (μm)	Degree of spatial incoherence, θ_0	Filament Frequency, α (μm^{-1})	Average time elapsed (s)
∞	6.1 ± 0.6	0	1.0 ± 0.1	3162 ± 535
46 ± 5	7.7 ± 0.9	0.0032 ± 0.0004	0.8 ± 0.1	2532 ± 366
25 ± 2	8 ± 1	0.0058 ± 0.0004	0.74 ± 0.09	1062 ± 140
15 ± 2	10 ± 1	0.009 ± 0.001	0.64 ± 0.06	950 ± 310
11 ± 1	13 ± 1	0.014 ± 0.001	0.47 ± 0.03	724 ± 38
6 ± 1	16 ± 1	0.024 ± 0.003	0.39 ± 0.03	550 ± 217
1.3 ± 0.2	18 ± 1	0.11 ± 0.02	0.35 ± 0.03	1476 ± 256
*0.3	75 ± 5	0.485	0.084 ± 0.006	N/A

*White light experiments[22]

From this data, it is evident that a decrease in spatial coherence length results in an increase of self-trapped filament diameter. The relationship between degree of spatial incoherence and the filament frequency can be further characterized by plotting the experimental data, and comparing it with the theoretical curve. The theoretical curve was generated by calculating theoretical filament frequency, α values, using a rearrangement of equation [1-4] (as with the 488 nm data): equation[3-1], for each of the incoherence, θ, values studied at the 532 nm wavelength. This theoretical curve can be seen in the following figure (in red), along with the corresponding experimental data (in blue). The theoretical curve was fit using a scaling as well as a displacement factor, determined using the least squares method.

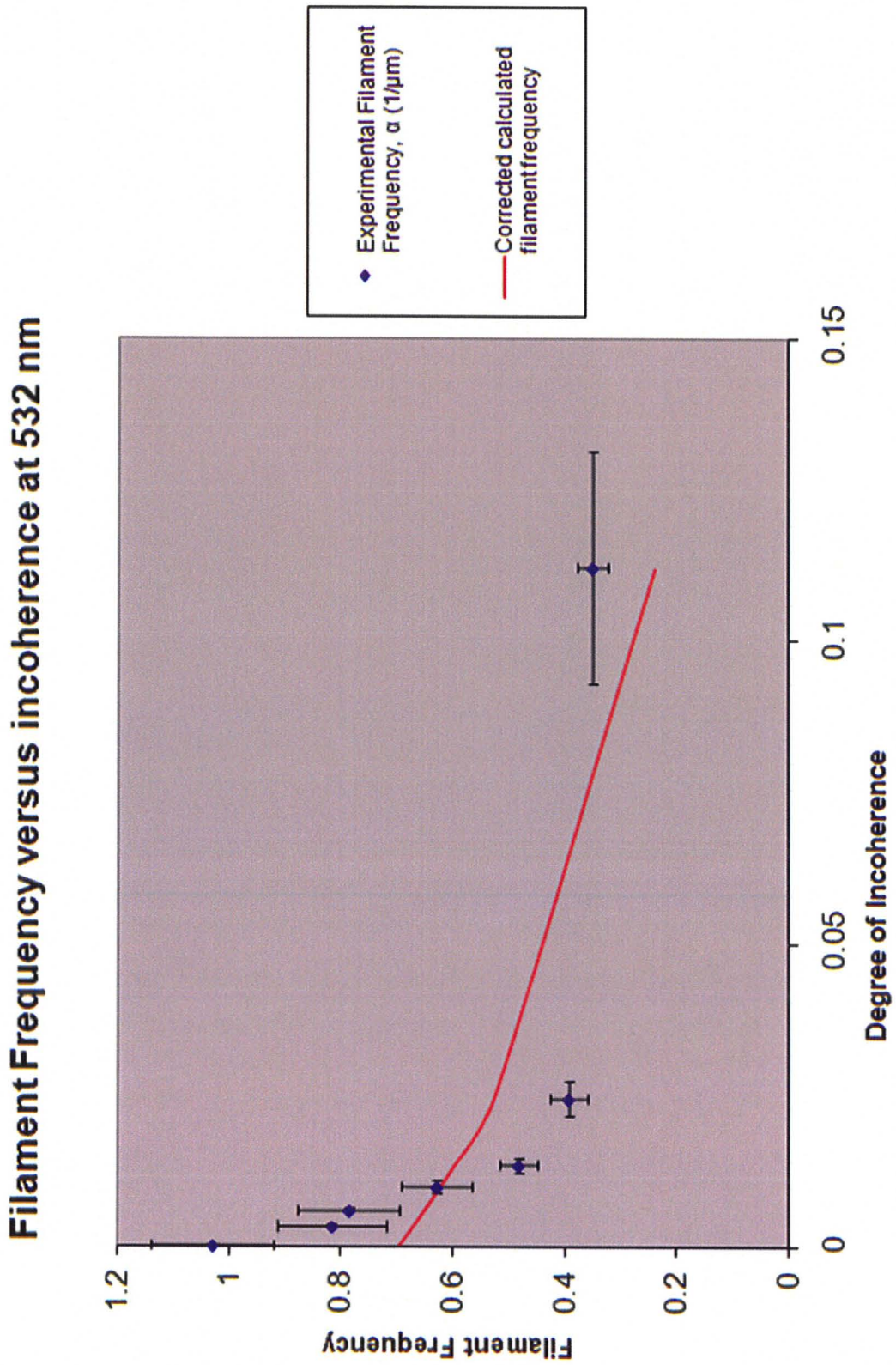

Figure 3.16 Plot of filament frequency versus degree of spatial incoherence for wavelength 532 nm

Here, both the theoretical and the experimental curves display a decrease in the filament frequency as the degree of incoherence becomes larger. The experimental data, however, shows a more pronounced inverse relationship than the theoretical curve, which takes much longer to level off. The fit of the theoretical curve, if the final point is excluded is much closer with respect to the data at smaller degrees of spatial incoherence, indicating that the deviation between theoretical and experimental data is larger at higher degrees of incoherence.

In addition to the relationship between filament diameter and spatial coherence length, a relationship can also be drawn between the self-trapped filament diameter and the wavelength of the incident light. Comparing the data from the 488 nm experiments (**Table 3.8**), to that of the 532 nm wavelength (**Table 3.16**), there is a trend that for corresponding degrees of incoherence, where as the wavelength increases, there is a decrease in the diameter of the resulting self-trapped filaments.

As with the 488 nm experiments, again there is a trend visible for not only the self-trapped filament diameter, but also the timing of the transition of the beam into individual self-trapped filaments due to the modulation instability process, dependant on the spatial coherence of the beam. The trend seen here also appears to be that this transition takes longer when the beam is more coherent.

3.3 Control experiment - modulation instability with speckled beam (stationary diffuser)

A control experiment was employed for the purposes of this study. This involved determining what occurred when the modulation instability experiments were done with the coherent laser light passing through a stationary diffuser – that is a multitude of coherent light speckles. This was done for two of the coherence lengths selected for this study: 27 ± 6 μm, and 45 ± 9 μm.

In contrast to the coherent light experiments, no convection appeared, and thus there was no noise along which preferential filamentation could occur. Each of the stationary diffuser experiments – at both coherence lengths – showed speckles that emerged without the appearance of one-dimensional stripes. Significant images exhibiting the 2D speckles are shown in **figure 3.17**.

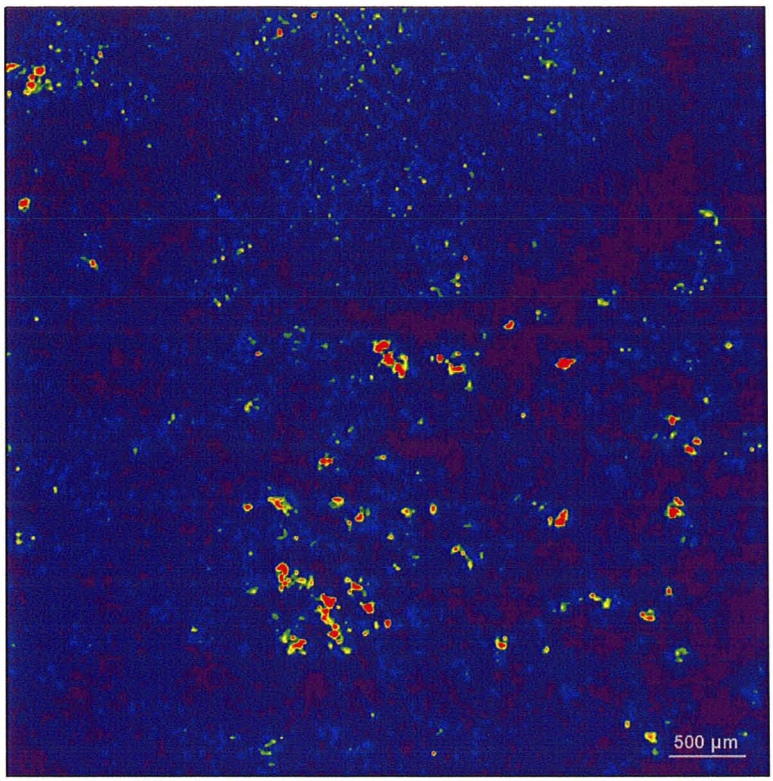

Figure 3.17 Modulation instability in a broad beam of coherent light speckles – with a stationary diffuser, a wavelength of 488 nm and a coherence length of 45 ± 9 µm, t = 1872 s.

Like the intensity profiles under linear conditions (as shown in **Figure 2.3**), the distributions of intensity under nonlinear conditions follows the same trend, where the shorter the coherence length, the more concentrated the spots are. With the longer coherence length, the speckles are again more widely distributed. Like with the experiments in the purely coherent light, the speckles were again measured for each trial. These results are summarised in **Table 3.17**.

Table 3.17 Modulation instability with coherent laser light speckles – stationary diffuser - experiment summary

Trial	1	2	3
Diffuser-cuvette separation distance (cm)	2.5	5.0	5.0
Coherence length (μm)	27 ± 6	45 ± 9	45 ± 9
Time elapsed (s)	2532	1608	1872
Age of sol used (days)	2	1	1
Cuvette material	Glass	Glass	Glass
# of spots measured	150	150	150
Average spot diameter (μm)	18 ± 4	15 ± 4	15 ± 4

It is clear from these results that the resulting intensity distribution is composed of clusters the size of the incident spots, some of which have divided further into smaller speckles which more closely resemble the filament diameter seen in the purely coherent case. This leads to an average speckle size which is between the size of the coherent speckle, and the self-trapped filament diameter seen in coherent light modulation instability. This reinforces the necessity of the rotation of the diffuser, as it is important for the photopolymerisable organosiloxane to experience the time-averaged profile of the beam rather than the individual speckles of coherent light.

3.4 Relating the optical profile to the physical structure – micrographs

As mentioned previously, the self-trapped filaments, which are represented in the optical intensity profiles seen in the above experiments, become indelibly inscribed in the nonlinear medium, resulting in a permanent physical structure in the photopolymer. These filaments appear as cylindrical waveguides as demonstrated in the following illustration.

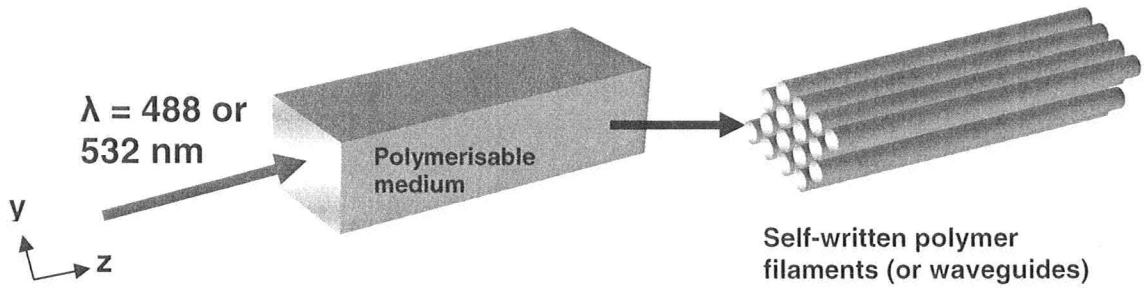

Figure 3.18 Schematic describing the formation of cylindrical waveguides within the photopolymerisable organosiloxane.

As the spatial coherence has a direct influence on the polymer microstructure, it is therefore important to quantify the structure of the polymer medium. This is done by analysing micrograph images of the samples after they have been removed from the partially spatially incoherent light source. As a result, the cylindrical waveguides imprinted in the medium are visible, and can be measured to verify that these physical structures are equivalent to the optical intensity profiles acquired as the waveguides formed. Selected micrographs are shown in the following figures, paired with the corresponding transverse (to the direction of light – and waveguide – propagation) optical intensity profiles.

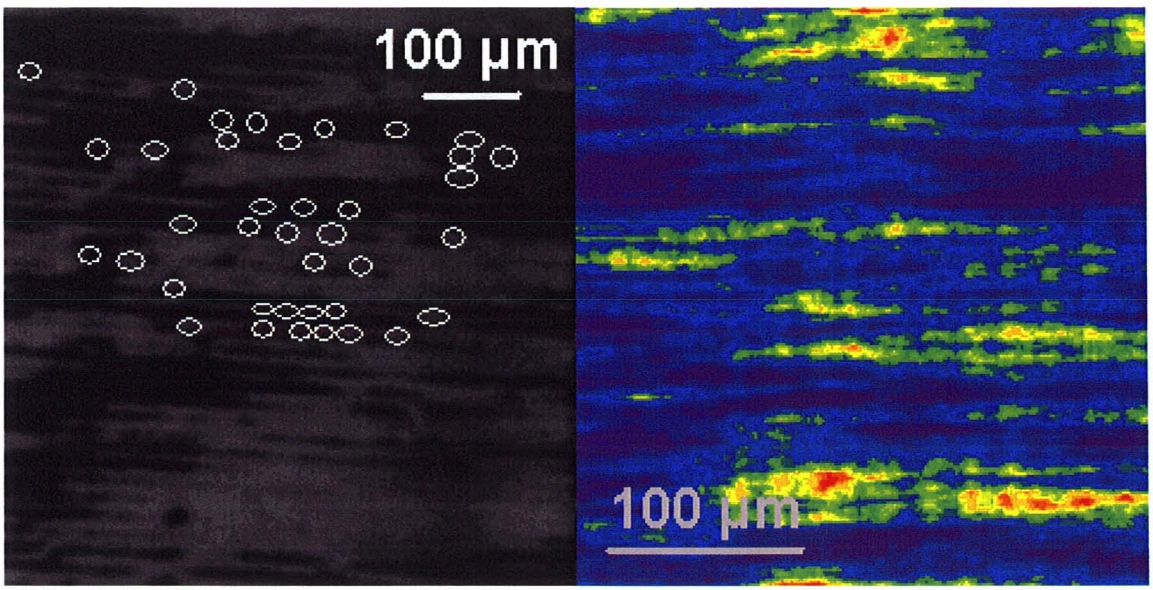

Figure 3.19 Micrograph (transverse cross-section) showing physical structure (left) and intensity profile showing optical structure (right) of a sample of the nonlinear medium after polymerization has induced the formation of waveguides. Wavelength of incident light is 488 nm, and the spatial coherence length is infinite.

Figure 3.19 shows the optical intensity profile of a sample irradiated with purely spatially coherent light with a wavelength of 488 nm, and the corresponding polymer microstructure. Both images appear similar, with a series of stripes running from left to right (this pattern is the result of the influence of striations on the plastic wall of the cuvette which contained the sample during the modulation instability process). These stripes are composed of spots which are able to guide light even after being removed from the incident light source. Measuring the spot diameters for both the optical and physical structures results in identical diameters for the self-trapped filaments – that is, approximately 7 µm. This provides evidence that the nonlinearity is permanently inscribed within the polymer, and thus, that the spatial coherence length of light provides a means to significantly control the polymer microstructure directly.

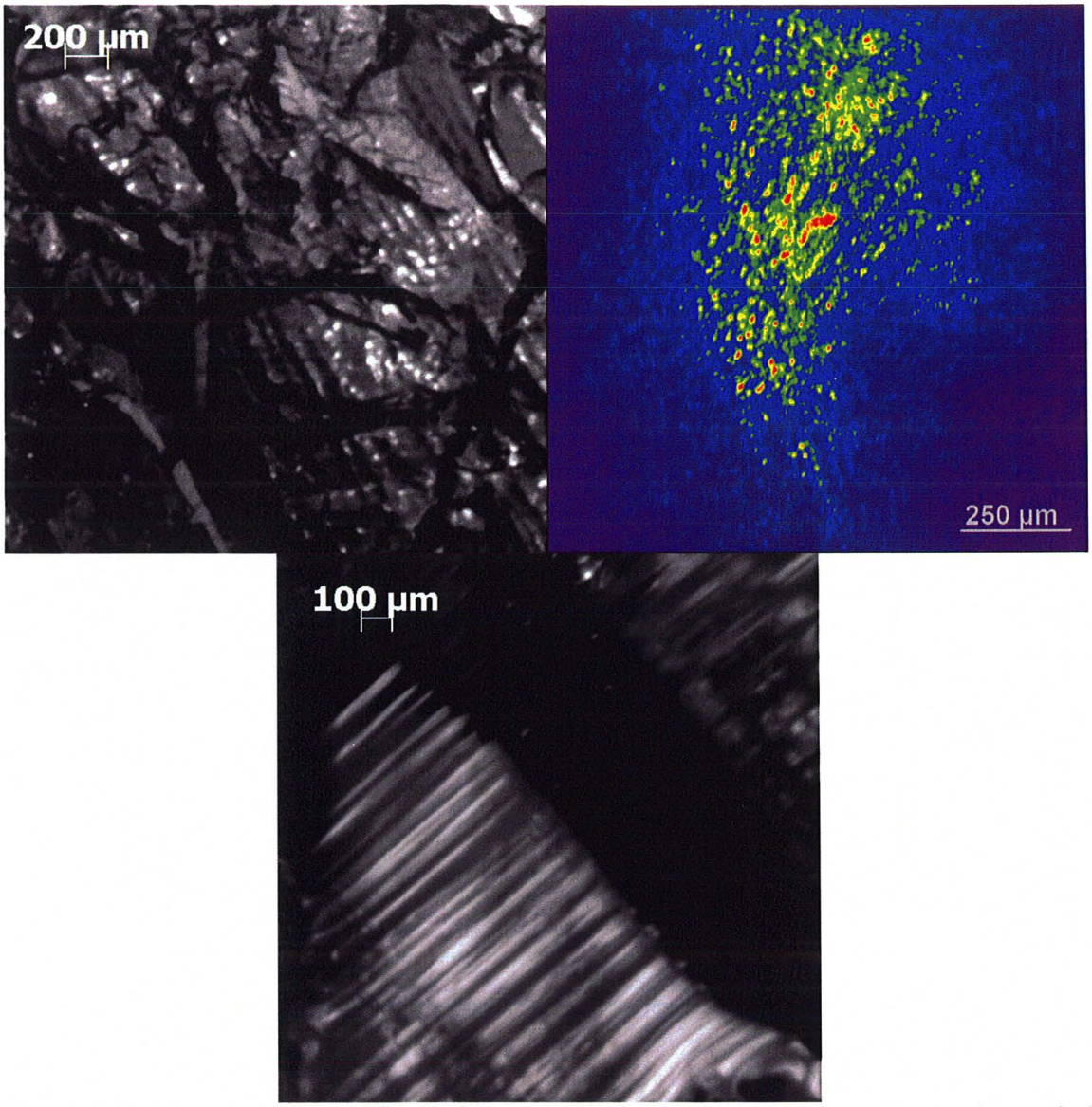

Figure 3.20 Micrograph showing physical structure (top left) and intensity profile showing optical structure (top right) of a sample of the nonlinear medium after polymerization has induced the formation of waveguides, in the plane transverse to the direction of beam propagation.
Bottom: Micrograph showing the physical structure of the self-trapped filaments propagating through the polymer medium. The direction of the filaments is on a diagonal, from bottom left, to top right. This is a (longitudinal) side view of the filaments seen in top left and top right. Wavelength of incident light is 488 nm, and the spatial coherence length is 34 µm.

All of the optical and physical profiles seen in **Figure 3.20** exhibit filaments approximately 15 µm in diameter. The waveguide structure can be further elucidated by examining a longitudinal view of the waveguides – that is, along the direction of

propagation. In this way, the cylindrical nature of the self-trapped beams becomes more evident. The third micrograph, which shows the longitudinal cross-section of the medium, (along the direction of beam propagation) demonstrates the cylindrical structure of the self-trapped filament waveguides. Measuring the width of the self-trapped beams as viewed from the side results in diameters that are commensurate to those measured in the transverse cross-section, as well as in the optical intensity profile.

Micrographs from the 532 nm wavelength experiments demonstrate the same relationship between optical profile, and physical structure. This can be seen in the following figure, in which both the physical and optical images show self-trapped filaments with an average diameter of approximately ten microns.

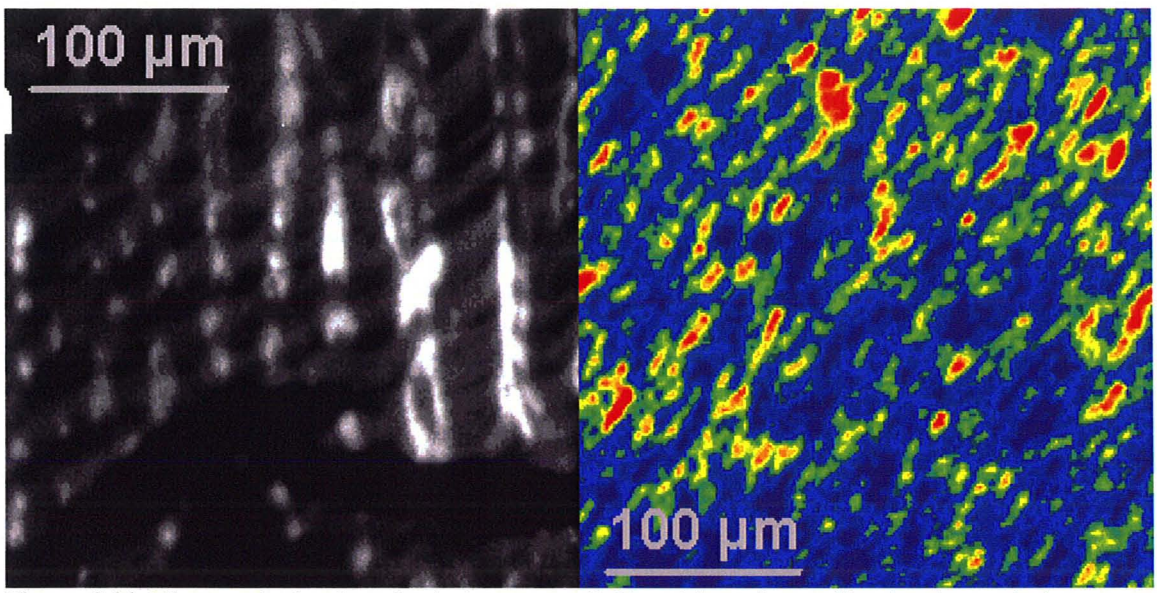

Figure 3.21 Micrograph showing physical structure (left) and intensity profile showing optical structure (right) of a sample of the nonlinear medium after polymerisation has induced the formation of waveguides. Wavelength of incident light is 532 nm, and the spatial coherence length is 25 ± 2 microns.

These results are significant, as they imply that the microstructure of polymers can be controlled directly by the characteristics of the light field – wavelength and spatial coherence length – using modulation instability. This is important as it is the first time that an experimental study of coherence-dependence has been applied to modulation instability in a photopolymerisable system. In addition, the results from this research have potential applications in the formation of photonic crystals. Using an optical mask to generate a periodic structure, in addition to this established diameter control via tuning of the spatial coherence, allows for complete control of the filament structure within the polymer, the consequence of which is the ability to create photonic crystals with very precise bandgaps. Typically, these periodic patterns have been produced using several mutually coherent beams, whereas this study provides a much simpler way to generate controlled optical structures.

4. Conclusions and Future Work

Modulation instability of partially spatially incoherent laser light at 488 nm was studied in a photopolymerisable organosiloxane. A rotating diffuser was used so that the photopolymer responded to a time-averaged version of the optical field. Refractive index changes due to polymerisation elicited a spontaneous division of the broad beam into multiple self-trapped filaments of light. By tuning the incoherence of the beam from 11 μm to 86 μm, it was possible to control the diameter of the filaments from 7 μm to 21 μm. Experiments were repeated at 532 nm. A similar trend was found where by tuning the incoherence of the optical field from 1.3 μm to 46 μm, it was possible to obtain filament diameters ranging from 6.1 μm to 18 μm.

These trends are consistent with a previously developed theoretical model relating filament frequency to spatial incoherence.[40,44] Specifically, tuning the degree of spatial incoherence to higher values (becoming increasingly incoherent) results in an overall decrease in the filament frequency, which is represented as an increase in the diameter of the self-trapped beams. Moreover, an increasing in the wavelength of the optical field results in smaller self-trapped filaments, which is also consistent with the theoretical model.

Refractive index changes due to modulation instability were irreversibly imprinted in the organosiloxane. Micrographs of the photopolymer show an array of self-

induced waveguides, each inscribed by a self-trapped filament of light. The diameters of the waveguides were commensurate with the diameters of the self-trapped filaments. The dependence of modulation instability on the incoherence of the optical field can in this way be exploited to tune polymer microstructure.

Future studies can examine this dependence further to precisely control the microstructure and array of self-induced waveguides in the photopolymer. Previous studies with incoherent white light demonstrated that precise positioning of self-induced waveguides could be achieved by introducing controlled noise with an optical mask. In this way, it was possible to create 2-D and 3-D periodic arrays of self-induced waveguides. Similar approaches could be used with the system examined in this thesis to create a wide variety of ordered structures with tunable periodicities. Such microperiodic structures have potential applications as linear and nonlinear photonic crystals.

5. Appendices

List of Figures and Tables

Appendix A

Introduction to optical waveguide theory

A waveguide is a structure that is capable of transmitting electromagnetic waves with minimal loss of signal. These structures are composed of two or more materials with different dielectric constants (and thus, different refractive indices). Due to this refractive index disparity, the waveguide is able to confine the electromagnetic wave to the region with the highest refractive index. This is possible due to total internal reflection, where the light that enters the region of higher refractive index is unable to pass into the lower index regions, due to the incident angle of the light being greater than that of the critical angle.[2, 46, 47, 48] The refractive index of a material describes the extent to which the velocity of the light decreases, as it enters the given material. It is defined by the following equation:[49]

$$n = \frac{c}{v} \qquad [A\text{-}1]$$

In this formula, n is the refractive index of the medium in question, c is the speed of light in a vacuum, 299 792 458 m/s[14], and v is the velocity of light in the medium.

Two common geometries of waveguide are the slab waveguide, and the fibre waveguide.[2, 46, 47, 48] The slab waveguide, also known as a planar waveguide, is composed of three layers of differing refractive index materials.

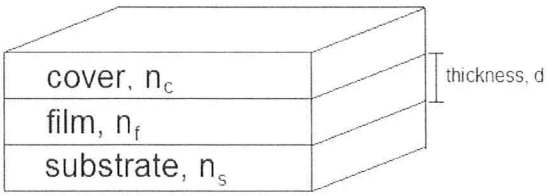

Figure A.1 Basic structure and refractive index profile of the optical planar waveguide[2, 47, 48]

These layers consist of a film – the region of highest refractive index, n_f, sandwiched between two layers – the substrate on the bottom, and the cover on the top – with lower refractive indices – n_s and n_c, respectively. If the refractive indices of the cover and the substrate are equivalent, $n_s = n_c$, then the planar waveguide is said to be symmetric. Otherwise the waveguide is asymmetric. Often, the cover material is simply air, $n_c = 1.000293$[50].

As light enters the film region of the slab waveguide, it may be unable to exit into the substrate or cover regions due to total internal reflection. This only occurs when the angle of incidence (as the light approaches the film/cover, or the film/substrate interface) is greater than the critical angle for the given boundaries. Critical angle is defined as follows:

$$\theta_{critical} = \sin^{-1}\left(\frac{n_2}{n_1}\right) \qquad \text{[A-2]}$$

In the case of an asymmetric planar waveguide, there are two critical angles to consider. First, the critical angle defined for the film/cover interface, and secondly, for the critical angle of the film/substrate interface.

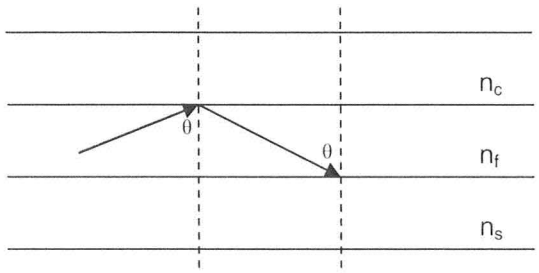

Figure A.2 Schematic showing the path of light rays in an asymmetric planar waveguide[2, 47, 48]

In the above figure, the angle, θ, has to be larger than the critical angles defined as follows, in order for total internal reflection to occur at both the upper and lower boundaries.

$$\theta_{1c} = \sin^{-1}\left(\frac{n_c}{n_f}\right) \qquad \text{and} \qquad \theta_{2c} = \sin^{-1}\left(\frac{n_s}{n_f}\right) \qquad \text{[A-3]}$$

There are three distinct scenarios that can come out of these equations. The first, where $\theta < \theta_{1c}$, where the light will penetrate both the cover and the substrate. This result in a radiation modes, which are not guided. The second situation occurs when $\theta_{1c} < \theta < \theta_{2c}$. This results in total internal reflection at the upper boundary, but penetration of light into the substrate, which is referred to as a substrate mode. The final example occurs when $\theta_{1c} < \theta > \theta_{2c}$, resulting in total internal reflection at both interfaces, and thus confinement of light in the central region. In order to achieve a guided mode, it is necessary to have this total internal reflection at both boundaries, as well as to have constructive interference of the light wave which occurs only at select discrete angles of propagation.

This means that the conditions for a guided mode also depend on the phase shift – or Goos Hänchen shift – that exists for the totally reflected light - which must be an integral multiple of 2π. This phase shift, Φ, depends on k_x, or lateral component of the wavevector, k_o, as well as on the thickness of the film, d, and on the phase shifts of total internal reflection at the upper (Φ_c), and lower (Φ_s) boundaries.[48]

$$\Phi = 2k_x d = 2k_o n_f d \cos\theta \qquad \text{[A-4]}$$

$$2k_o n_f d \cos\theta - \Phi_c - \Phi_s = 2\pi m \qquad \text{[A-5]}$$

The integral multiple of 2π, called m, in equation 1-8, is the mode order. The minimum allowed angle θ, that satisfies equation [A-5], corresponds to the fundamental mode, $m = 0$. Higher order modes (where $m \geq 1$), occur with larger angles. Each accessible mode can be described by its propagation vector, β_m.[48]

$$\beta_m = k_o n_f \sin\theta_m \qquad \text{[A-6]}$$

In which θ_m is the angle of a given mode, m.

The following figure shows the fundamental and first order modes of a planar waveguide.

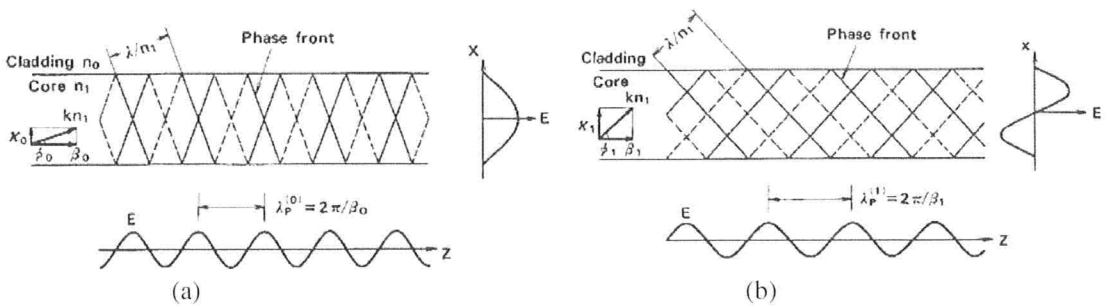

(a) (b)

Figure A.3 The formation of modes (a) the fundamental mode (m=0), and the first higher order mode (m=1)[48] Reprinted from Fundamentals of Optical Waveguides, 2nd edition, Katsunaro Okamoto, Chapter 1 - Wave Theory of Optical Waveguides, page 12, 2006, with permission from Elsevier.

The wave equations for optical waveguides can be described using Maxwell's equations.[46, 47, 48, 51]

$$\nabla \times \mathbf{E} = -\mu \frac{\partial \mathrm{H}}{\partial t} \qquad \text{[A-7]}$$

$$\Delta \times \mathbf{H} = \varepsilon \frac{\partial \mathrm{E}}{\partial t} \qquad \text{[A-8]}$$

The fields described in this equation are the electric field strength, **E**, and the magnetic field strength, **H**. The values μ and ε represent the permeability and permittivity of the medium, respectively.

$$\mu = \mu_0 \qquad \text{[A-9]}$$

$$\varepsilon = \varepsilon_0 n^2 \qquad \text{[A-10]}$$

, where μ_0 and ε_0 correspond to the free space permeability and permittivity respectively, and n is the refractive index. Equations [A-9] and [A-10] can be inserted into [A-7] and [A-8], and the curl of each can be taken. Combining [A-7] and [A-8] into these curl functions and using the vector identity $\nabla \times \nabla \times \mathrm{E} = \nabla(\nabla \cdot \mathrm{E}) - \nabla^2 \mathrm{E}$, the following inhomogeneous wave equations emerge:[46, 47, 48, 51]

$$\nabla^2 \mathrm{E} + \nabla\left(\frac{1}{n^2} \nabla n^2 \mathrm{E}\right) - \varepsilon_0 \mu_0 n^2 \frac{\partial^2 \mathrm{E}}{\partial t^2} = 0 \qquad \text{[A-11]}$$

$$\nabla^2 \mathrm{H} + \frac{1}{n^2} \nabla n^2 \times (\nabla \times \mathrm{H}) - \mu_0 \varepsilon_0 n^2 \frac{\partial^2 \mathrm{H}}{\partial t^2} = 0 \qquad \text{[A-12]}$$

Since a waveguide structure is composed of materials of different refractive indices, the medium is considered to be optically inhomogeneous. This means that its

properties (especially refractive index) are dependent on position. Thus, the inhomogeneous wave equations, [A-11], and [A-12], can be solved for monochromatic waves:[48, 51]

$$E(r,t) = E(x,y)e^{i(\omega t-\beta z)} \qquad \text{[A-13]}$$

$$H(r,t) = H(x,y)e^{i(\omega t-\beta z)} \qquad \text{[A-14]}$$

Where r is the position in the plane transverse to the axis of propagation (z-axis).

These solutions can be combined with Maxwell's equations, [A-7], and [A-8], to obtain the following set of equations describes wave propagation in slab or planar waveguides, in Cartesian coordinates:[48,51]

$$\begin{cases} \dfrac{\partial E_z}{\partial y} + i\beta E_y = -i\omega\mu_0 H_x \\ -i\beta E_x - \dfrac{\partial E_z}{\partial x} = -i\omega\mu_0 H_y \\ \dfrac{\partial E_y}{\partial x} - \dfrac{\partial E_x}{\partial y} = -i\omega\mu_0 H_z \\ \dfrac{\partial H_z}{\partial y} + i\beta H_y = i\omega\varepsilon_0 n^2 E_x \\ -i\beta H_x - \dfrac{\partial H_z}{\partial x} = i\omega\varepsilon_0 n^2 E_y \\ \dfrac{\partial H_y}{\partial x} - \dfrac{\partial H_x}{\partial y} = i\omega\varepsilon_0 n^2 E_z \end{cases} \qquad \text{[A-15]}$$

Another common type of waveguide is the fibre waveguide, which is composed of a core and cladding. In three-dimensional self-trapping, the self-induced waveguide is an optical fibre waveguide.

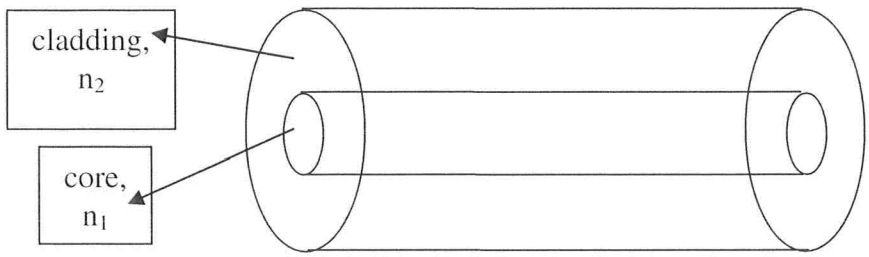

Figure A.4 Basic Structure and refractive index profile for an optical fibre waveguide

Optical fibre waveguides have a cylindrical core, with refractive index, n_1, surrounded by a cladding with refractive index, n_2. These fibre waveguides are very similar to those of the planar waveguides in that they must experience total internal reflection in order to be able to produce guided or propagation modes. Like planar waveguides, the central region must have a higher refractive index than in the exterior region. That is $n_2<n_1$.

For the analysis of wave propagation in optical fibre waveguides – which have cylindrical symmetry – the solutions need to be described by cylindrical coordinates:[48, 51]

$$\begin{cases} \frac{1}{r}\frac{\partial E_z}{\partial \theta} + i\beta E_\theta = i\omega\mu_0 H_r \\ -i\beta E_r - \frac{\partial E_z}{\partial r} = -i\omega\mu_0 H_\theta \\ \frac{1}{r}\frac{\partial}{\partial r}(rE_\theta) - \frac{1}{r}\frac{\partial E_r}{\partial \theta} = -i\omega\mu H_z \\ \frac{1}{r}\frac{\partial H_z}{\partial \theta} + i\beta H_\theta = i\omega\varepsilon_0 n^2 E_r \\ -i\beta H_r - \frac{\partial H_z}{\partial r} = i\omega\varepsilon_0 n^2 E_\theta \\ \frac{1}{r}\frac{\partial}{\partial r}(rH_\theta) - \frac{1}{r}\frac{\partial H_r}{\partial \theta} = i\omega\varepsilon_0 n^2 E_z \end{cases} \quad [A\text{-}16]$$

These expressions produce infinite solutions for the electromagnetic field, so it is important to note that only the solutions which fulfill the boundary conditions are accepted. That is to say that even though there are discontinuities in the refractive indices at the interfaces between substrate/film/cover or core/cladding, the electric fields must remain continuous.

Appendix B

Figures for repeat trials of modulation instability experiments

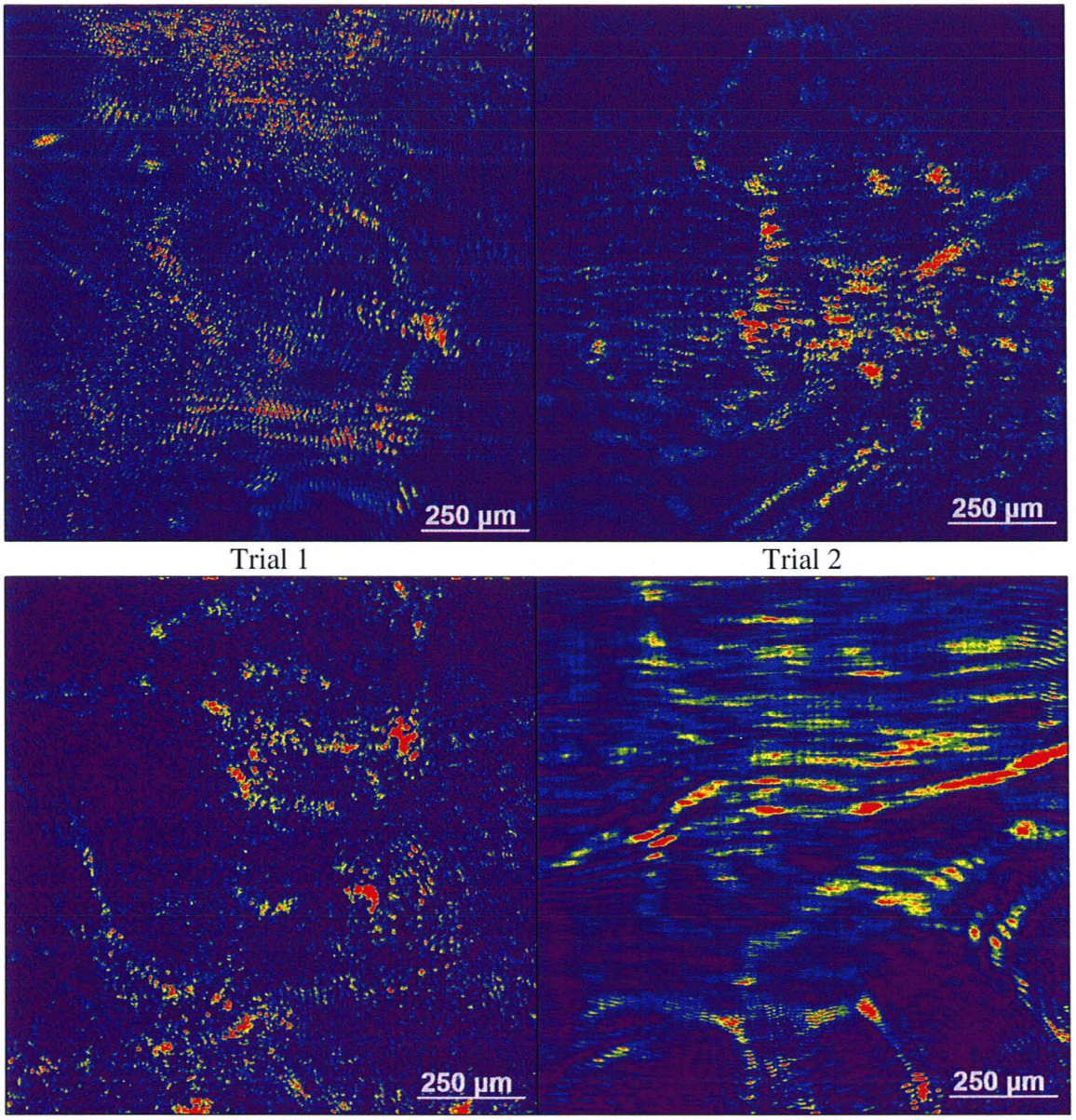

Figure B.1 Wavelength: 488 nm, spatial coherence length: ∞

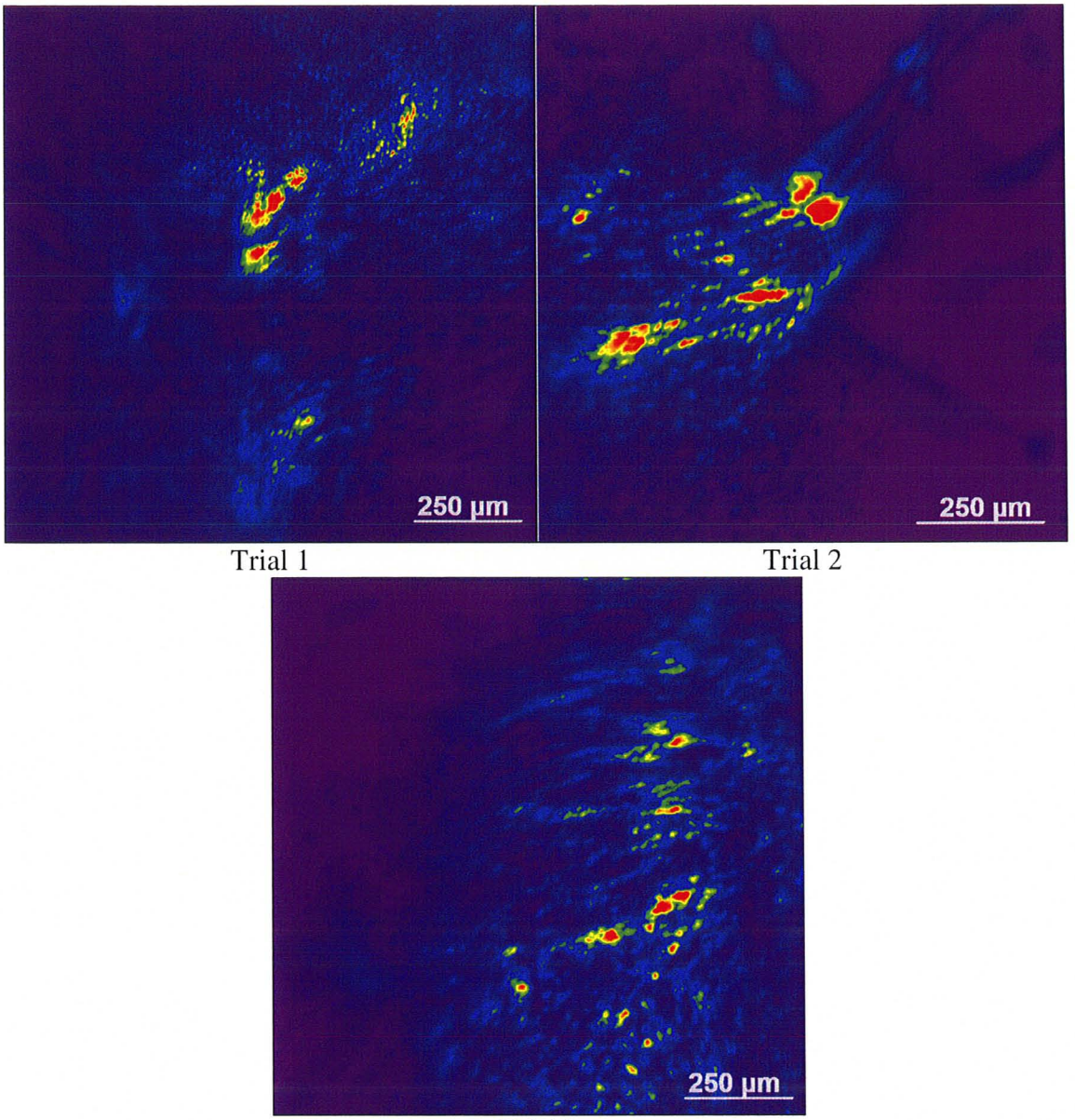

Trial 1 Trial 2

Trial 3

Figure B.2 Wavelength: 488 nm, spatial coherence length: 86 ± 12 µm

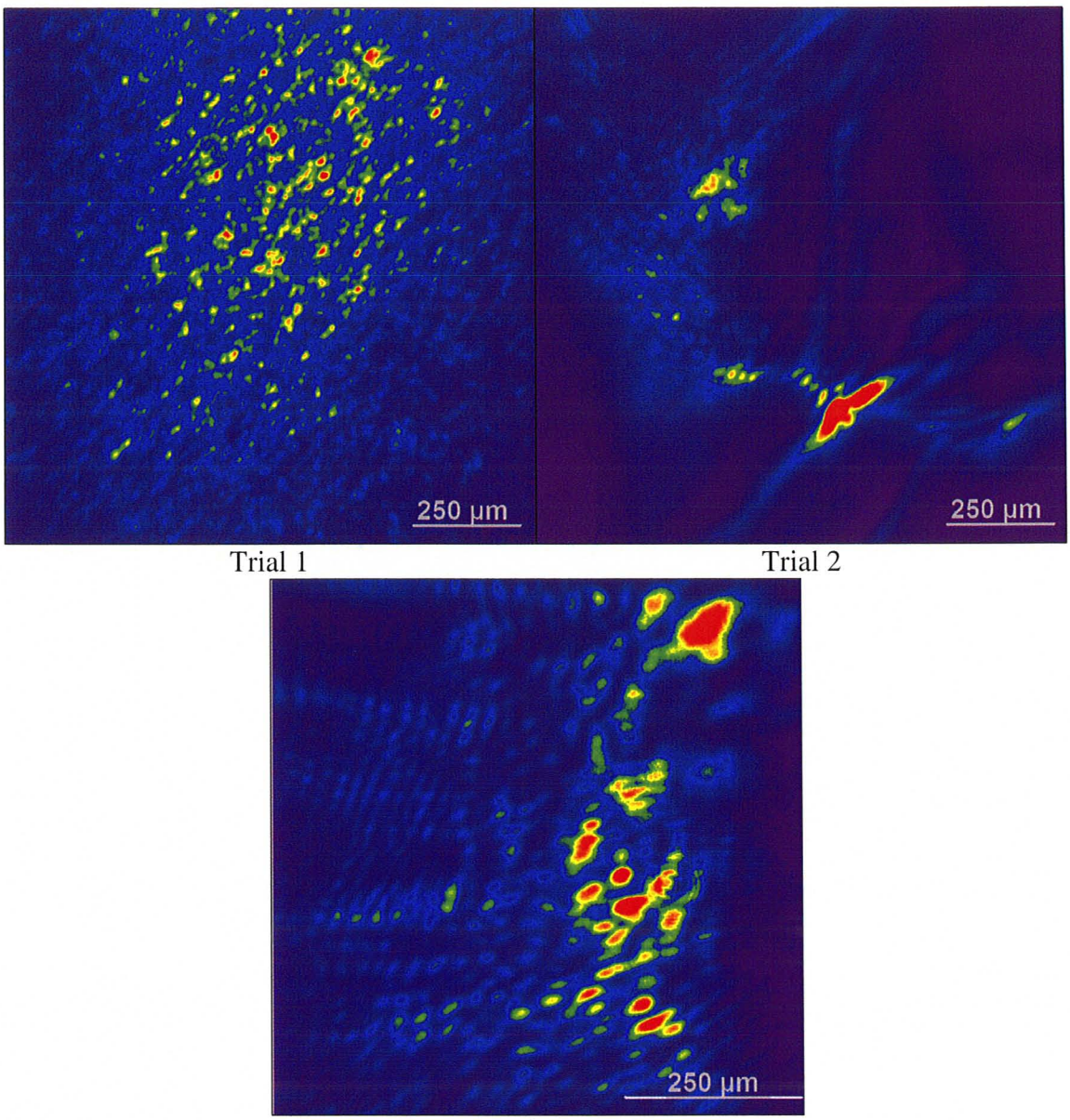

Trial 1 Trial 2

Trial 3

Figure B.3 – Wavelength: 488 nm, spatial coherence length: 45 ± 9 µm

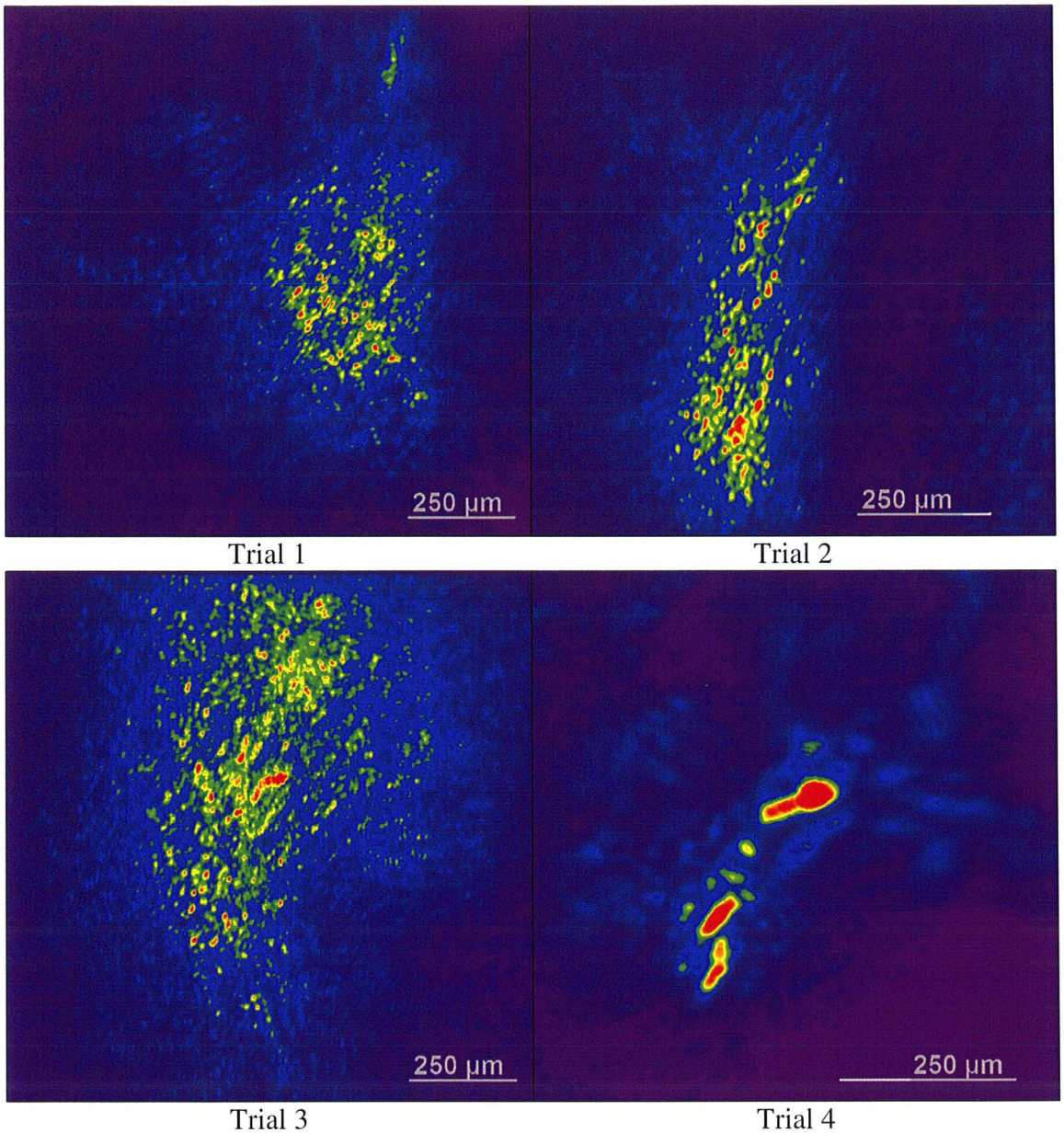

Figure B.4 Wavelength: 488 nm, spatial coherence length: 34 ± 6 µm

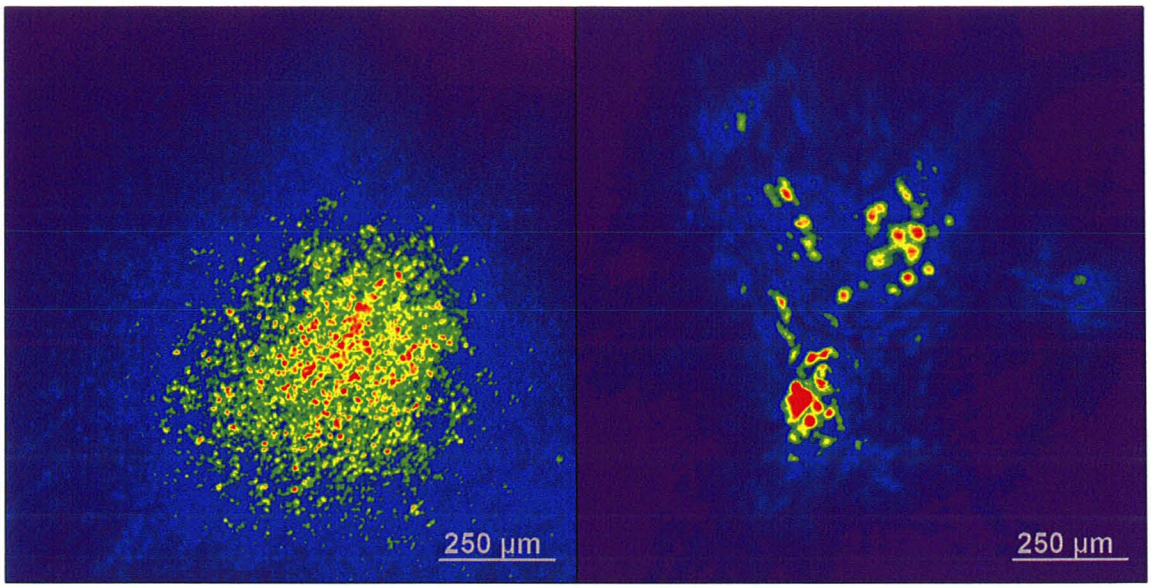

Trial 1 Trial 2

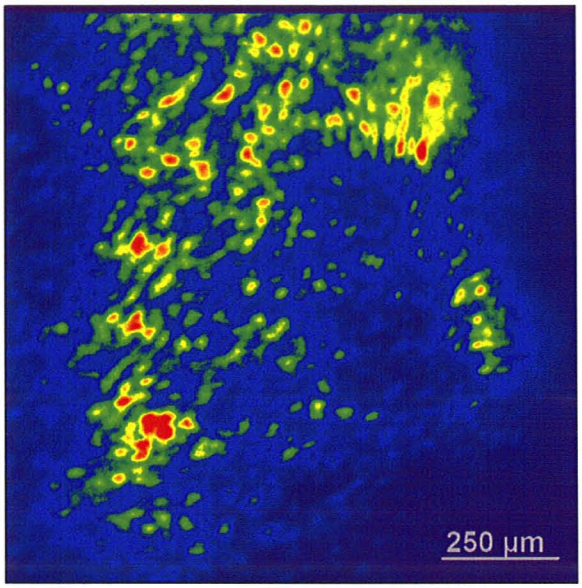

Trial 3

Figure B.5 Wavelength: 488 nm, spatial coherence length: 27 ± 6 µm

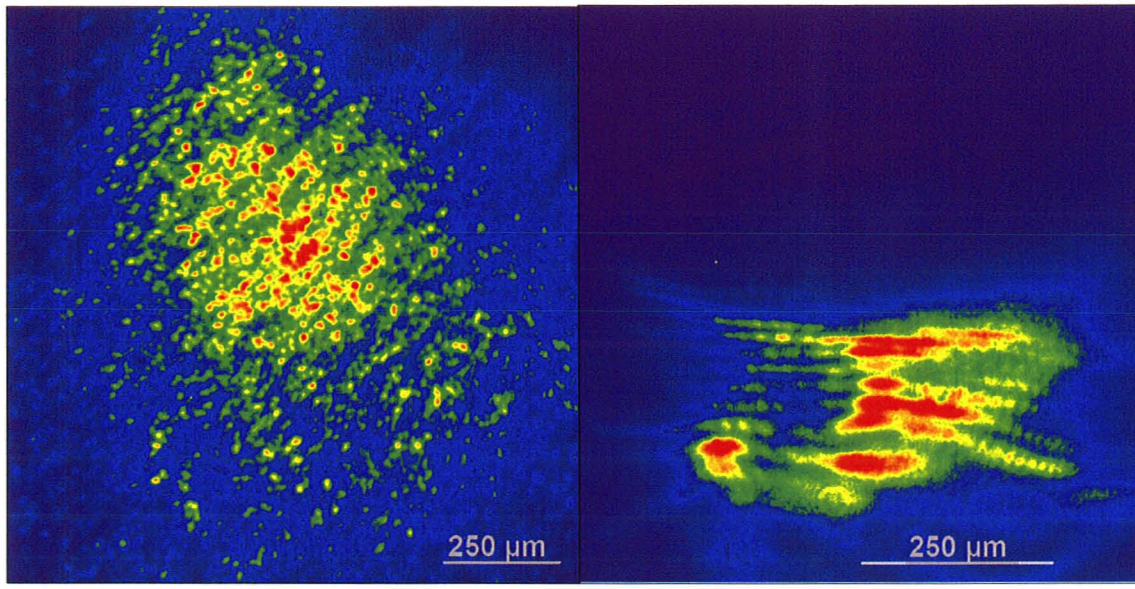

Trial 1 Trial 2

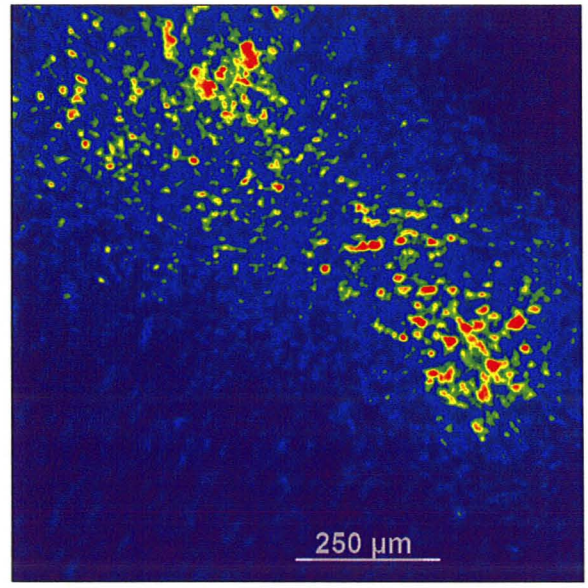

Trial 3

Figure B.6 Wavelength: 488 nm, spatial coherence length: 15 ± 3 µm

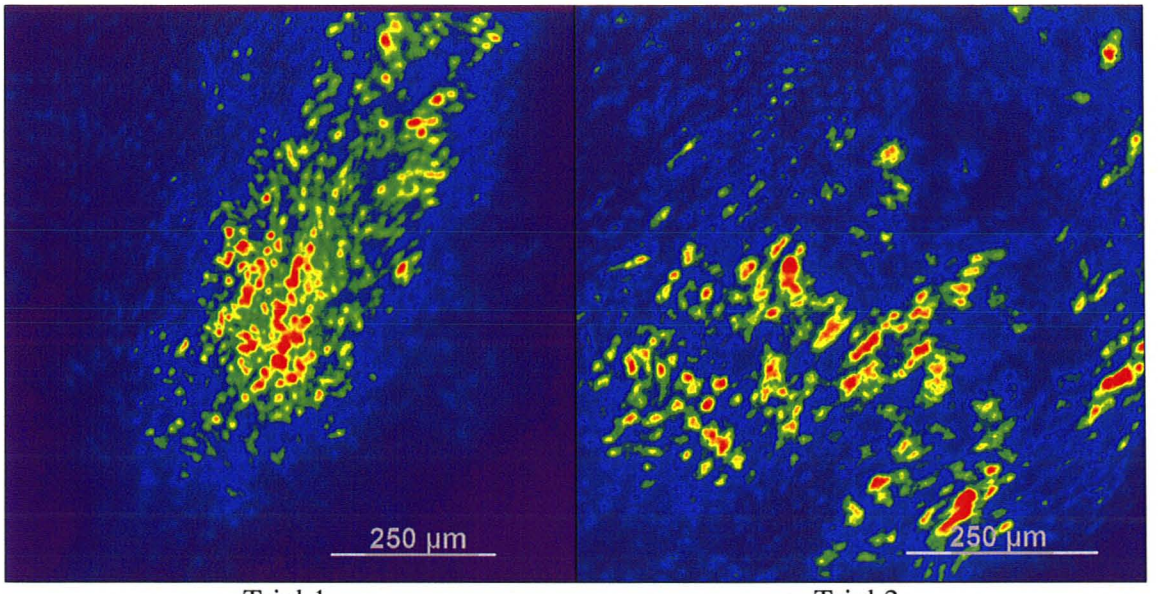

Trial 1 Trial 2

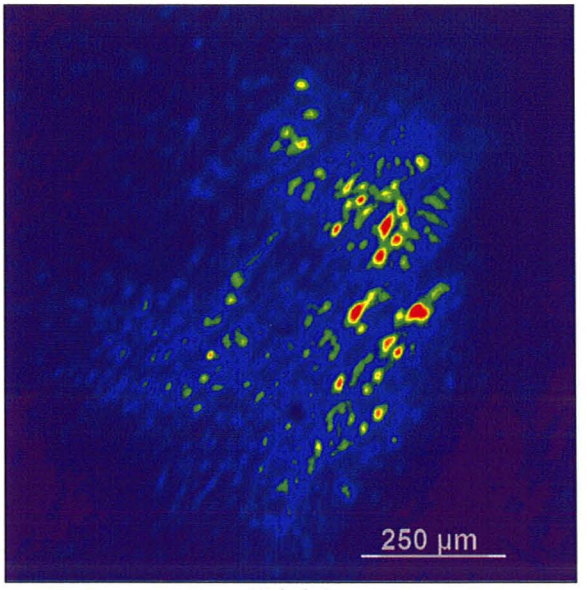

Trial 3

Figure B.7 Wavelength: 488 nm, spatial coherence length: 11 ± 2 µm

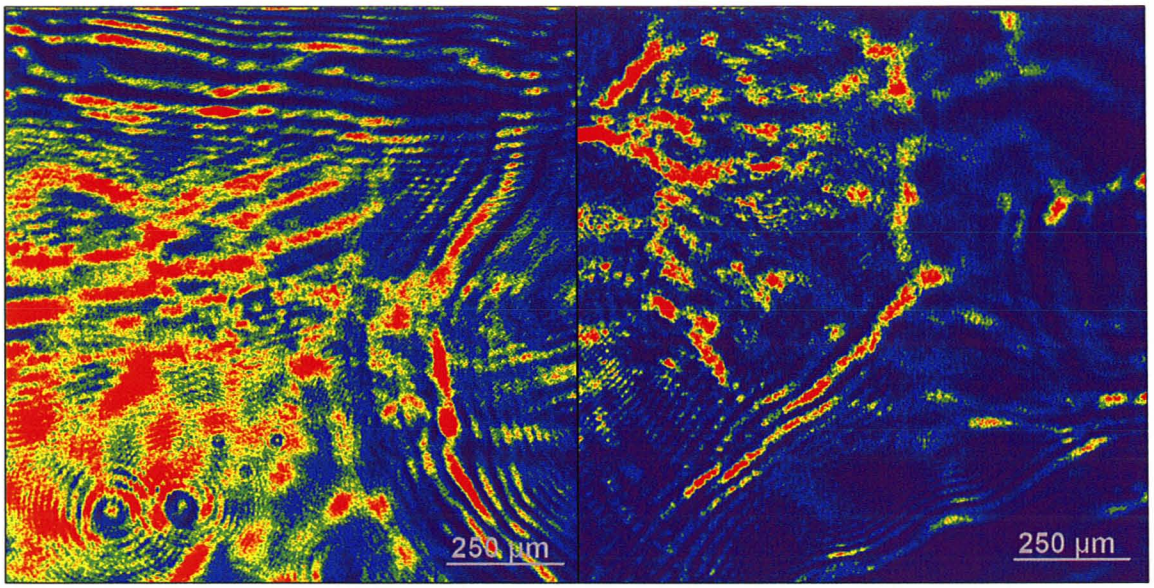

Trial 1 Trial 2

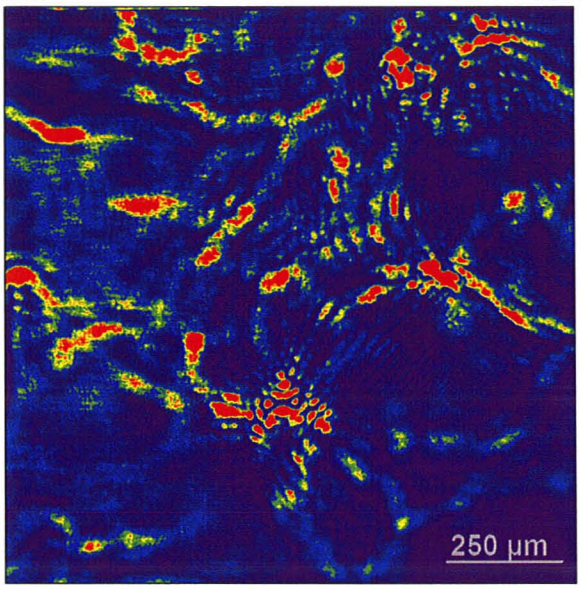

Trial 3

Figure B.8 Wavelength: 532 nm, spatial coherence length: ∞

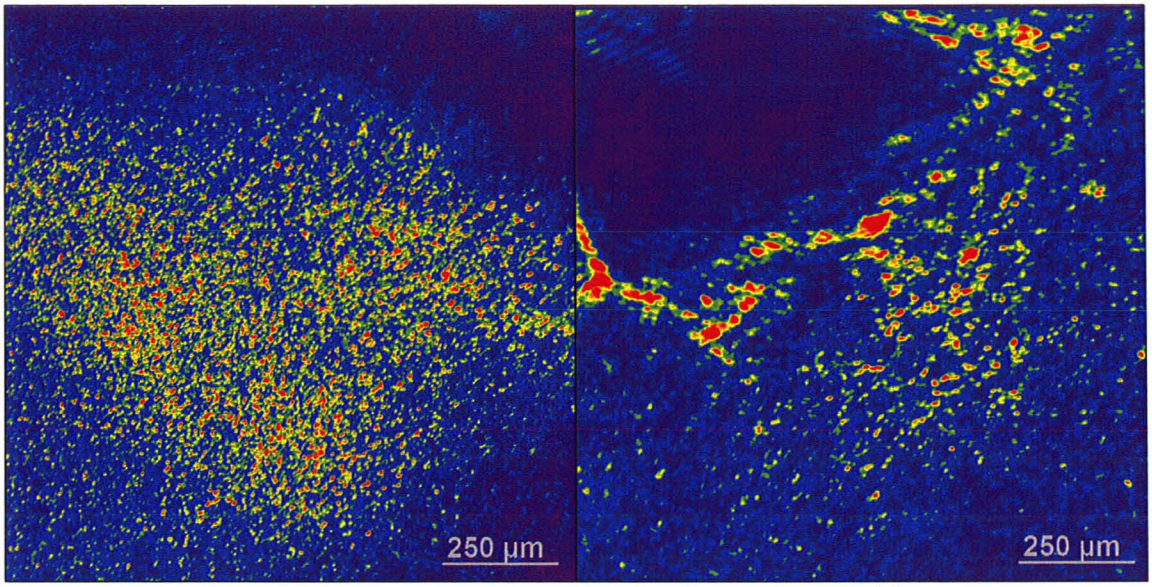

Trial 1 Trial 2

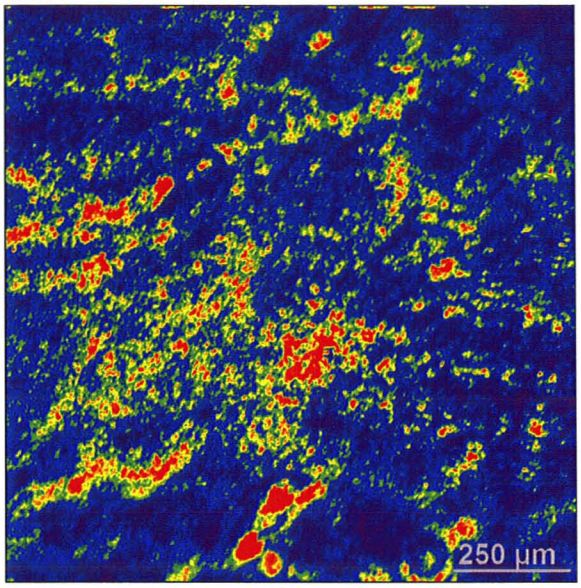

Trial 3

Figure B.9 Wavelength: 532 nm, spatial coherence length: 46 ± 5 µm

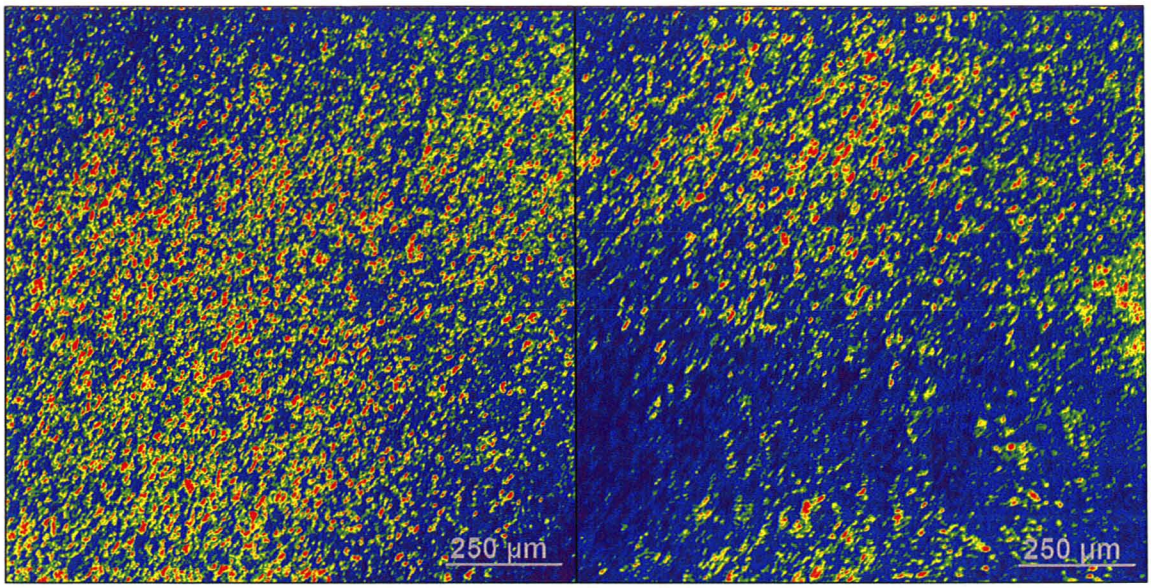

Trial 1 Trial 2

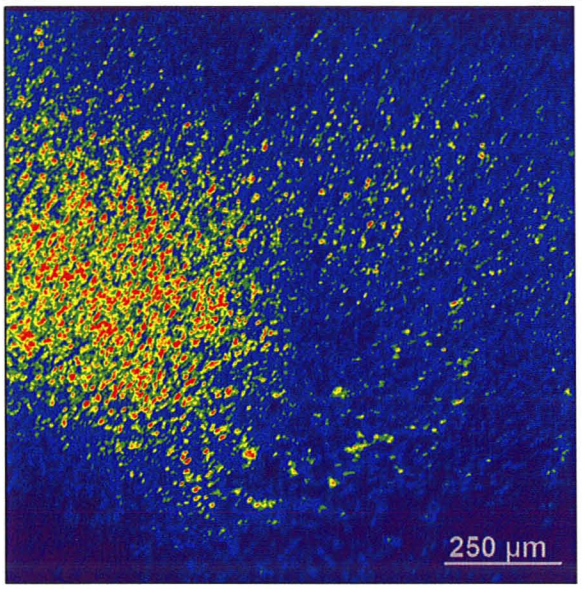

Trial 3

Figure B.10 Wavelength: 532 nm, spatial coherence length: 25 ± 2 µm

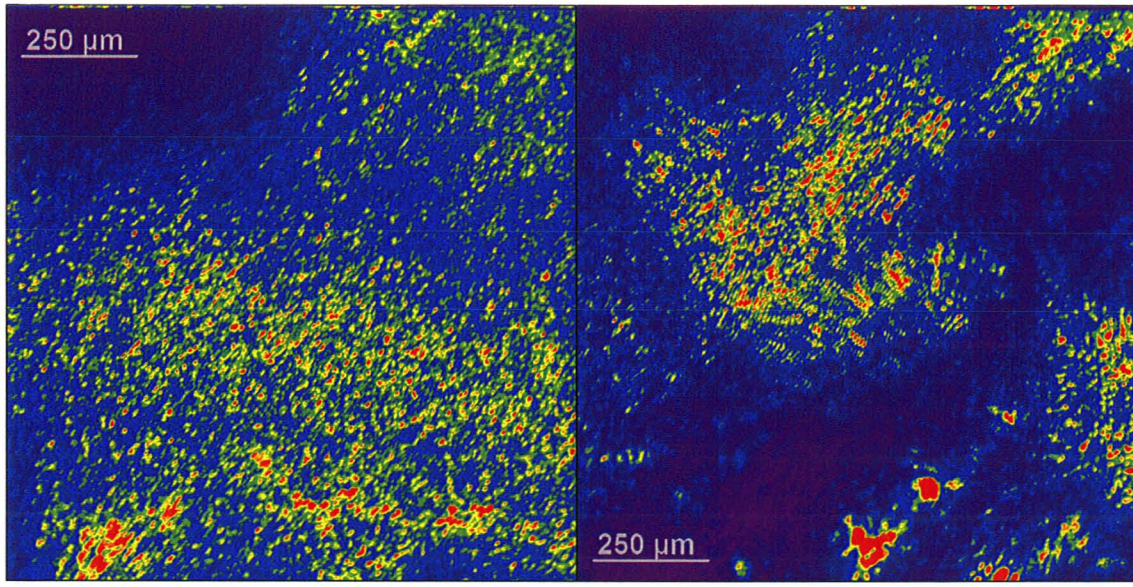

Trial 1 Trial 2

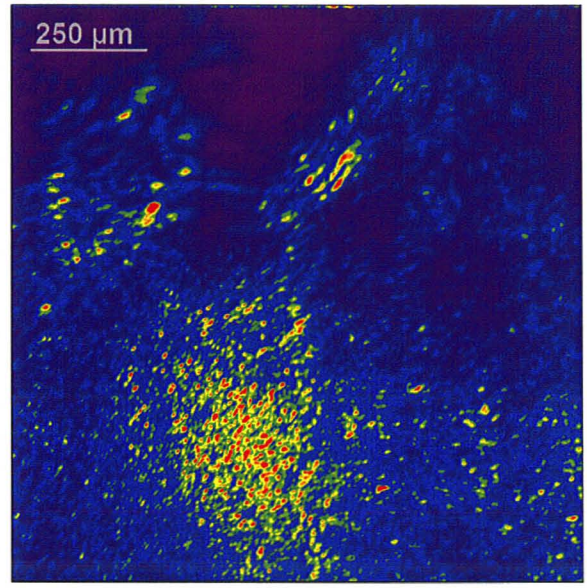

Trial 3

Figure B.11 Wavelength: 532 nm, spatial coherence length: 15 ± 2 µm

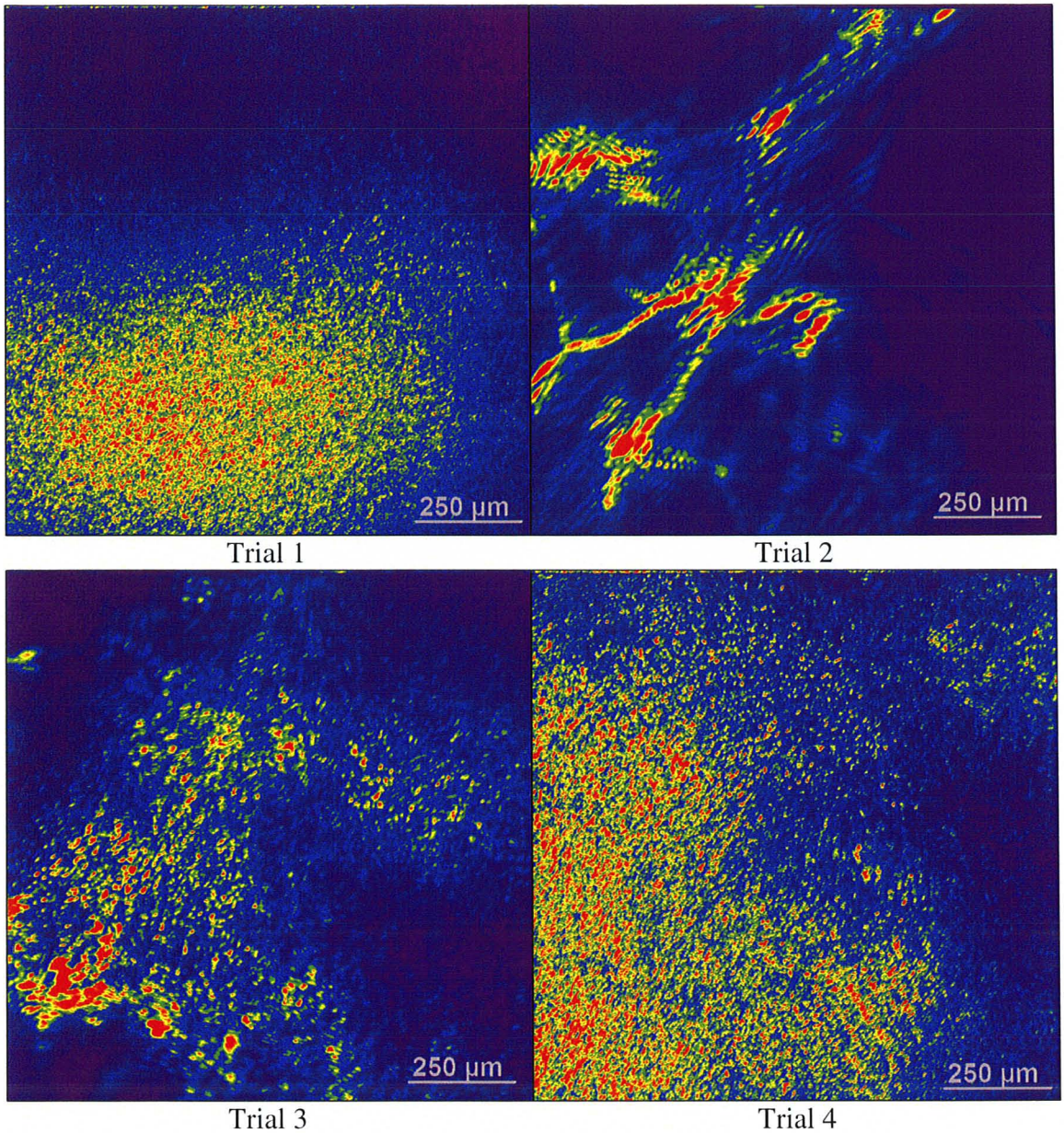

Figure B.12 Wavelength: 532 nm, spatial coherence length: 11 ± 1 µm

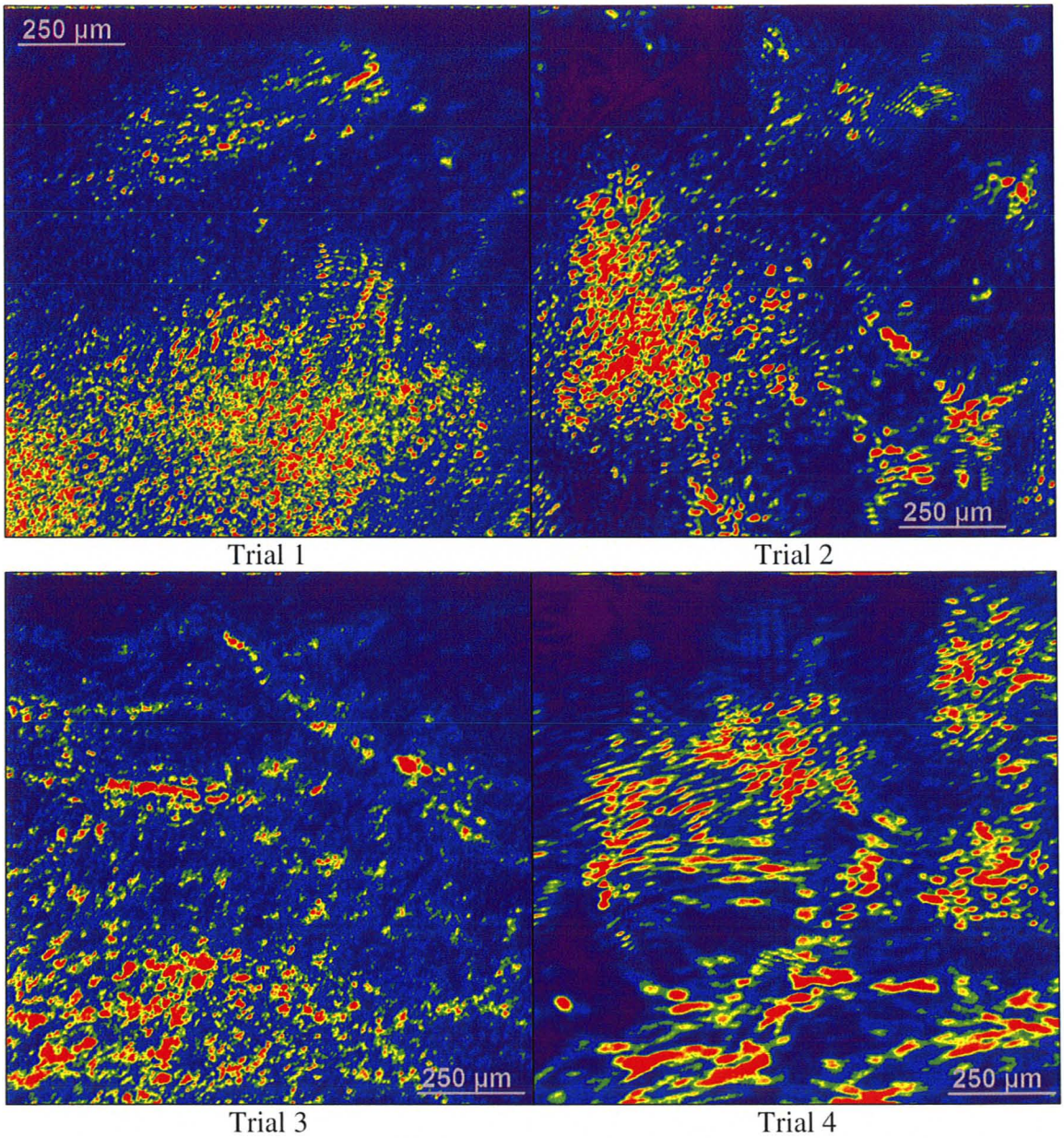

Figure B.13 Wavelength: 532 nm, spatial coherence length: 6 ± 1 µm

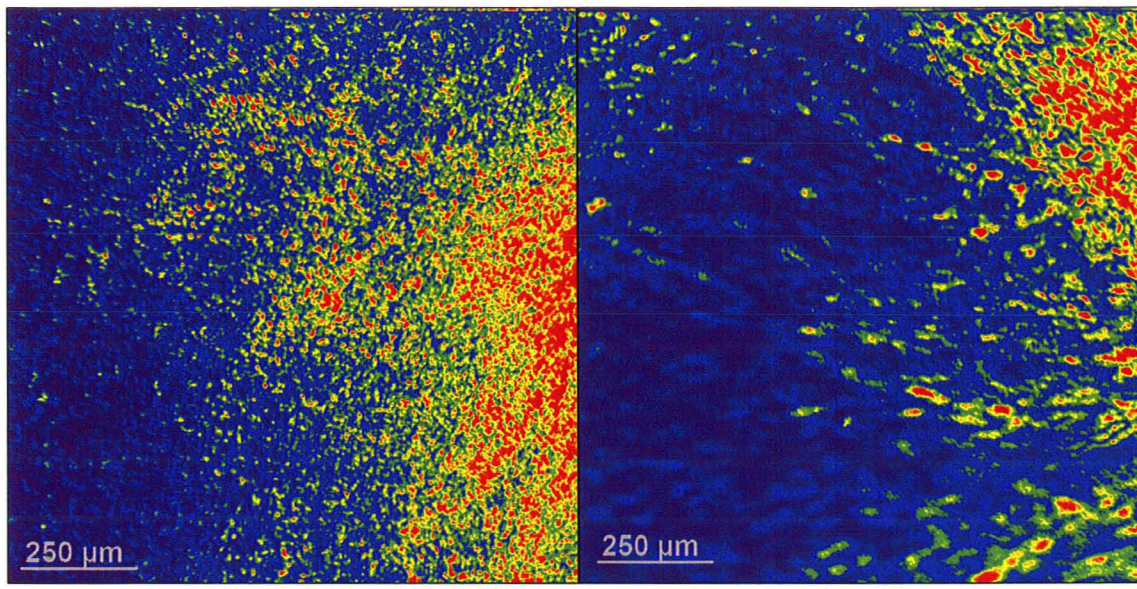

Trial 1 Trial 2

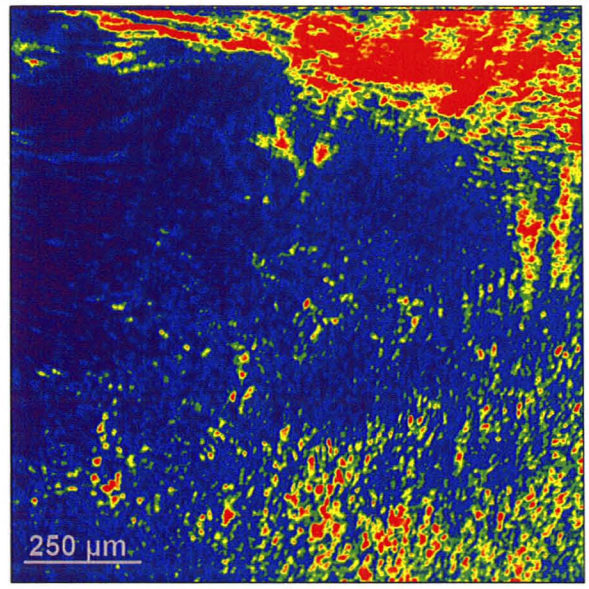

Trial 3

Figure B.14 Wavelength: 532 nm, spatial coherence length: 1.3 ± 0.2 µm

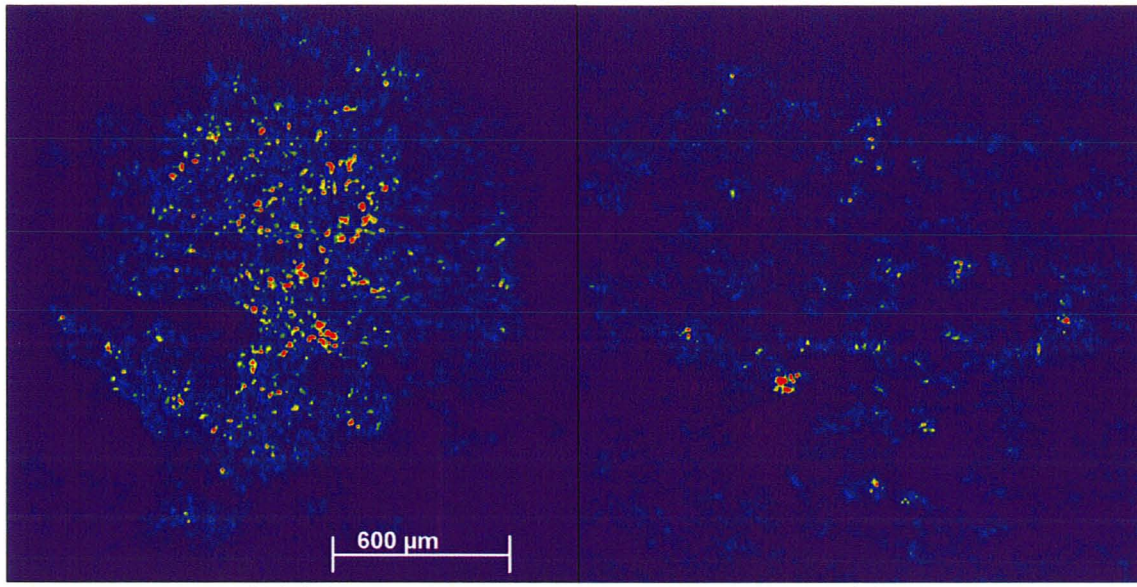

Trial 1 Trial 2

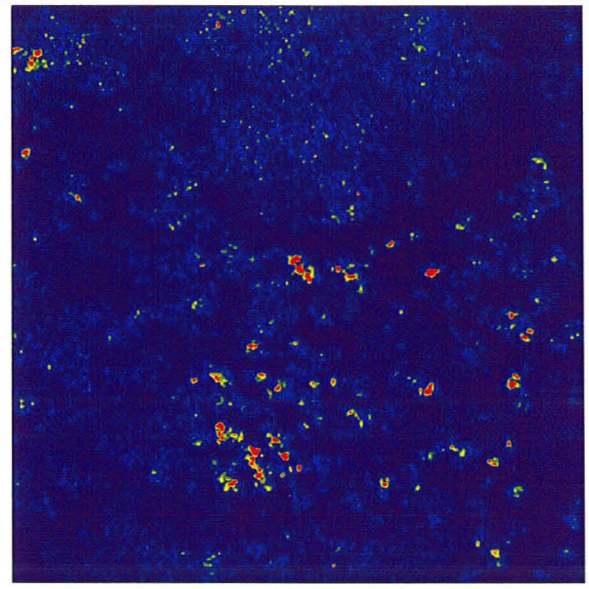

Trial 3

Figure B.15 Control Experiments – Diffuser at rest. Wavelength: 488 nm, Trial 1: Coherence length = 27 ± 6 µm, t = 2532 s; Trial 2: Coherence length = 45 ± 9 µm, t= 1608 s; Trial 3: Coherence length = 45 ± 9 µm, t = 1872 s.